Computer Modelling of Directional Coupler Based Optical Devices

by

Tiparatana Wongcharoen

A thesis submitted to City University for the Degree of Doctor of Philosophy in Electrical and Electronic Engineering

City University

Measurement and Instrumentation Centre
Department of Electrical, Electronic and Information Engineering
Northampton Square, London EC1V 0HB, UK.

August 1995

This work is lovingly dedicated

to

Royal Kingdom of Thailand

Table of Contents

List of Tables

List of Figures

Acknowledgements

I wish to express my sincere appreciation to Professor Kenneth Grattan for his advice and guidance throughout this work.

I am deeply indebted to Dr. Azizur Rahman for his excellent supervision of this work and also for providing his valuable time to discuss problems of all sorts.

I wish to acknowledge the support provided by the Bangkok University for allowing me to study for this degree through a grant.

Also, I gratefully appreciates the sharing of expertise and the many constructive comments in the area of computer made by Dr. Zoheir Mouaziz, Dr. Zhiyi Zhang, Dr. Xhang Shan, and Mr. Brian Burns during the years of working with the Photonic Devices Modelling group, at City University.

I would like to take this opportunity to thank Sow Fun Pit Dawson, Saloma Gilling, Pam Parker, Sue Ciccone, Joan Rivellini, Lynn Pilley, Linda Carr, and Roger Valsler for their help and the friendly, joyful atmosphere surrounding me in the course of this work.

Finally, my deepest gratitude is devoted to my father, mother, brothers, sisters, and husband, Surapong Pinitglang. It is only with their loves, patiences, and encouragements that my research is made possible. I offer this work as one instalment towards repaying my immense debt to them with gratitude and admiration and love.

Declaration

I grant powers of discretion to the University Librarian to allow this thesis to be copied in whole or in part without further reference to the author. This permission covers only single copies made for study purposes, subject to normal conditions of acknowledgements.

Abstract

This work is a study of the important parameters of synchronous and nonsynchronous, weakly and strongly coupled optical directional couplers, primarily using the finite element method. This method can be used to find accurate modal solutions of the isolated waveguides or the coupled waveguides with arbitrary shapes, index profiles, and anisotropies. Unlike the traditional coupled mode theory, the vector supermodes obtained by using the finite element method are orthogonal to each other, even when the guides are strongly coupled or when they are not identical. From an accurate knowledge of the propagation constants of the two supermodes, the coupling length of the system can also be calculated.

However, the finite element method cannot provide directly the power-transfer efficiency or the cross-talk between the coupled waveguides. Calculations of the important coupling parameters can be achieved by introducing the coupled mode approach along with the accurate modal solutions obtained by using the finite element method. In this approach, the overlap integrals of the isolated modes and the coupling factors are calculated numerically and these values are subsequently used to find the power coupling efficiency from one waveguide to another. Recently, there have been several innovative approaches to improving the traditional coupled mode theory by enforcing orthogonality of the supermodes or by maintaining the power conservation criteria. In this work, some of these new coupled mode approaches have been implemented to study the coupling parameters along with the exploitation of the accurate modal solutions obtained using the finite element method.

As an alternative, the least squares boundary residual method can be applied to find the excitation coefficients of the two supermodes by considering the butt-coupling between the input waveguide and the directional coupler section. In this approach, the continuity of the tangential electric and magnetic fields is achieved in a least squares sense at the junction discontinuity interface. Once the transmission coefficients of the two guided even- and odd- like supermodes are calculated, the power carried by the two guides along the axial direction can be easily evaluated.

In this work, the power transfer from one optical waveguides to another by the use of the finite element based propagation model has also been studied. Simulation results are presented for a wide range of directional coupler based-devices including electro-optic switches and semiconductor filters. To show the advantages of the finite element-based approaches, the power transfer efficiency between coupled waveguides with two-dimensional confinement is also presented.

Symbols and Abbreviations

OIC	Optical Integrated Circuit
DBR	Distributed Bragg Reflector
DFB	Distributed Feedback
FEM	Finite Element Method
FDM	Finite Difference Method
VM	Variational Method
MAM	Multilayer Approximation Method
BEM	Boundary Element Method
PMM	Point-Matching Method
MMM	Mode-Matching Method
TE	Transverse Electric mode
TM	Transverse Magnetic mode
LSBR	Least Squares Boundary Residual
AN	Analytical solution
HS	Hardy and Streifer
MA	Marcatili
CH	Chuang
FDBPM	Finite-Difference based Beam Propagation Method

OCMT	The Orthogonal Coupled Mode Theory
NCMT	The Nonorthogonal Coupled Mode Theory
α	Penalty parameter
λ	Wavelength in μm.
β	Propagation constant
π	pi $\cong$ 3.142
ε	Permittivity
μ	Permeability
k	Wave number
L_c	Coupling length

Chapter 1

Introduction

1.1 Historical development of Lightwave Technology

From a historical perspective there is one particularly noteworthy date in the development of lightwave technology, the year 1880, in which Alexander Graham Bell invented the "photophone". This was a device that varied the intensity of sunlight incident upon it in response to the amplitude of speech vibrations. At receiver, the light variations were reconverted into an electrical signal by means of a selenium detector, and subsequently back into sound. While the photophone itself was impractical due to the rapidity with which its optical signal intensity weakened with propagation distance, the concept of optical communication that it demonstrated is in many ways responsible for the development of the field of lightwave and integrated optics. The transmission and processing of signals carried by optical beams rather than by electrical currents or radio waves has been a topic of great interest ever since the early 1960s, when the development of the laser first provided a stable source of coherent light for such applications. In spite of the tremendous potential bandwidth offered by the laser, strong absorption by rain,

snow, fog, and smog prevented the effective propagation of laser light through the atmosphere for practical distances for communication. It was not until the development of low-loss optical fibers that optical communications could become a reality. Their development, along with that of compact single-mode semiconductor lasers, has led to the demonstration of communication systems that can transmit information at a rate of over two billion bits per second over 130 kilometres with an error rate of one per billion bits. With the capacity to transmit optical signals also came the necessity periodically to reamplify and recondition them by the use of "repeater" spaced every so often along the transmission path. It is here that the classical optics approach was unsatisfactory. The optical telephone repeater typically involved a laser, detector, lenses, and mirrors, spread out on an optical bench. Although the initial research in integrated optics was primarily directed toward the optical communications area, other potential applications for combining the unique properties of light into an extremely small package were apparent.

The history of radio communications technology has seen a steady increase of the carrier frequency used for the transmission of information. With the invention of the laser, this steady climb made a huge jump from the millimetre wavelength to the optical frequency range, an increase by three to four orders of magnitude. There is now little doubt that guided wave optical devices will have a lasting impact on electrical engineering in the coming years. In the last two decades the optical fibre has finally allowed the practical use of light as a carrier of

information. The semiconductor laser is also a guided wave device. It can emit light of the wavelength at which silica fibre shows minimum dispersion and minimum propagation loss, near λ_o = 1.3 and 1.55 μm, respectively. With careful design, the output can also consist of very nearly a single optical frequency. This is an important advantage for communications, since it reduces the effect of modal dispersion. Together, these are currently in the process of revolutionising the telecommunications industry, and making considerable advances in a variety of other new and exciting application areas. The appreciation that optical fibres could be used as a method of conveying information, with the availability of huge bandwidth, generated a new technology through which telecommunications companies throughout the world have been able to gain massive economies of scale. Now that optical techniques are well established in telecommunications, there is increasing interest in using optics to extend and replace electronics for some purposes. One major activity in research laboratories throughout the world is the demonstration of various *optical integrated circuits* (OIC) to replicate and enhance the performance of *electronic integrated circuits*, and also to perform novel functions particularly suited to optics. An essential feature of these optical components is a method of optically linking various parts of the circuit, and optical waveguides can be considered as equivalent to the connecting *wires* of optical circuits.

The optical integrated circuit has a number of advantages when compared to either its counterpart, the electrical integrated circuit, or to conventional optical

signal processing systems composed of relatively large discrete elements. The major advantages of the optical integrated circuits (OIC) are increased bandwidth, the possibility of expanded frequency (wavelength) division multiplexing, low-loss couplers, including bus access types, expanded multipole switching (number of poles, switching speed), smaller size, weight, lower power consumption, batch fabrication economy, improved reliability, improved optical alignment and immunity to vibration. The major disadvantage is high cost of developing new, associated fabrication technology.

The OIC inherently has the same large characteristic bandwidth as the optical fiber because, in both cases, the carrier medium is a lightwave rather than an electrical current. Thus, the frequency limiting effects of capacitance and inductance can be avoided. The design and fabrication of a practical OIC with a bandwidth to match that of an optical fiber, while feasible in principle, probably will require many years of technology development. Light can be guided, modulated, deflected, filtered, radiated into space or, by using laser action, it can also be generated within a thin-film structure. Integrated optical devices promise to provide optical communication systems with components such as the lasers, modulators, filters, optical switches, and directional couplers. However, practical applications of OICs have already been accomplished, and the future is promising. In order to develop new optical communication systems or optical devices, we need fully to understand the principles of optical guiding, while obtaining accurate

quantitative propagation characteristics of waveguides and utilising them effectively in actual design.

Maxwell's equations are need to be solved to calculate the propagation characteristics of optical waveguides. It is, however, rather rare to obtain a precise analytic solution, and therefore, a precise analysis of optical waveguides is generally considered to be difficult. For this reason, various methods of optical waveguide analysis have been developed. These methods may be broadly classified into two categories: analytical approximate solutions and numerical solution using computers. In order to analyze and design optical waveguides, it is necessary to study these analysis methods in depth, and to be able to use these methods as tools. Some of the representative analytic solutions and numerical solutions are introduced in this thesis.

Historically, planar waveguide integrated optics was the first system to be developed, followed shortly by the more sophisticated and successful channel waveguide integrated optics system. An optical waveguide that is uniform in the direction of propagation is the most basic type of waveguide, but this alone is not sufficient for the construction of an optical integrated circuit. In reality, an appropriate combination of various forms of optical waveguides is placed on the substrate to construct an optical circuit with the desired features. These may be, for example, corner-bent waveguides, S-shaped waveguides, and bent waveguides which are used to change the direction of the lightwaves. Tapered waveguides are used to alter the width of waveguides; branching waveguides and crossed

waveguides are used for splitting, combining, and interference; and optical waveguide directional couplers and two-mode waveguide couplers are used for coupling. Waveguide gratings, with a periodic structure in the direction of propagation, play many important roles in optical integrated circuits containing components, such as wavelength filters, mode converters, reflectors, resonators, demultiplexers, etc. Waveguide gratings are also used widely as a laser element, such as a distributed Bragg reflector (DBR) laser or a distributed feedback (DFB) laser.

Although waveguides come in various forms and with a variety of functions, the fact remains that the optical waveguide that is uniform in the direction of propagation is the essential form of waveguide. The information regarding the propagation characteristics of the optical waveguide is thus the most basic and important information required when designing this type of waveguides. Therefore, the discussion in this thesis will be restricted to optical waveguides in which material constants such as structure and refractive index do not change in the direction of propagation.

1.2 Analysis of Optical Waveguides

Some of the major reasons for a study of the propagation of light in optical waveguides are listed below. Firstly, it is necessary to establish how many optical modes the structure will support. Most applications will require the propagation of one or two modes. Some factors such as small changes in dimensions or refractive

indices can frequently result in the structure being either at "cut-off" *i.e.* not able to support a propagating mode or supporting more than one mode. The circular symmetry of an optical fibre as shown in Fig. 1.1a ensures that one or more modes will always be supported whatever the value of d, the core diameter as long as $n_g > n_s$, where n_g and n_s are the refractive indices in guide and substrate respectively. In a nonsymmetrical planar structure, such as is shown in Fig. 1.1b, however, this is not necessarily the case, and if n_g, n_s and d are sufficiently small, the structure will be "cut-off" and no mode can be supported. However, for symmetrical planar structure if $n_s = n_c$ then this cutoff will not occur for the fundamental mode.

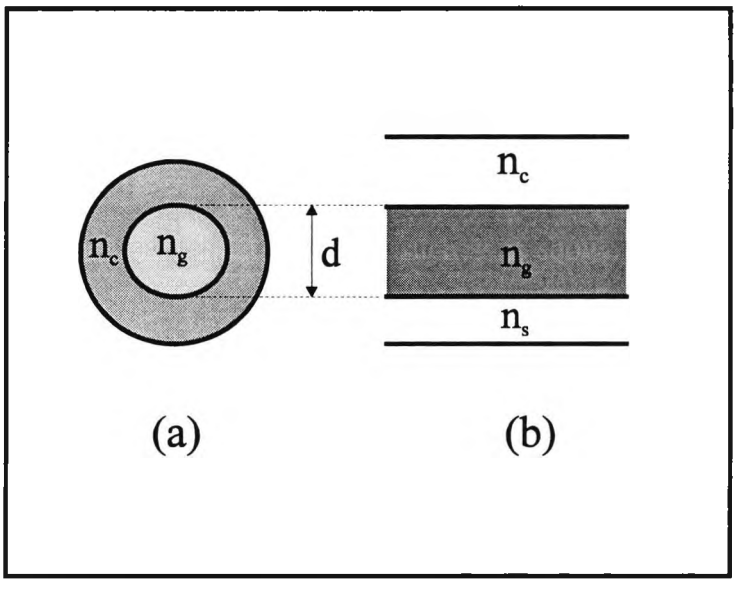

Fig. 1.1 Refractive index profile of (a) an optical fibre and (b) a planar waveguide structure.

Secondly, it is often desirable to know the precise field profile of the mode. This is important when designing devices for high coupling efficiency between planar waveguides and optical fibres. Also, the performance of some practical

waveguides is limited by scattering losses caused by roughness induced by the fabrication process, and detailed information about the magnitude of the field at the rough edges allows these losses to be assessed.

Thirdly, it may be necessary to know the propagation constant (β) of a mode in a waveguide. For single mode propagation, knowledge of this parameter is not usually very important. However, for most optical switching functions, the operating principle is the interference between two modes, and an exact knowledge of the difference between the β value of the two modes is necessary. This difference is usually a very small percentage of β, and so a precise calculation of β for each guide is very important, and for this, the most accurate techniques for calculating β for practical waveguides are needed.

1.3 Optical Waveguide Analysis Techniques

1.3.1 Analytical Approximation Solution and the Numerical Solution

The propagation characteristics of optical waveguides can be calculated by solving Maxwell's equations, but this is not an easy task. There are many reasons that optical waveguide analysis is difficult; some of the major reasons are listed below:

-Practical optical waveguides have complex structures,

-The general propagation mode is the hybrid mode,

-Some optical waveguides have an arbitrary refractive index distribution (graded optical waveguides), as in doped optical waveguides and non-uniform-core optical fiber,

-The electromagnetic field extends outside the guide core and guides are not of the closed type,

-Anisotropic materials and nonlinear optical materials may be used to increase the range of performance,

-Materials with a complex refractive index, such as semiconductors and metals, are also used.

To overcome these difficulties, various methods have been developed for the analysis of optical waveguides. Such methods may be roughly classified into two groups, analytical approximation solutions and numerical solutions using computers.

1.3.1.1 Analytical Approximation Solutions for Optical Waveguides

An exact analytical solution can be obtained for a simple stepped 1-D optical waveguide and a stepped optical fiber. If, however, the waveguide has an arbitrary refractive index distribution, such an exact analysis is no longer possible. Therefore, various types of analytical approximation solutions have been developed for 1-D optical waveguides in which the refractive index changes gradually in the thickness direction, and for optical fiber whose refractive index changes gradually only in the radial direction. In the case of 2-D optical

waveguides for optical integrated circuits and nonaxisymmetrical optical fiber, hybrid-mode analysis is required to satisfy the boundary conditions, even if the individual materials that constitute the waveguide are homogeneous. However, the analytical approximation solutions developed for these optical waveguides generally do not treat them as a hybrid mode, and therefore, the accuracy of the solution deteriorates near the cutoff frequency.

1.3.1.2 Numerical Solutions for Optical Waveguides

Numerical solutions can grouped into the *domain solution*, which includes the whole domain as the operational area, and the *boundary solution*, which includes only the boundaries as the operational area. The former is also called a *differential solution*, and the latter, an *integral solution*. The domain solutions include the finite element method (FEM), the finite difference method (FDM), the variational method (VM), and the multilayer approximation method (MAM). The boundary solutions include the boundary element method (BEM), the point-matching method (PMM), and the mode-matching method (MMM). Among these are the perturbation technique, the method of conformal transformation, the mode matching technique, the finite difference method, and the variational method (Koshiba, 1992).

The perturbation techniques are particularly useful, and can produce quite good results if there exists a compact solution for the unperturbed waveguide and the perturbation of the physical configuration is so small that the unperturbed fields

are only slightly disturbed. When the perturbation terms are large, the perturbation methods become tedious and the physical meaning of the results is clouded by the complexity of the expressions used and normally, in such a case, the use of the perturbation techniques will yield a relatively poor approximation. When the perturbation becomes large, it becomes an inconvenient procedure, when the variational method becomes is more appropriate (Davies, 1980).

The development of new ideas in theory and in applications in numerical methods for partial differential equations has been particularly influenced by the innovation brought about by the computer era. In general, a numerical method leads to an algorithm for the solution of a problem, and to get an overall picture, it may have to be solved separately for each set of values of the parameters. However, this algorithm may be simple in many problems where an analytical solution is difficult or impossible. Before numerical, computer-based solutions of real problems dealing with complex continua can be solved, it is necessary to limit their infinite degrees of freedom to a finite number of unknowns. Such a process of discretization was first successfully performed by the use of the finite difference method which was, until recently, one of the most popular numerical methods.

The basic idea behind the finite difference formulation of a problem is the discretization of the differential operator equations which represent the physical system by a set of difference equations. This can be done by expanding the field at a point in terms of its value and derivatives at a neighbouring point by a Taylor series and suitably truncating this series. In this way a relation between the field

value for the central point of a cluster with the field values of neighbouring nodal points can be derived. Operations are then performed not upon continuous functions but rather approximately, in terms of fields over a discrete point set. The main disadvantages of finite difference methods are the lack of geometrical flexibility in fitting irregular boundary shapes, and in concentrating points in regions of the solution domain where the variable changes most rapidly. The other difficulties experienced in using the finite difference methods are the treatment of singular points and when any boundary or interface boundary does not coincide with constant coordinate surfaces.

An alternative approach, the variational method, is becoming increasingly more important than other approximate methods. If the domain does not conform to one of the major coordinate systems, the problem is often more readily solved by using a finite element method. This method is in essence a variational method which makes use of the Rayleigh-Ritz procedure. The ability of the finite element to represent a complex shape is a point in its favour. Isoparametric elements are well adapted for problems with curved boundaries (Miniowitz and Webb, 1991; Koshiba and Inoue, 1992). In this thesis, the finite element method with its simple numerical integration and its simple logic makes it ideally suited to implementation using a computer.

The finite element method, which is one of the domain solutions, can be very easily applied not only to optical waveguides of any shape, but also to optical waveguides with any refractive index distribution and to those with any anisotropic

materials or nonlinear optical materials. In Chapter 5 and in subsequent chapters, actual analysis examples are given to demonstrate that the finite element method can be used effectively for the analysis of various optical waveguides, including 2-D optical waveguides, as discussed in Chapter 8 and Chapter 9.

The finite element method enables a solution of the problem by applying the variational principle to the functional of the subject system, instead of solving directly the differential equation for the system. The distinctive feature of the finite element method is that it first divides the subject domain into small sections called elements, develops an equivalent digitising model for each of these elements, and then re-assembles the whole. Another words, the finite element method is a type of Ritz-Galerkin method, or a numerical analysis technique, that uses a partitioned polynomial expression as an approximating function and converts a continuous system into an equivalent discrete system. In recent years, there has been a trend to call any method that employs division into elements a finite element method, even if it does not use the variational principle, as in the Galerkin method and other weighted-residual methods. As a result, the range of application of the finite element method has expanded, and the definition of the term has also broadened.

1.3.2 Methods for analyzing waveguides

Many of the simpler techniques that may be used are based on the solution for a one dimensional slab waveguide which can be solved semi-analytically and calculated to any specified degree of accuracy. If a typical slab waveguide of

thickness a, and refractive index n_a confined by two semi-infinitely thick layers of refractive indices n_c and n_b, as shown in Fig. 1.2, supports a TE mode given (without the exp(jωt) time dependence) by

$$\psi(x,z) = A(x)e^{-j\beta z} \tag{1.1}$$

where β is the propagation constants, z the direction of propagation, $\psi(x,z)$ is the field component of the TE modes and $A(x)$ the field profile of the mode and β is given by the solution of the transcendental equation

$$\tan(aq - N\pi) = \frac{(p+r)q}{(q^2 - pr)} \tag{1.2}$$

where

$$p^2 = \beta^2 - n_b^2 k^2 \tag{1.3}$$

$$q^2 = n_a^2 k^2 - \beta^2 \tag{1.4}$$

$$r^2 = \beta^2 - n_c^2 k^2 \tag{1.5}$$

$$k = \frac{2\pi}{\lambda} \tag{1.6}$$

with λ being the free-space wavelength, and N is an integer 0,1,2,... corresponding to different modes.

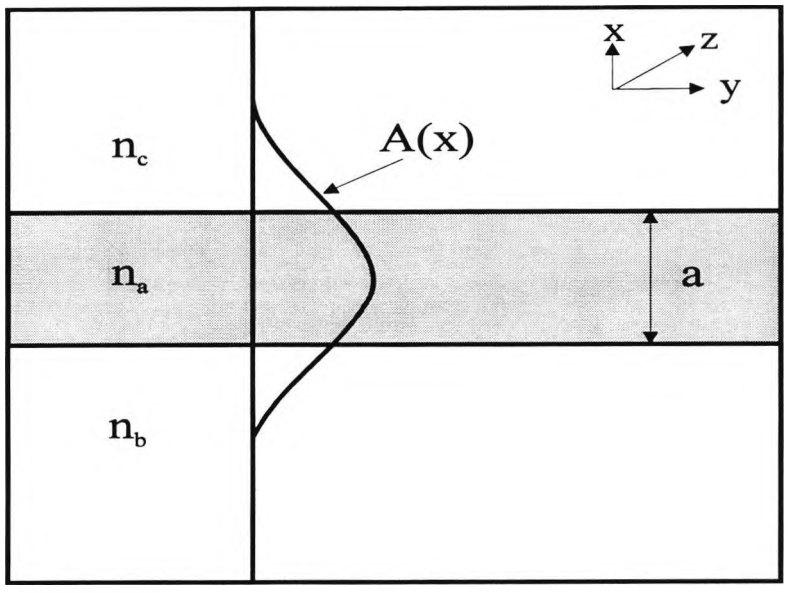

Fig. 1.2 Schematic of a slab waveguide, showing waveguide of thickness a, and refractive index n_a confined by two semi-infinitely thick layers of refractive indices n_c and n_b supporting a TE mode.

1.4 Multilayer Planar Waveguide Couplers

While butt coupling can be used to couple two planar waveguides, the more commonly used method is to bring the guides in question into close proximity and allow coupling to occur through phase coherent energy transfer (optical tunnelling). The indices n_O and n_2 in the guiding layers, as shown in Fig. 1.3, must be larger than the indices in the separation region and the substrate region, n_1 and n_3, respectively, and the thickness of the confining layer of separation must be small enough that the evanescent tails of the guided modes overlap. In order for efficient energy transfer to occur between the two guides, they must have identical propagation constants. Thus, the indices and the thicknesses of the waveguiding layers must be very carefully controlled to provide matching propagation constants, during the fabrication process of any such coupler system.

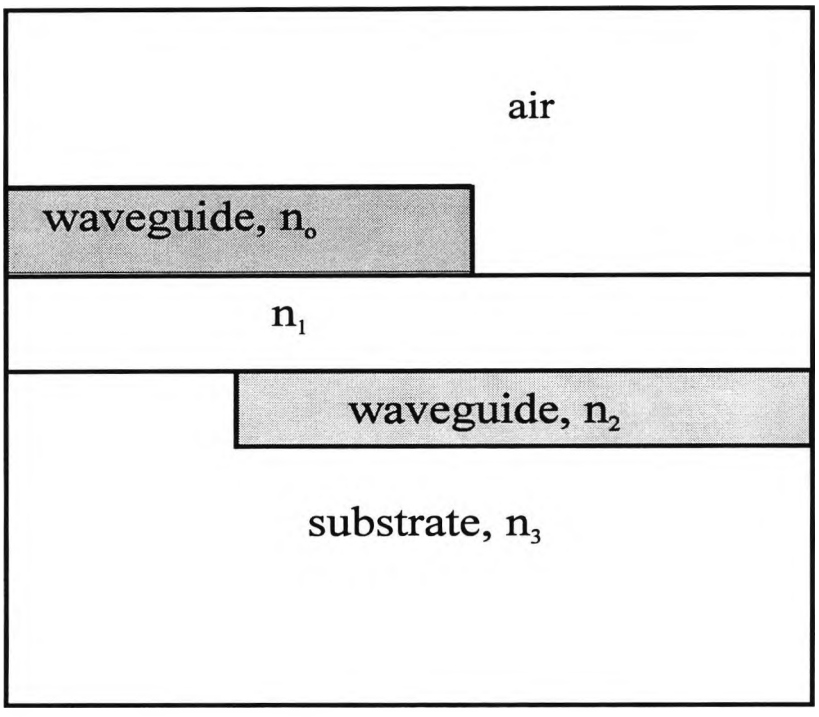

Fig. 1.3 Coupling between two planar waveguides by optical tunnelling. Transfer of energy occurs by phase coherent synchronous coupling through the isolation layer with index n_1.

1.5 Dual-Channel Directional Couplers

The dual-channel directional coupler, which is analogous to the microwave dual-guide multihole coupler (Lance, 1964), consists basically of two parallel channel optical waveguides sufficiently closely spaced so that energy is transferred from one to the other by optical tunnelling, as shown in Fig. 1.4. This energy is transferred by a process of synchronous coherent coupling between the overlapping evanescent tails of the modes guided in each waveguide. Photons of the driving mode, say in guide *a*, transfer into the driven mode in guide *b*, maintaining a phase coherence as they do. This process occurs cumulatively over a significant length; hence, the light must propagate with the same phase velocity in each channel in

order for this synchronous coupling to occur. The fraction of the power coupled per unit length is determined by the overlap of the modes in the separate channels. Thus, the coupling factor depends on the separation distance, *s*, and the interaction length, *L*, in particular.

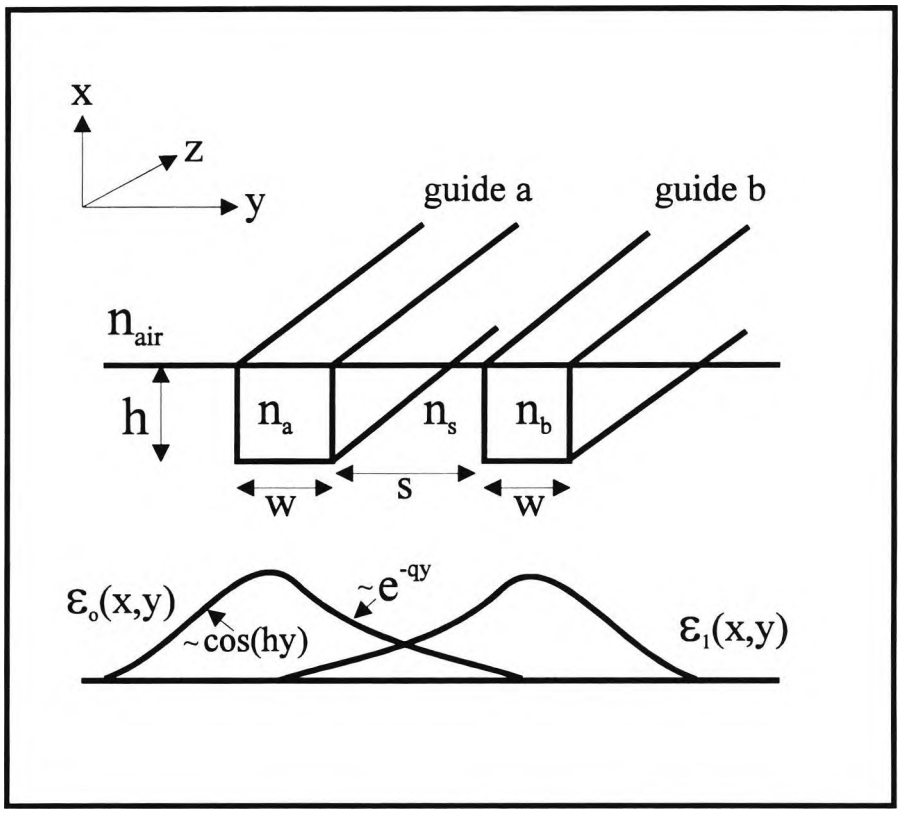

Fig. 1.4 Diagram of a dual channel directional coupler. The amplitudes of the electric field distributions in the guides are shown below them.

1.6 Coupled-Mode Theory of Synchronous Coupling

A concise theory of operation of the dual-channel directional coupler can be developed by following the coupled mode theory approach of Yariv (1973). The electric field of the propagating mode in the waveguide is described by

$$\overline{E}(x,y,z) = A(z)\,\overline{\mathcal{E}}(x,y) \tag{1.7}$$

where A(z) is a complex amplitude which includes the phase term $\exp(-j\beta z)$. The term $\overline{\mathcal{E}}(x,y)$ is the solution for the field distribution of the mode in one waveguide, assuming that the other waveguide is absent. By convention, the mode profile $\overline{\mathcal{E}}(x,y)$ is assumed to be normalised to carry one unit of power. Thus, for example, the power in guide *b* is given by

$$P_b(z) = A_b(z)^2 = A_b(z)A_b^*(z) \tag{1.8}$$

where $A_b^*(z)$ is a complex amplitude in guide *b*.

The coupling between modes is given by the general coupled mode equation for the amplitudes of the two modes. Thus,

$$\frac{dA_a(z)}{dz} = -j\beta_a A_a(z) + \kappa_{ab} A_b(z) \tag{1.9}$$

and

$$\frac{dA_b(z)}{dz} = -j\beta_b A_b(z) + \kappa_{ba} A_a(z) \tag{1.10}$$

where β_a and β_b are the propagation constants of the modes in the two guides, and κ_{ab} and κ_{ba} are the coupling coefficients between the modes.

The guides shown in Fig. 1.4 may be considered, and it can be assumed that these guides are identical and that they both have an exponential optical loss coefficient, α. Thus,

$$\beta = \beta_r - j\frac{\alpha}{2} \tag{1.11}$$

where $\beta = \beta_a = \beta_b$, and β_r is the real part of β. For the case of identical guides, it is obvious from reciprocity that

$$\kappa_{ab} = \kappa_{ba} = -j\kappa \tag{1.12}$$

where κ is real. Then, using (1.11) and (1.12), Eq. (1.9) and (1.10) can be rewritten in the form

$$\frac{dA_a(z)}{dz} = -j\beta A_a(z) - j\kappa A_b(z) \tag{1.13}$$

and

$$\frac{dA_b(z)}{dz} = -j\beta A_b(z) - j\kappa A_a(z) \tag{1.14}$$

If it is assumed that light is coupled into guide *a* at the point $z = 0$, so that the boundary conditions for the problem are given by

$$A_a(0) = 1 \quad \text{and} \quad A_b(0) = 0 \tag{1.15}$$

then the solutions are described by

$$A_a(z) = \cos(\kappa z)e^{-j\beta z} \tag{1.16}$$

and

$$A_b(z) = -j\sin(\kappa z)e^{-j\beta z} \tag{1.17}$$

Thus, the power flow in the guides is given by

$$P_a(z) = A_a(z)A_a^*(z) = \cos^2(\kappa z)e^{-\alpha z} \tag{1.18}$$

and

$$P_b(z) = A_b(z)A_b^*(z) = \sin^2(\kappa z)e^{-\alpha z} \tag{1.19}$$

From (1.18) and (1.19), it can be seen that the power does indeed transfer back and forth between the two guides as a function of length. Note also, in equations (1.16) and (1.17), the distinct phase difference that exists between the amplitude of the fields in the two guides. The phase in the driven guide always lags the phase of the driving guide by 90°. Thus, initially at $z = 0$, the phase in guide b lags 90° behind that in guide a. That lagging phase relationship continues for increasing z, so that at a distance z that satisfies $\kappa z = \pi/2$, all of the power has been transferred to the guide b. Then, for $\pi/2 \leq \kappa z \leq \pi$, the phase in guide a lags behind that in guide b. This phase relationship results from the basic mechanism

which produces the coherent transfer of energy. The field in the driving guide causes a polarization in the dielectric material which is in phase with it, and which extends into the region between the guides because of the presence of the mode tail. This polarization then acts to generate energy in the mode of the driven guide. It is a basic principle of field theory that such generation occurs when the polarization leads the field, while dissipation occurs when the polarization lags the field. Thus, the lagging field in the driven guide is to be expected. Because of this definite phase relationship, the dual-channel coupler is a directional coupler. No energy can be coupled into a backward wave travelling in the -z direction in the driven waveguide. This is a very useful feature in many applications.

From (1.18) and (1.19), it can be seen that the length, L, necessary for complete transfer of power from one guide to the other is given by

$$L = \frac{\pi}{2\kappa} + \frac{m\pi}{\kappa} \tag{1.20}$$

where m = 0,1,2,.... In a real guide, with absorption and scattering losses, β is complex. Hence, the total power contained in both guides decreases by a factor $\exp(-\alpha z)$.

The coupling coefficient, κ, is a strong function of the shape of the mode tails in the guides. For well confined modes, in which the overlapping of the tails causes only a negligible perturbation of the basic mode shape, it can be shown that the coupling coefficient is given by (Somekh, 1974)

$$\kappa = \frac{2h^2 q e^{-qs}}{\beta W(q^2 + h^2)} \tag{1.21}$$

where W is the channel width, s is the separation, h and β are the propagation constants in the y and z directions, respectively, and q is the extinction coefficient in the y direction. It will be recalled that these parameters have been assumed to be identical for both waveguides. In a practical situation, it may be difficult to fabricate two identical waveguides to form a coupler. If, for example, the guides do not have exactly the same thickness and width, the phase velocities will not be the same in both. This will not necessarily destroy the coupling effect entirely. If the difference in phase constants, $\Delta\beta$, is small, it can be shown that the power distributions in the two guides are given by (Somekh *et al.*, 1974a)

$$P_a(z) = \cos^2(gz)e^{-\alpha z} + \left(\frac{\Delta\beta}{2}\right)^2 \frac{\sin^2(gz)}{g^2} e^{-\alpha z} \tag{1.22}$$

and

$$P_b(z) = \frac{\kappa^2}{g^2}\sin^2(gz)e^{-\alpha z} \tag{1.23}$$

where

$$g^2 \equiv \kappa^2 + \left(\frac{\Delta\beta}{2}\right)^2 \tag{1.24}$$

It can be seen from (1.22-1.24) that, in the presence of a constant phase difference, $\Delta\beta$, a transfer of power will still occur. However, the transfer will be incomplete, since (1.22) will never go to zero for any values of z.

The preceding equations can be used to calculate the expected performance of dual-channel directional couplers for the case of slightly non-identical guides, with a non-zero $\Delta\beta$.

1.7 Applications Involving Directional Couplers

The dual-channel directional couplers are among the more useful of integrated optic devices. They can be used as power dividers, input or output couplers, and directionally selective taps on an optical data bus. The foregoing are all examples of passive applications, in that the fraction of power coupled in each case is a constant. However, the most important application of the dual-channel coupler is an active modulator or switch, in which the coupled power is electronically controlled. It has been shown in (1.22) and (1.23) that the coupled power is a strong function of any phase mismatch between the two waveguides.

1.8 Aims and Objectives of the thesis

The information given so far has provided a background to the work which is reported in this thesis and has provided several objectives for the research undertaken in this field. The following presents the primary aims of the work presented here which are

(1) To investigate established work on the structure of optical devices, based on a directional coupler analysis. First, to carry out a study on planar structures for calculating the coupling length, L_c, and making a comparison of the results obtained using the finite element and the analytical approaches. Next, the aim is to calculate the coupling length, L_c, in 2-D confinement using the finite element method.

(2) To implement an improved coupled-mode theory to study the influence of the coupling parameter, along with the exploitation of the accurate modal solutions obtained using the finite element method.

(3) To study three separate approaches, namely the coupled mode approach, the least squares boundary residual method and the propagation model in detail and to use them to calculate the power transfer efficiency in a planar waveguide directional coupler and then to make a comparison with alternative methods. However, to our knowledge so far, a numerical simulation of the power transfer efficiency in 2-D confinement has not been previously reported.

(4) To develop an extension of the system, once the results obtained from the first stage of the application are achieved, to be implemented in a further, more detailed study to characterize 2-D confinement directional coupler waveguides.

The objective of this work is to do these by testing the 1-D results obtained using the coupled mode approaches, the propagation model and the least squares

boundary residual method. Finally, these methods are then extended to calculate the power transfer efficiency in a 2-D confinement directional coupler problem, where the advantages of these more sophisticated methods can be more clearly seen.

1.9 Structure of the Thesis

This thesis is comprised of work carried out by the author in the use of the finite element method, the coupled-mode theory and the least squares boundary residual approach in the analysis of certain types of interesting optically guiding devices. The subsequent discussion gives an outline of the carefully structured thesis, beginning with an Introduction to the subject in a review of optical waveguides as presented in this first Chapter.

In Chapter 2, the relevant theoretical background on the finite element method and a comparison of several variational formulations are presented. A detailed study of the finite element approach along with the use of triangular coordinates and shape functions is undertaken, to calculate the eigenvectors and the propagation constants. Since the analysis of an axially-uniform waveguide is essentially a two-dimensional problem, the application of the method is restricted to two-dimensional domains. The application of finite elements to waveguides of optical structures is first studied. The variationally-based finite element analysis of the modes in a uniform waveguide is then considered. Scalar and vector formulations are also employed, as is the choice of the variational form. This leads

to the difficulty of spurious modes, which is addressed in the work. By applying the penalty approach, the relation $\nabla \cdot H = 0$ is satisfied and the spurious modes do not appear. Methods for their avoidance are considered at the end of the Chapter.

In Chapter 3, the implementation of this approach will be described, along with matrix solution techniques. An abrupt discontinuity problem, in the transverse plane $z = 0$, between two quite arbitrary uniform waveguides is also considered. The use of the least squares boundary residual (LSBR) method along with the vector finite element method for accurate calculation of this wide range of optical waveguide discontinuity problems is also presented at the end of this Chapter.

General coupled-mode theory and an implementation of the three approaches used in this part of the work is described in Chapter 4, with the aim of calculating the power transfer efficiency. In this Chapter the various forms of the coupled-mode theory for two parallel uniform optical waveguides is first reviewed, with the aim of describing subtle distinctions between different forms of the conventional theory. Then, a comparison between different coupled mode approaches is applied to the analysis of optical directional couplers made of slab waveguides. The power transfer efficiency of the couplers is also studied, based on the use of the theory developed.

Chapters 5, 6, 7, 8, and 9 will deal with the results of the application of these methods to various types of important and relevant optical waveguide problems. Our solutions will be proved by comparing the results obtained with

analytical and other alternative results available. In Chapter 5, results are presented on a study of the important parameters of synchronous and nonsynchronous, weakly and strongly coupled optical directional couplers using the finite element method. Accurate propagation constants and field profiles have been obtained for the modes of the isolated guides and supermodes of the coupled system. The power transfer efficiency and cross-talk are calculated from the individual guide modes using improved coupled mode approximations and from the supermodes using the least squares boundary residual method. The results of an adjustment of the length of the directional coupler, both in terms of the separation distance between two waveguides and width of guide are also presented in this chapter. The effect of mesh divisions is also presented. The results for an electro-optic directional coupler switch showing the effect of Δn and the separation distance are presented in Chapter 6. In this Chapter also, the power coupling efficiency between two optical waveguides is presented.

In Chapter 7, the coupling length and power transfer variation with wavelength are presented for both synchronous and nonsynchronous directional couplers. The effect of mesh divisions is also shown in this Chapter. The accurate calculation of coupling parameters is of considerable interest, more specifically for strongly coupled nonidentical guides, as may be used in the design of wavelength filters or a polarizer.

The results of an analysis of the characterization of optical channel waveguide directional couplers is shown in Chapter 8. A discussion of coupling

length variation with fabrication tolerances and asymmetry for directional couplers used as elements of optical devices is presented using the finite element method, employing an accurate vector **H**-field formulation. The effect of the curved guide sections, leading to the directional couplers, on the coupling length of the device is also presented.

The coupled mode theory, so far, has been based on the mode coupled equations introduced by Miller (1954). The analytical methods based on mode coupling between weakly coupled waveguides are difficult to apply to strongly coupled waveguides. In Chapter 9, the coupling properties in strongly coupled waveguides are given theoretically using a method based on the interference between the waveguide modes supported by the coupled waveguide system, say for two even and odd modes. In this method, the coupling coefficient is defined as the power transfer ratio between the two waveguides. The power transfer efficiency between the two guides in an electro-optic channel waveguide directional coupler is presented in this chapter.

Finally, general conclusions arising from the whole research programme are explored and summarized in the last Chapter. The future trends and possible extensions of the work are also suggested. Finally, a list of references used in this thesis is presented.

Chapter 2

The Finite Element Method

2.1 Introduction

The finite element method, first developed for application to continuous and structural mechanics, is widely used in different fields of science and technology. It is a numerical technique for obtaining approximate solutions to boundary-value problems of mathematical physics. The method has a history of about fifty years. It was first proposed in the 1940s and its use began in the 1950s for aircraft design. Turner, Clough and their associates (1956) at the Boeing Aircraft Company used this method to calculate the stress-strain relations for complicated aircraft structures for which no known solution existed. In 1960, Clough introduced the term "finite elements" to describe the new technique for plane stress analysis. Although the finite element method originated in structural engineering, within a decade the basic concepts were being recognised as having wider applicability and were being used for the solution of problem in various areas like structural and fluid mechanics, heat transfer, electromagnetic theory, acoustics, and biomedical engineering. Subsequent development has been rapid,

and the techniques are now well established within many scientific and engineering disciplines. Obviously, the finite element method, because of its tremendous utility, is in a rapid process of evolution. The basic idea of the finite element method is that any piecewise-continuous function can be approximated by a set of piecewise-continuous polynomials, each defined over a part of the field of domain of the above function. Instead of the function itself, its values at several points of the domain are calculated.

Mathematically, this method is an extension of the Rayleigh-Ritz-Galerkin technique (Zienkiewicz, 1977). It is therefore applied to a wide class of partial differential equations. When the method was first used it was not recognised at the start as an instance of the Rayleigh-Ritz principle. The whole procedure became mathematically respectable at the moment when the unknowns were identified as the coefficients in a Ritz approximation, and the discrete equations were seen to be exactly the conditions for minimising the system potential energy.

The Rayleigh-Ritz method has been used to yield approximate solutions for variationally formulated problems in many areas of physics and engineering. It is, however, associated with certain difficulties which prevent it from being used in a wider class of problems.

Firstly there is no systematic way of choosing the trial functions used in the approximation. Besides, for irregular-shaped boundaries, the required enforcement of the essential boundary conditions can be really problematic. Therefore the class

of problems is immediately limited to those involving geometrically simple boundaries. Also for non-positive definite operators, the matrices obtained are often ill-conditioned.

There are also certain difficulties inherent in the fact that the Rayleigh-Ritz approximation is applied over the whole domain. Generally, very high degree polynomials have to be used to give an accurate description of the unknown function. In this case the procedure becomes more complicated, if the domain contains interfaces at which discontinuous changes of the material properties occur. Besides, the method does not offer the possibility of concentrating more on areas of interest or where the unknown function varies more rapidly.

Given the above shortcomings of the Rayleigh-Ritz method, the finite element approximation offers a very attractive alternative. The method is applied in a discretized way, free of the difficulties associated with "overall" techniques. Irregular boundaries and discontinuous domains can be easily handled and the mesh can be refined or expanded where appropriate. Even linear polynomials are sufficient to approximate almost any function and the discretized nature of the finite element method enables the systematic selection of the trial functions. The finite element technique also lends itself easily to computer implementation because it involves a large number of repetitive steps.

In particularly, it is suitable for automatic computation, and has been formulated to take maximum advantage of the capabilities of modern computers.

With the introduction and advancement of computers, engineers realised that the solution of a large number of simultaneous equations no longer posed an insurmountable problem and this stimulated many new fields of applied research.

The electromagnetic waveguide can be classified into two categories from its cross-sectional shape. One is a planar waveguide or an axially symmetrical waveguide, which can be treated as an equivalent one-dimensional problem. The other is the more general arbitrarily shaped waveguide, which should be treated as a two-dimensional problem. Furthermore, depending on the eigenmode property in a waveguide, either a scalar wave analysis will be acceptable, or a vectorial wave analysis will be required.

This Chapter is concerned with the use of one- and two-dimensional finite element techniques applied to optical waveguide problems. The arbitrarily shaped optical waveguide can be considered, as shown in Fig. 2.1, being composed of several different materials, each of which can be described by arbitrary permittivity and permeability tensors ε and μ. The waveguide is assumed to be uniform along its longitudinal z axis. Assuming the time (t) and z variation are given by $\exp(j\omega t)$ and $\exp(-j\beta z)$ functions respectively, the electromagnetic fields, $\mathcal{H}(x, y, z, t)$ and $\mathcal{E}(x, y, z, t)$ which are the magnetic field and the electric field at the angular frequency, ω, have the form:

$$\mathcal{H}(x,y,z,t) = H(x,y) \exp\left[j(\omega t - \beta z)\right] \tag{2.1}$$

$$\mathcal{E}(x,y,z,t) = E(x,y)\exp[j(\omega t - \beta z)] \tag{2.2}$$

where β is the propagation constant in the positive z-direction. $H(x,y)$ and $E(x,y)$ are the spatial time-independent magnetic field and the spatial time-independent electric field respectively. The general geometry of the guide can, if necessary, be quite complicated, with an arbitrary permittivity profile $\varepsilon(x, y)$ in the transverse (*i.e.* the x-y) directions.

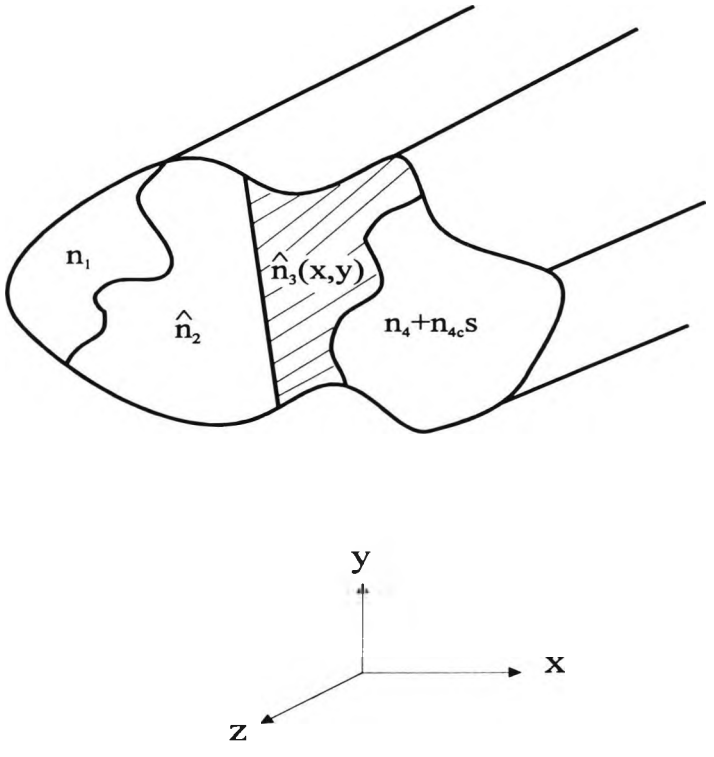

Fig. 2.1 A general arbitrarily shaped optical waveguide geometry, which consists of several regions, where each may be of different type of materials.

2.2 Variational formulations

Finite element formulations are usually established via a variational or a Galerkin (method of moment (Harrington, 1968) or weighted residuals) approach.

The latter is more flexible but when it is possible, it is advantageous to take a variational approach, especially when one global parameter such as the propagation constant is required. This form of derivation only will be considered in this chapter.

2.2.1 Maxwell's equations

Maxwell's equations are a set of fundamental equations governing all macroscopic electromagnetic phenomena. The equations can be written in both differential and integral form, but here they are presented only in differential form, since they lead to differential equations to be dealt with by the finite element method.

For general time-varying fields, the familiar Maxwell's equations in differential form can be written as

$$\nabla \times \mathbf{E} + \frac{\partial \mathbf{B}}{\partial t} = 0 \qquad \text{(Faraday's law)} \qquad (2.3)$$

$$\nabla \times \mathbf{H} - \frac{\partial \mathbf{D}}{\partial t} = \mathbf{J} \qquad \text{(Maxwell-Ampere law)} \qquad (2.4)$$

$$\nabla \cdot \mathbf{D} = \rho \qquad \text{(Gauss's law)} \qquad (2.5)$$

$$\nabla \cdot \mathbf{B} = 0 \qquad \text{(Gauss's law-magnetic)} \qquad (2.6)$$

where

E = electric field intensity (volts/meter)

D = electric flux density (coulombs/ meter^2)

H = magnetic field intensity (amperes/meter)

B = magnetic flux density (webers/meter^2)

J = electric current density (amperes/meter^2)

ρ = electric charge density (coulombs/meter^3)

Another fundamental equation, which is known as the equation of continuity, can be written as

$$\nabla \cdot \mathbf{J} = -\frac{\partial \rho}{\partial t} \tag{2.7}$$

which specifies the conservation of charge.

The associated constitutive equations for the medium may be written as:

$$\mathbf{D} = \varepsilon \mathbf{E} \tag{2.8}$$

$$\mathbf{B} = \mu \mathbf{H} \tag{2.9}$$

where ε is the permittivity and μ is the permeability of the medium.

It is convenient to assume a complex time dependence through the factor $\exp(j\omega t)$, where j is the imaginary unit, ω is the radian (circular) frequency, and t denotes the time. With this assumed time variation, all time derivatives may be replaced by $j\omega$. We will not include the factor $\exp(j\omega t)$ explicitly as this factor always occurs as a common factor in all terms.

2.2.2 The Scalar Approximations

Several different variational formulations have been proposed for use (Koshiba *et al.*, 1982; Silvester, 1969; Mabaya, 1981) with the finite element method. The simplest one is scalar, given in terms of only one field component and this type of formulation has been used for solving optical waveguide problems. This formulation is valid only in situations where the modes can be described as being predominantly TE or TM and one form suitable for quasi-TE modes can be written as (Mabaya *et al.*, 1981) :

$$J(\phi) = \int_{\Omega} \left[\left\{ \frac{\partial \phi}{\partial x} \right\}^2 + \left\{ \frac{\partial \phi}{\partial y} \right\}^2 + \left\{ \beta^2 - k_o^2 n^2(x,y) \right\} \phi^2 \right] dx\, dy \qquad (2.10)$$

where β is the propagation constant, $n(x,y)$ is the refractive index profile and the integration is carried out over the waveguide cross-section domain, Ω. A finite element program based on this formulation can yield β^2 as the eigenvalue of the matrix equation for a given free-space wave number, k_o, and the eigenvector, $\phi(x,y)$ is the transverse field distribution which is the E_x field component for the quasi-TE modes. Similarly, the scalar variational formulation for the quasi-TM modes can be written as (Mabaya *et al.*, 1981) :

$$J(\psi) = \int_{\Omega} \frac{1}{n^2(x,y)} \left[\left\{ \frac{\partial \psi}{\partial x} \right\}^2 + \left\{ \frac{\partial \psi}{\partial y} \right\}^2 + \left\{ \beta^2 - k_o^2 n^2(x,y) \right\} \psi^2 \right] dx\, dy \qquad (2.11)$$

In this formulation $\psi(x,y)$ is the transverse field distribution, which is the H_x field component for the quasi-TM modes.

In the finite element approximation, the primary dependent variables are replaced by a system of discretized variables over the domain of consideration. To achieve this, the entire waveguide cross section is first divided into a patchwork of subregions or elements, usually triangles or quadrilaterals. Elements can have various shapes, such as triangles or rectangles, and they can also be of various sizes. Triangles are commonly used because they are easy to adapt to complex shapes. Using many elements, any cross-section with a complex boundary and with an arbitrary permittivity distribution can be accurately approximated. The simplest triangular element assumes a linear interpolation between the field values at the vertices of the triangle. Higher order interpolation polynomials are also used, with a larger number of nodal values which are unknowns of the problem in each element. By expressing the fields in terms of nodal values and with the assumed shape functions, the resulting field components are continuous over the whole domain.

To find these nodal fields, the usual (Rayleigh-Ritz) procedure is to force stationarity of the functional with respect to each nodal variable. This yields a matrix eigenvalue equation, with vector $\{\mathbf{x}\}$ of nodal field variables :

$$[A]\{\mathbf{x}\} - \lambda [B]\{\mathbf{x}\} = 0 \qquad (2.12)$$

where [A] and [B] are real symmetric matrices, and [B] is also positive definite. The eigenvalue λ may be k_o^2 or β^2 depending on the variational formulations. It should be emphasised that it is most desirable for the resulting matrix equation to be of this canonical form, to allow for an efficient and robust solution. This equation can be solved by one of various standard subroutines to obtain the different modal eigenvalues and associated eigenvectors.

2.2.3 The Vector formulations

The single scalar formulation is inadequate (except as an approximation) for the inherently hybrid mode situation of anisotropic or genuinely two dimensional, inhomogeneous optical waveguide problems. A vector formulation is necessary to represent accurately the general waveguide fields, of which there are at least two field components. However, as will be seen later, some vector formulations are affected by spurious or non-physical solutions which appear mixed with those which are correct in the computation.

One of the first vector formulations used for microwave and optical waveguides was in terms of the axial field components, E_z-H_z (Csendes and Silvester, 1970). This E_z-H_z formulation (Mabaya *et al.*, 1981; Yeh *et al.*, 1975; Vandenbulcke and Lagasse, 1976; Ikeuchi *et al.*, 1981) cannot treat general anisotropic problems without destroying the canonical form of equation (2.12). Also, for a waveguide with an arbitrary dielectric distribution, enforcing boundary conditions in this approach can be quite difficult. Another fundamental

disadvantage for optical waveguide problems is that this E_z-H_z formulation is based on axial field components which are the least important of the six components of the two vector **E** and **H** fields. For the H^y_{mn} mode, H^y is dominant but for the H^x_{mn} mode, H^x and E^y are dominant. Additionally, this formulation is also affected by spurious solutions, and techniques to reduce them (Mabaya *et al.*, 1981) can be at the expense of greatly increasing the computing cost.

In 1956, Berk (1956) presented a number of vector variational formulations in the form of Rayleigh quotients for loss-free anisotropic microwave waveguides and resonators in terms of the **H** field, the **E** field or a combination of both. Later, Morishita and Kumagai (1977) and Chen and Lien (1980) established general procedures to derive variational formulations for self-adjoint and non-self-adjoint operators.

A vector **E** formulation has been applied to analyze cylindrical waveguides (English and Young, 1971), optical fibers (Katz, 1982), and magnetically anisotropic waveguides used for the solution of a variety of optical (and microwave) waveguides. These formulations have attracted attention because they can be used to analyze general anisotropic but loss-less problems. The natural boundary conditions for the **E**-field formulation are equivalent to a magnetic wall and so an electric wall has to be specifically implemented (i.e. $\hat{n} \times E = 0$). It is because of this need to force electric boundary conditions, that the **E**-field formulation is extremely difficult to implement for irregular shaped waveguides.

However, the main problem is the enforcement of the field continuity across the dielectric interfaces.

When considering the **H**-field formulation, the natural boundary condition is that of an electric wall and so for the majority of electromagnetic problems it can be left free. However to force $\hat{n} \cdot H = 0$, on an arbitrary shaped waveguide is considerably easier than $\hat{n} \times H = 0$ where $\hat{n}$ is the unit vector normal to the boundary, and it can be specifically implemented to reduce the size of the matrices involved in the solution, and thus reduce the computational time. Another advantage of the **H**-field formulation is that for variations of the refractive index through the cross section of the waveguide there is no need to impose interface boundary conditions. The **H**-field formulation is more suited to dielectric waveguide problems where the magnetic field is continuous everywhere; furthermore, as the natural boundary condition corresponds to that of an electric wall boundary condition, there is no need to force the trial fields at conducting boundaries. This formulation can be written as (Berk, 1956; Rahman and Davies, 1984):

$$\omega^2 = \frac{\int (\nabla \times H)^* \cdot \hat{\varepsilon}^{-1} \cdot (\nabla \times H)\, d\Omega}{\int H^* \cdot \hat{\mu} \cdot H\, d\Omega} \tag{2.13}$$

Integration is carried over the waveguide cross-section, Ω, where an asterisk denotes complex conjugation and $\hat{\varepsilon}$ and $\hat{\mu}$ are respectively the

permittivity and permeability (which may be of arbitrary anisotropy) of the loss-free medium. Application of the Rayleigh-Ritz procedure to equation (2.13) leads to a similar eigenvalue problem as shown in equation (2.12), where now [A] is a complex Hermitian matrix which can be reduced to the real symmetric case by using a suitable transformation (Rahman and Davies, 1984a) for the loss-free condition, [B] is real symmetric and positive definite, and the eigenvectors $\{\mathbf{x}\}$ represent the unknown field components at the nodal points for different modes with ω^2 as their corresponding eigenvalues. Unfortunately, spurious solutions also appear in this formulation (as in the **E**-field formulation), but however, it will be seen later that these nonphysical modes can be avoided. In order to obtain a solution for a given wavelength, the β value has to be changed iteratively until the output eigenvalue corresponds to the correct wavelength.

The vector formulation has a disadvantage over the scalar formulation in that its matrix problem is larger than for the scalar approach. However, with this program, the use of the subspace iteration method (Bathe and Wilson, 1976) to solve the matrix problem makes this a less important issue.

Variational formulations in terms of the transverse **H**-field or **E**-field components have also been recently considered, including an implicit satisfaction of the divergence-free condition. These formulations use the minimum number of variables required and can completely eliminate spurious solutions but at the expense of the complexity of the matrix problem or the sparsity of the matrices

(Hayata *et al.*, 1986). In this case, the matrix order can be reduced to two thirds of what is needed in the full vector formulation but more work will be required in the future, particularly in the development of the formulations and in efficient matrix solution techniques (Fernandez and Lu, 1990) before this formulation becomes more popular.

The full 6-component **E** and **H** formulation (English, 1971a; Svedin, 1989) does not appear to have much advantage over the **H**-field or **E**-field formulation, since in this case, the degrees of freedom per node double. Apparent advantages reside in the simpler modelling of the basic equations, which allows the elimination of spurious modes, and this can be important when considering problems with special material properties.

2.3 Natural Boundary Conditions

The boundary condition which is automatically satisfied in the variational procedure is called the natural boundary condition. The advantage of the variational formulation is that the natural boundary condition can be automatically satisfied if left free. The functional defined in equation (2.10) has the continuity $\frac{\partial \phi}{\partial \hat{n}}$ as the natural boundary condition, whereas the functional in equation (2.11) has the continuity $\left[\left(\frac{1}{n^2}\right)\left(\frac{\partial \psi}{\partial \hat{n}}\right)\right]$ as the natural boundary condition where $\hat{n}$ is the outward unit normal vector. By contrast, the vector **H**-formulation given in equation (2.13) has the $\hat{n} \cdot H = 0$ (electric wall) as the natural boundary condition.

If necessary, if the natural boundary condition may also be enforced to reduce the matrix order, and even these boundary conditions are satisfied if automatically left free. However, in some cases, it may be necessary to change the unsuitable natural boundary condition by introducing an additional surface integral around the desired boundary. If symmetry of a waveguide exists, then the advantage of that should be taken by imposing that waveguide symmetry. However, it may be necessary to analyze the structure with complementary symmetry conditions to get all the modes, but exploitation of the symmetry greatly reduces the computational cost.

2.4 Finite Element Formulation

The finite element method is based on the following principle. The differential operator equations which describe the physical problem are replaced by an appropriate extremum functional J, which is the variational for the desired quantity and is written in Euler density form. The problem may be regarded as that of constructing a solution surface $H(x,y)$ over a specified region of the x-y plane, such as to satisfy the boundary conditions as well as the extremum requirement on J.

Most real problems are three dimensional. With certain assumptions, it is possible to approximate most of them as two-dimensional problems. For uniform waveguide problems an axial dependence in the form of $\exp(-j\beta z)$ is assumed and the transverse plane is considered for the further characterization.

2.5 Discretization of the problem

The use of the Finite element method starts with the subdivision of the region of physical interest into smaller regions called elements. There are a great many competing element shapes and it is not clear whether it is more efficient to subdivide the region into triangles or into quadrilaterals. Each element is essentially a simple unit within which the unknown can be prescribed in a simple manner. For the problem in hand, the continuum is separated by imaginary lines into a number of triangles, as shown in Fig. 2.2

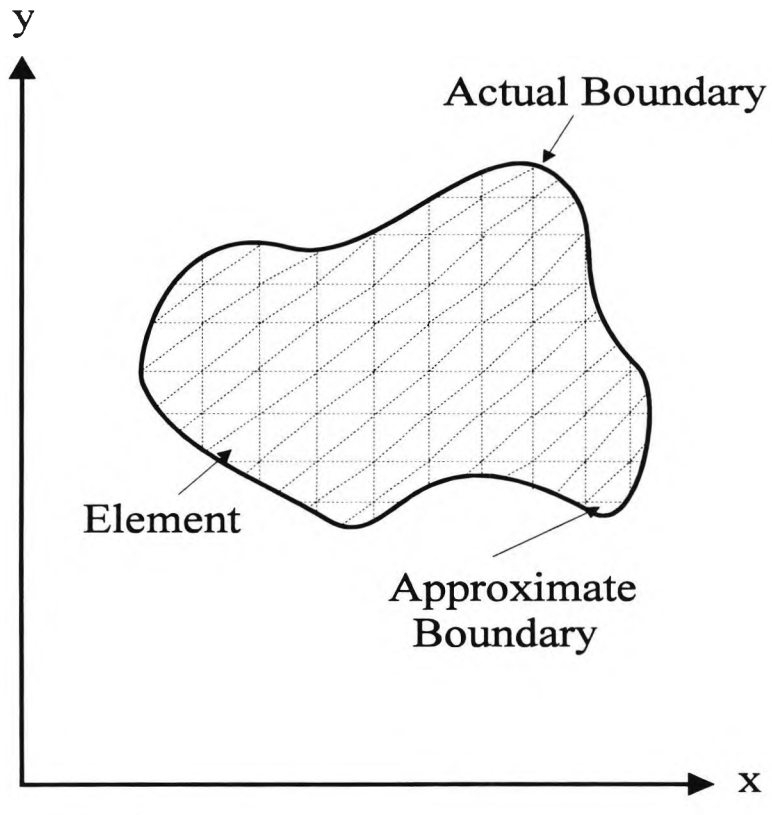

Fig. 2.2 Waveguide cross-section subdivided into finite elements.

A consequence of such a division is that the distribution of the unknown **H** is also discretized into corresponding subzones. The subdivided elements are now easier to examine, as compared to the entire body and the distribution of **H** over it.

In this scheme of grading, a number of vertices are generated and a set of field values is assigned to these vertices. The intersections of the sides of the elements are called nodes or nodal points, and the interfaces between the elements are called nodal lines. The elements are assumed to be interconnected at a discrete number of nodal points on their boundaries. The values of **H** at these nodal points will be the basic unknown parameters. In a two-dimensional problem, the triangular elements are better able to deal with curved or awkward boundaries. Owing to the flexibility of their size and shapes, the finite elements are able to represent a given domain more faithfully, however complex its shape may be. Problems with curved boundaries or surfaces have lead to the development of elements with curved edges or faces (Koshiba and Inoue, 1992; Miniowitz and Webb, 1991).

2.6 Shape Functions

Having decided on the discretization, the next choice is that of the representation of the element approximation, the shape functions, in terms of the variational parameters. The most common form of approximation in each element is the polynomial approximation. This is probably due to the fact that polynomials are relatively easily manipulated, both algebraically and computationally.

Polynomials are also attractive from the point of view of the Weierstass approximation theorem, which states that any continuous function may be approximated, arbitrarily closely, by a suitable polynomial. The chosen functions should possess continuity, of the type required by the variational basis of the formulation, within the element and across the element boundaries. Without this interelement continuity, the functions are not admissible for the variational formulation, and the energy over the domain cannot be found by adding the separate contributions from within each element.

Within the domain described by an element, the pattern or shape for the distribution of the unknown field quantity, **H**, is approximated by some complete set of polynomials called shape functions. The shape functions are chosen uniquely to define the field within each finite element under consideration and which are linearly dependent on the values of fields assigned to the vertices of the element. A number of mathematical functions such as polynomials and trigonometric functions can be used for this purpose. The polynomials are specially used because of the ease and simplification they provide in the finite element. In this method, the actual field over the entire domain may be approximated by a finite number of trial sets of algebraic functions which are uniquely defined and differentiated.

The solution needs to be independent of the orientation of the local coordinate system geometrically, and this requirement implies that the solution surface is permitted an equal complexity of curvature in any direction. In order to guarantee this solution isotropy, the polynomial expression applicable to each

subregion must be a complete polynomial ; that is, if the highest order term in it is x^N and y^N, and it must also contain all possible terms $x^m y^n$, $0 < m+n < N$ but no other terms. The polynomial will then contain, altogether, $M = (N+1)(N+2)/2$ terms. The necessary terms for all possible polynomials up to a complete quadratic are shown below in Fig. 2.3. This figure is effectively the Pascal triangle.

	degree of polynomial
1	*constant*
x y	*1 linear*
x^2 xy y^2	*2 quadratic*
x^3 x^2y xy^2 y^3	*3 cubic*
x^4 x^3y x^2y^2 xy^3 y^4	*4 quartic*

Fig. 2.3 Polynomial terms for complete polynomials in the two-dimensional analysis.

2.7 Representation of fields

The continuous field function $\phi(x,y)$ in the problem domain may be replaced by a set of discrete values (ϕ_p, p=1,2,3,...,m) where *m* is the total number of nodes. This function will be continuous across adjacent triangles, so that if the potential is interpreted like a third dimension, it can be viewed as a surface with many triangular facets. To be admissible functions, they must satisfy some specific conditions between the elements; usually the continuity of the field across the boundaries is preferred.

Inside each first order triangle and between the discrete nodes, ϕ is interpolated continuously. This can be achieved by introducing the "nodal shape functions", $N_i(x,y)$. The field inside an element, $\phi_e(x,y)$ when m = 3, can be written as

$$\phi_e(x,y) = \sum_{i=1}^{3} N_i(x,y) \cdot \phi_i \tag{2.14}$$

where ϕ_i are the nodal field values. Equation (2.14) can be written in the matrix notation as,

$$\phi_e(x,y) = \begin{bmatrix} N_1 & N_2 & N_3 \end{bmatrix} \begin{Bmatrix} \phi_1 \\ \phi_2 \\ \phi_3 \end{Bmatrix} \tag{2.15}$$

$$\phi_e(x,y) = [N] \{\phi_e\} \tag{2.16}$$

where the row vector $[N]$ is called the shape function matrix and the column vector $\{\phi_e\}$ is the vector corresponding to nodal field values of the element. The simplest use of triangular elements is by *first order* elements, where a first-degree polynomial ($a + bx + cy$) is used over each element. It can be shown that element shape function $\{N\} \equiv [N]^T$ can be written as (Reddy, 1993)

$$[N]^T = \begin{bmatrix} N_1 \\ N_2 \\ N_3 \end{bmatrix} = \frac{1}{2A_e} \begin{bmatrix} x_2y_3 - x_3y_2 & y_2 - y_3 & x_3 - x_2 \\ x_3y_1 - x_1y_3 & y_3 - y_1 & x_1 - x_3 \\ x_1y_2 - x_2y_1 & y_1 - y_2 & x_2 - x_1 \end{bmatrix} \begin{bmatrix} 1 \\ x \\ y \end{bmatrix} \tag{2.17}$$

where T denotes a transpose, A_e the area of the triangle and x_1, x_2, x_3, y_1, y_2, and y_3 are the x, y coordinates of the three nodes respectively. $[N]^T$ can also be written as

$$[N]^T = \begin{bmatrix} N_1 \\ N_2 \\ N_3 \end{bmatrix} = \begin{bmatrix} a_1 & b_1 x & c_1 y \\ a_2 & b_2 x & c_2 y \\ a_3 & b_3 x & c_3 y \end{bmatrix} \tag{2.18}$$

By comparing equation (2.17) and (2.18) the coefficients a_i, b_i and c_i are calculated as

$$a_1 = \frac{x_2 y_3 - x_3 y_2}{2A_e} \tag{2.19}$$

$$b_1 = \frac{y_2 - y_3}{2A_e} \tag{2.20}$$

and

$$c_1 = \frac{x_3 - x_2}{2A_e} \tag{2.21}$$

Similarly a_2, b_2, c_2, a_3, b_3, and c_3 can be calculated by cyclic exchange of $1 \rightarrow 2 \rightarrow 3$ in equations (2.19) to equation (2.21).

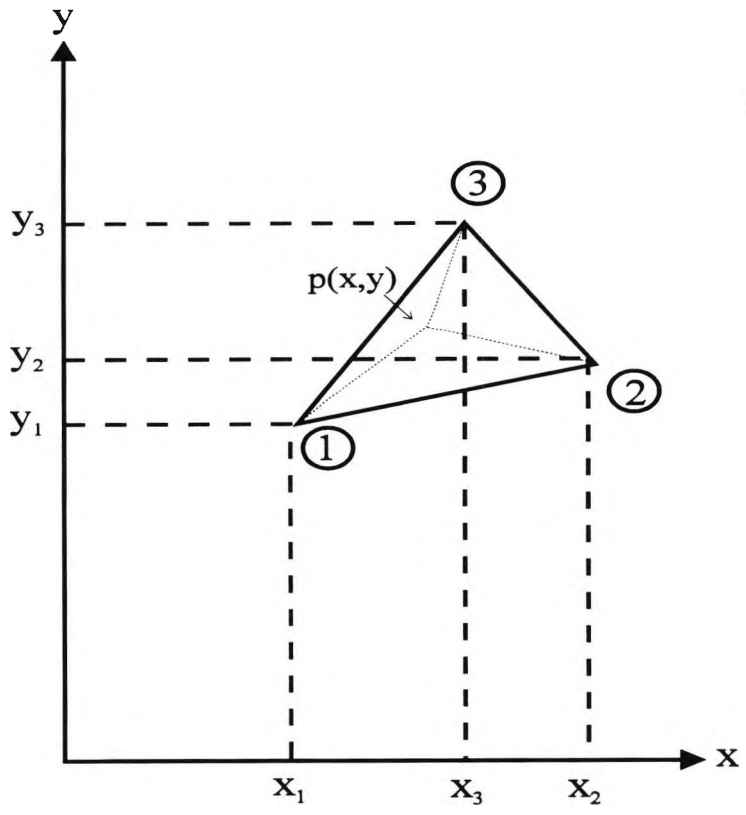

Fig. 2.4 This figure shows coordinates and node numbers of a typical first order three-noded triangular element.

The typical point P somewhere in the triangle of Fig. 2.4 with vertices 1,2 and 3 can be considered, and thus N_i can also be denoted by

$$N_1 = \frac{area\ of\ the\ triangle\ P12}{area\ of\ the\ triangle\ 123} \tag{2.22}$$

Similarly N_2 and N_3 can be defined. It immediately follows from the area definition that

$$N_1 + N_2 + N_3 = 1 \tag{2.23}$$

2.8 Infinite Elements

In this section, the implementation of so-called infinite elements is described. The field extends up to infinity for open-type problems where this is particularly important for the solution close to cutoff. In this case, the field decays slowly and the region of significant field value is considerably bigger. In orthodox finite element discretization, the region of consideration cannot extend up to infinity, yet in many of the waveguide problems, the problem domain extends up to infinity. Rahman (1984a) has developed the infinite element approach, which is found to be very useful to extend the effective region of interest up to infinity, as shown in Fig. 2.5. However, the use of the infinite element will extend the domain up to infinity with the shape functions decaying exponentially. For open types of structures, a small number of infinite elements need to be added starting from the end of the regular element boundaries. One "free" parameter, the decaying shape function parameters for the fields needs to be assumed and contributions to the functional are calculated from these infinite elements in a separate subroutine and added with the original global matrices. This is done by assigning a value to an integer through BLOCK DATA which can switch this subroutine ON or OFF according to the requirements. Simple shape functions were used to develop the formulation for isotropic materials. Assumptions were made using the linear field variation for the finite dimensional side, and on the other side, the field decaying exponentially. Similar assumptions lead to the development of two dimensional infinite elements, suitable for use at the corners.

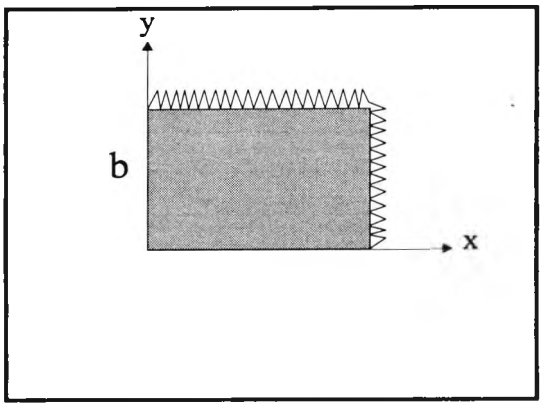

Fig. 2.5 Infinite strip

Suppose the infinite element extends toward the positive x direction up to infinity (shown in Fig. 2.6), then, any field component, such as H_x, can be written as

$$\begin{aligned} H_x &= f(x,y)H_{x_i} \\ &= \sum_{1}^{2} N_i H_{x_i} \end{aligned} \tag{2.24}$$

where H_{x_1} and H_{x_2} are the x-components of the magnetic field at nodes 1 and 2 respectively.

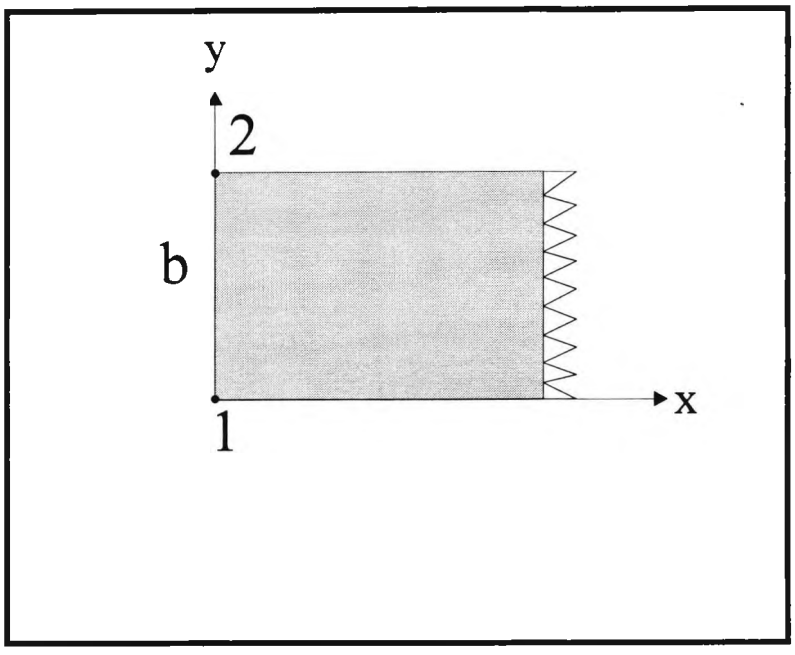

Fig. 2.6 Two dimensional strips that one dimension extend up to infinity.

For the simplest case, this can be written as

$$H_x = (a_1 + b_1 y)e^{(-x/L)}H_{x_1} + (a_2 + b_2 y)e^{(-x/L)}H_{x_2} \tag{2.25}$$

where L is the free parameter related to the field decay and a_1, a_2, b_1, and b_2 can be evaluated in terms of the finite width of the infinite element, then

$$\begin{aligned} H_x &= \frac{y}{b}e^{(-x/L)}H_{x_1} + \left(1 - \frac{y}{b}\right)e^{(-x/L)}H_{x_2} \\ &= [N_1, \quad N_2]\{H_{x_1}, \quad H_{x_2}\} \end{aligned} \tag{2.26}$$

where b is the width of infinite strip and

$$N_1 = \frac{y}{b}e^{(-x/L)} \tag{2.27}$$

$$N_2 = \left(1 - \frac{y}{b}\right) e^{(-x/L)} \tag{2.28}$$

H_y and H_z can be expressed in a similar way, and thus the vector field **H** can be described by

$$H = \begin{Bmatrix} H_x \\ H_y \\ H_z \end{Bmatrix} = \begin{bmatrix} N_1 & 0 & 0 & N_2 & 0 & 0 \\ 0 & N_1 & 0 & 0 & N_2 & 0 \\ 0 & 0 & N_1 & 0 & 0 & N_2 \end{bmatrix} \begin{Bmatrix} H_{x_1} \\ H_{y_1} \\ H_{z_1} \\ H_{x_2} \\ H_{y_2} \\ H_{z_2} \end{Bmatrix} \tag{2.29}$$

$$= [N]\{H\}$$

Using these shape functions, the denominator of equation (2.13) can be evaluated as

$$\begin{aligned} \int_{\Delta} \{H\}^*[N]^* \mu [N]\{H\} ds &= \{H\}^* \int_{\Delta} [N]^* \mu [N] ds \{H\} \\ &= \{H\}^* [B_e] \{H\} \end{aligned} \tag{2.30}$$

Components of the $[B_e]$ matrix can be evaluated, as discussed in Appendix 1.

Similarly the numerator of the equation (2.13) can also be calculated as follows:

$$\int_{\Delta} \{H\}^* [\nabla \times [N]]^* \varepsilon^{-1} [\nabla \times [N]] \{H\} ds = \{H\}^* [A_e] \{H\} \tag{2.31}$$

and this is also shown in Appendix 1.

The infinite elements extending in the y direction, or in two dimensions can be solved by using this technique.

2.9 Element and Global Matrices

For any one triangular element, the functional, J^e can be calculated and the total functional, J, associated with the assemblage of many elements is, in general, the sum of all the individual elements

$$J = \sum_{1}^{m} J^e \tag{2.32}$$

$$\begin{aligned} &= \left[\sum_{e=1}^{m} \int_{\Delta} \{\phi_e\}^T \left(\frac{\partial \{N\}}{\partial x} \cdot \frac{\partial [N]}{\partial x} + \frac{\partial \{N\}}{\partial y} \cdot \frac{\partial [N]}{\partial y} \right) dxdy \right] \{\phi_e\} \\ &+ \left[\sum_{e=1}^{m} \int_{\Delta} \{\phi_e\}^T \left(\beta^2 \{N\}[N] - k_o^2 n_e \{N\}[N] \right) dxdy \right] \{\phi_e\} \end{aligned} \tag{2.33}$$

where m is the number of the element, and $\int_{\Delta}$ represents integration carried over each element.

The spatial derivative matrices [X] and [Y] can also be written in matrix form as

$$\frac{\partial [N]}{\partial x} = \begin{bmatrix} b_1 & b_2 & b_3 \end{bmatrix} = [X] \tag{2.34}$$

$$\frac{\partial [N]}{\partial y} = \begin{bmatrix} c_1 & c_2 & c_3 \end{bmatrix} = [Y] \tag{2.35}$$

where b_i and c_i are constant values only depending on the coordinate values of the three nodes for a given element, which are given by the equations (2.20) and (2.21)

The integration required in Equation (2.33) can be easily carried out by using the following relation for a triangular element

$$\int_{\Delta} N_1^i N_2^j N_3^k \, d\Omega = \frac{i!\, j!\, k!\, 2!}{(i+j+k+2)!} A_e \tag{2.36}$$

After carrying out the integration, equation (2.33) can be written as

$$J = \{\phi_e\}^T [A]\{\phi_e\} - \lambda \{\phi_e\}^T [B]\{\phi_e\} \tag{2.37}$$

where the eigenvalue $\lambda = \beta^2$ and the [A] and [B] matrices, for the scalar formulation (2.10) are given by

$$A = \sum_{1}^{m} \int_{\Delta} \left[\{X\}[X] + \{Y\}[Y] - k_0^2 n^2 \{N\}[N] \right] d\Omega \tag{2.38}$$

and

$$B = \sum_{1}^{m} \int_{\Delta} \{N\}[N] \, d\Omega \tag{2.39}$$

where {X} and {Y} are the transposed column matrix of [X] and [Y] respectively. Since the energy expression of equation (2.38) is quadratic in nodal potentials, $\{\phi_e\}$, to minimise the energy functional, it is sufficient to set

$$\frac{\partial J}{\partial \{\phi_p\}} = 0 \tag{2.40}$$

Following the minimization, the standard eigenvalue equation may be obtained as shown in equation (2.12).

The vector formulation can be similarly derived, except that instead of one unknown potential per node there are three unknown field components given by H_x, H_y and H_z. Over each element, the three components of the magnetic field can be written in the matrix form as

$$\left.\begin{aligned} H_x(x,y) &= [N]\left\{H_e^x\right\} \\ H_y(x,y) &= [N]\left\{H_e^y\right\} \\ H_z(x,y) &= [N]\left\{H_e^z\right\} \end{aligned}\right\} \tag{2.41}$$

where $\left\{H_e^x\right\}$, $\left\{H_e^y\right\}$, and $\left\{H_e^z\right\}$ are the three nodal field vectors of an element representing the x, y, and z component of the magnetic field. The full vector magnetic field over an element can be written as

$$\left\{\boldsymbol{H}_e\right\} = \begin{Bmatrix} \hat{x}\left\{H_e^x\right\} \\ \hat{y}\left\{H_e^y\right\} \\ \hat{z}\left\{H_e^z\right\} \end{Bmatrix} \tag{2.42}$$

where $\hat{x}$, $\hat{y}$, $\hat{z}$ are the unit vectors in the x, y and z directions.

The application of the standard finite element techniques to find the stationary condition to the vector **H**-formulation given in equation (2.13) will yield the same generalized eigenvalue equation as shown in equation (2.12). However, for this vector formulation matrix [A] will be a complex Hermitian matrix and [B] will be a real symmetric positive definite matrix.

2.10 Matrix generation

As mentioned earlier, the denominator of the equation (2.13), can be represented by matrix [B], as shown below.

$$[B] = \int_{\Delta} H^{*} \hat{\mu} H \, d\Omega \tag{2.43}$$

where Δ shows integration over a given triangle.

However, from equation (2.41)

$$\left.\begin{aligned} [B] &= \int_{\Delta} (\{H\}[N])^{*} \hat{\mu} ([N]\{H\}) \, d\Omega \\ [B] &= \{H\}^{*} \mu \int_{\Delta} [N]^{*}[N] \, d\Omega \, \{H\} \end{aligned}\right\} \tag{2.44}$$

where {H} is a column vector.

By considering μ as scalar, the $[B_e]$ element matrix can be defined as

$$[B_e] = \int_{\Delta} [N]^{*}[N] \, d\Omega \tag{2.45}$$

From equation (2.44) the 9×9 $[B_e]$ matrix can be calculated and so, for example,

$$B_{e_{ij}} = \mu \int_{\Delta} i_{th} \; row \; of \; N^{*}, \; j_{th} \; column \; of \; N \, d\Omega \tag{2.46}$$

The generation of the element matrices are shown in Appendix 2.

In this way all the components of the element matrix, $[B_e]$, can be calculated. The numerator of equation (2.13) can be written by the [A] matrix and

1. If ε is isotropic, then it is scalar and it can be taken outside the integral.
2. If ε is a tensor, then it is represented by 3×3 matrix and ε^{-1} is also a 3×3 matrix.

If it is assumed it is isotropic, then ε is a scalar, and it can be taken out of the integration.

$$[A] = \varepsilon^{-1} \int_{\Delta} (\nabla \times [N]\{H\})^{*} \cdot (\nabla \times [N]\{H\})\, d\Omega \tag{2.47}$$

then

$$[A] = \frac{1}{\varepsilon} \int_{\Delta} \left(\{[\mathrm{Q}] \cdot [H]\}^{*} [Q][H] \right) d\Omega \tag{2.48}$$

where

$$[Q] = \begin{vmatrix} 0 & -\frac{\partial}{\partial z} & \frac{\partial}{\partial y} \\ -\frac{\partial}{\partial z} & 0 & -\frac{\partial}{\partial x} \\ -\frac{\partial}{\partial y} & \frac{\partial}{\partial x} & 0 \end{vmatrix} [N] \tag{2.49}$$

$$[A_e] = \frac{1}{\hat{\varepsilon}} \int_{\Delta} [Q]^{*} [Q]\, d\Omega \tag{2.50}$$

From equation (2.50) the A_e element matrices can be calculated. All the elements of the matrix are assembled to form a global matrix $[A_e]$ and $[B_e]$ in order to generate the eigenvalue problem. The most important parameter for the Global matrix is the sparsity, which is related to the number of non-zero elements. In solving waveguide problems by finite elements, the key factor affecting storage

requirements and the computational effort is the choice of algorithm to solve the matrix equation.

2.11 Spurious solutions

A problem associated with the vector formulation of the finite element method is the presence of *spurious solutions* that arise along with the desirable physical solutions.

To eliminate these spurious solutions, the penalty function has been utilised, a method which has been successful (Rahman and Davies, 1984b) in eliminating these solutions previously resulting in problems associated with microwaves and optical waveguides.

The first stage in the elimination is the identification of solutions being either real solutions or spurious. This is achieved using the principle that for a real solution, its eigenvector should satisfy **divH = 0**. Thus, in essence, **divH** is calculated over the guide cross-section. The nature of **divH** variations for different eigenvectors are then examined and only those solutions are considered which have a low value of **divH**. Now since only the eigenvectors with low divergence are checked, a real solution can readily be identified among the spurious.

To implement this logic as the penalty function method, an integral is added to the functional (equation 2.13) which satisfies **divH = 0**. Thus the divergence-free constant is imposed by the using the penalty technique, and it can be written in the new expression for the functional

$$\omega^2 = \frac{\int_{\Delta} (\nabla \times H)^* \, \hat{\varepsilon}^{-1} \, (\nabla \times H) \, d\Omega + \left(\frac{\alpha}{\hat{\varepsilon}_0}\right) \int (\nabla \cdot H)^* \cdot (\nabla \cdot H) \, d\Omega}{\int_{\Delta} H^* \, \hat{\mu} \, H \, d\Omega} \qquad (2.51)$$

This method is comparable to the classical addition of an integral which changes the natural boundary conditions. The penalty function method thus reduces the spurious solutions, and it has been shown (Rahman and Davies, 1984b) to improve the quality of the field eigenvectors.

A separate subroutine can be introduced to implement the penalty function method and which adds the contributions from the second term of the numerator (2.51), when it is necessary to reduce the spurious solutions and improve the eigenvectors. It can be noted that this applies only to the vector solutions and not to the scalar approximations because they satisfy $\nabla \cdot H = 0$ condition.

Mabaya, Lagasse and Vandenbulcke presented an approximate scalar finite-element formulation for the analysis of the isotropic optical waveguide (Mabaya *et al.*, 1981). This approach has as main advantages the smaller matrix dimensions, the requirement for less computer time, the presence of no spurious modes and the capability of easily computing higher-order modes. Spurious modes do not occur with the scalar approximation, and when appropriate this can be used to flush out spurious modes from the vector formulation, but much effort has gone into their proper removal from the accurate approaches over the last 8 years (Rahman *et al.*, 1991). Davies presented two ways of properly avoiding spurious modes (Davies, 1993). One is the use of a new vector formulation in terms of the transverse

magnetic field, H_t. It solves the difficulty by a new formulation with no need for special new finite elements. It follows that these spurious solutions will no longer appear if the basis functions are chosen to be divergence-free. This leads to the second which is the use of the original variational form of (2.13) but applying a more appropriate choice of basis vector functions from the armoury of finite elements. This is done by taking advantage of the recent introduction of "edge elements" (Bossavit and Mayergoyz, 1989). This method uses established formulations but with new finite elements some form of vector finite elements.

2.12 Summary

This chapter has considered the history and formulation of the finite element method. Various aspects of the use of the method have been considered, including the natural boundary conditions, the discretization of the problem, the shape function, and the representation of fields. The infinite element was also considered for open-type problems where the field extends up to infinity, and then the use of method to eliminate the spurious solutions that arise along with the desirable physical solutions was discussed. This lays the basis for the work described in subsequent Chapters on the use of the method to solve the problems defined in later chapters, forming the core of this thesis, starting with the implementation of the finite element method and consideration of the power transfer in the next Chapter.

Chapter 3

Implementation of the Finite Element Method and the Power Transfer Efficiency

3.1 Introduction

In Chapter 2, the formulation and general theory of the finite element method has been presented. The prime objective in this chapter is to discuss some important computational aspects related to the implementation of the finite element analysis. Here, briefly, the technique to obtain solutions of the eigenvalue problems will be mentioned.

Since the nature of the finite element method has been described previously, here only the *implementation* of the finite element method will be discussed. In general, using many elements, any continuum with a complex boundary and with an arbitrary index distribution can be approximated to such a degree that an accurate analysis can be carried out, even though the execution of the programme will require a large amount of computational time when the number of elements used is increased. The time to prepare the input data and to interpret

the results will be discussed, as will the steps involved to obtain the results in the next section.

3.2 Flow Chart

The steps involved in the use of the finite element method are expressed in the flow chart given in Fig. 3.1. The required data for the implementation of the finite element method is entered through a data file. For example, the x and y coordinates of all the nodes and the relationship between the node identifiers and node numbers for all elements has to be defined and entered for an arbitrary two dimensional problem.

The required time for the preparation of these data should be considered, and to minimize the volume for these input data, it is necessary to develop problem-dependent mesh generators. In this semi-automatic approach, the problem domain is divided into a few large zones and the fineness of element subdivisions within each is specified. The initial input data about the large zones and refinements required are given as an input in the normal way in **BLOCK DATA** form, and the subdivisions are processed automatically. Alternatively, they can be input as "*parameters*" or can be read from a data file. For a particular problem, the nonidentical directional coupler waveguide, the input data are shown along with the structure in Fig. 3.2

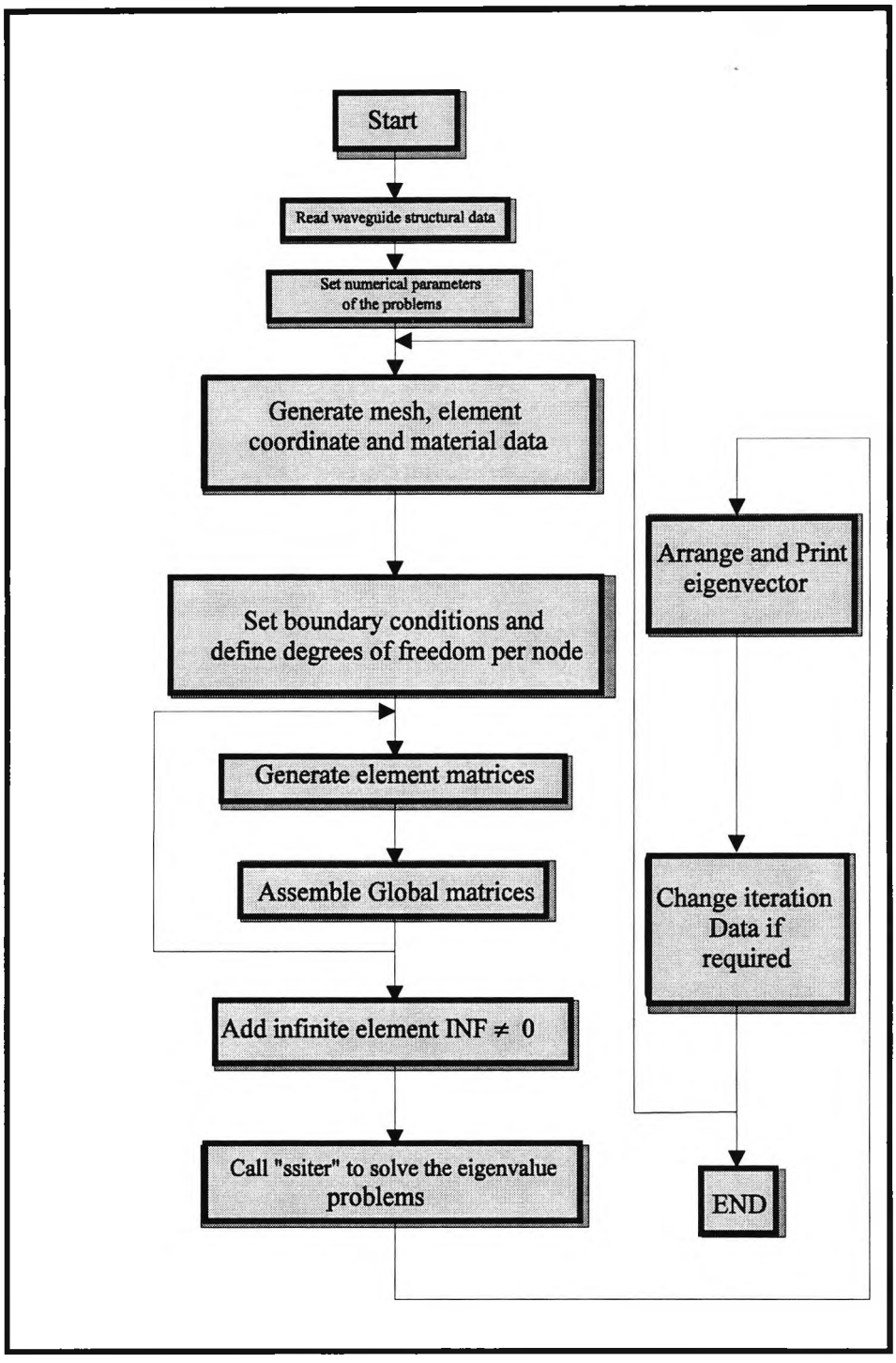

Fig. 3.1 Flow chart for the implementation of the finite element method.

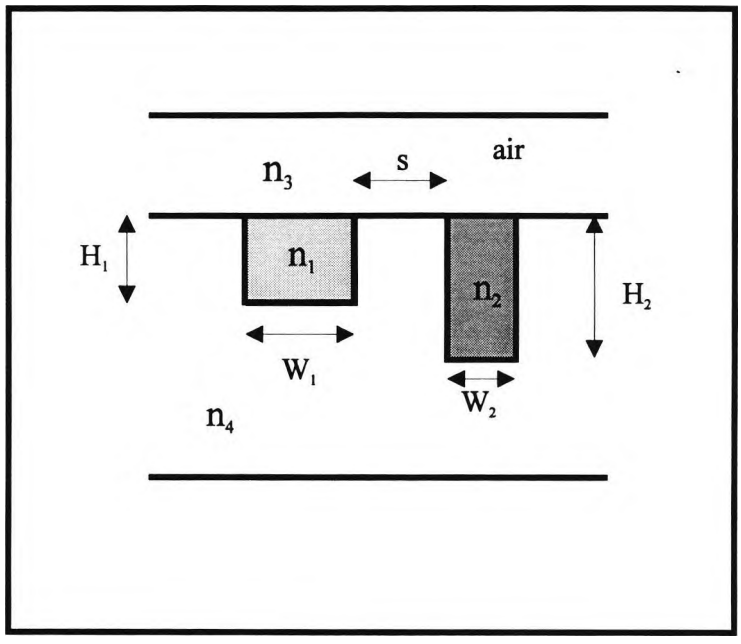

Fig. 3.2 Input data for a nonidentical directional coupler

Once the geometry of the structure has been defined, it is necessary to specify the boundary conditions. When the required boundary condition is same as the natural boundary condition of the variational formulation, then it can be left free. Since forcing of the boundary conditions reduces the size of the matrices, for regular or semi-regular structures, it is advantageous to implement it. The implementation of the boundary conditions also reduces the size of the matrices, and however, also to reduce the required storage, these boundary conditions are applied at the time of assembling the global matrices, resulting in only the reduced matrices being assembled.

For problems with one-fold symmetry, only half of the region of interest need to be considered. Similarly for problems with two fold symmetry, only one

quarter of the problem need be taken into account. So in problems with two-fold symmetry, for the same mesh sizes, the matrix orders are reduced to one-fourth. However, one obvious drawback for this exploitation of symmetry is that the given waveguide must be solved four times for different possible **ODD/EVEN** symmetric combinations, if all the modes are required. However, by considering the direct matrix eigenvalue solution, as the matrix order is one-fourth of the original system, so its associated computational time is only one-sixty-fourth. Although the problem may need to be solved four times, however, the overall savings could be considerable.

It is also necessary to specify the degrees of freedom associated with each node. For the vector formulation, each node has three degrees of freedom, namely H_x, H_y, and H_z, the x, y and z components of **H** field, respectively. The degrees of freedom can be different for different formulations. For the solution of a new problem, initially it may be useful to attempt a solution by using an approximate scalar formulation. This is because the scalar formulation is free from spurious solutions and it requires a smaller computer time. In this scalar run "rough" eigenvalues for different modes can be found and these values can be used to choose an optimum "*input beta*" for subsequent runs using vector formulations. The present computer program can consider both the vector and scalar formulations and a particular formulation can be selected by giving different values to an integer variable.

3.3 Output arrangements for Finite Element Method

The output of any solution should be checked properly, this being particularly important in the vector formulation, as the physical and spurious solutions can be intermixed, and because of the presence of the spurious solutions, eigenvectors along with their eigenvalues should be printed. However, a contour plot of the H_x, H_y, and H_z fields, the variation of the fields and power contours can be obtained by using a simple semi-automatic mesh generation program (or "*APPLE*" software package)

In this thesis, the least squares boundary residual (LSBR) method has been used along with the vector finite element method to analyse the power transfer from a single waveguide section to a guided wave section. The vector **H**-field finite element method is capable of providing accurate eigenvalues and eigenvectors for a wide range of optical waveguide problems including those of arbitrary shape, arbitrary index distribution, and using anisotropic materials. The least squares boundary residual method matches the continuity of the tangential electric and magnetic fields in the least squares sense by including many modes at the discontinuity plane, to yield the general scattering matrix.

In the next section, a brief account of the principles of the least squares boundary residual method will be given. The use of the LSBR method along with the vector finite element method is discussed and the results of its application to a

series of relevant problems are presented in Chapters 5 to 9. A final discussion follows in Chapter 10.

3.4 Least Squares Boundary Residual (LSBR) Method

Discontinuity problems in optical waveguide devices are of considerable theoretical and practical interest. They play an important role in designing practical devices such as an isolated abrupt step discontinuity as in butt joints or as finite cascade sections such as gratings, tapers, bendings, or y-junctions. The problem considered here is an abrupt discontinuity, in the transverse plane, at $z = 0$, between two arbitrarily shaped uniform waveguides. Each guide can have a scalar or tensor permittivity that varies arbitrarily in the two transverse directions, and an incident wave is presumed in respect of one mode.

3.4.1 Basic theory of the Least Squares Boundary Residual method.

The Least Squares Boundary Residual method was introduced as an alternative to point-matching (and Galerkin) methods, satisfying the boundary conditions in the usual least-squares sense over the discontinuity interface. The method is rigorously convergent, the error minimization being global rather than sampled, and has the flexibility of introducing an electric/magnetic weighting factor.

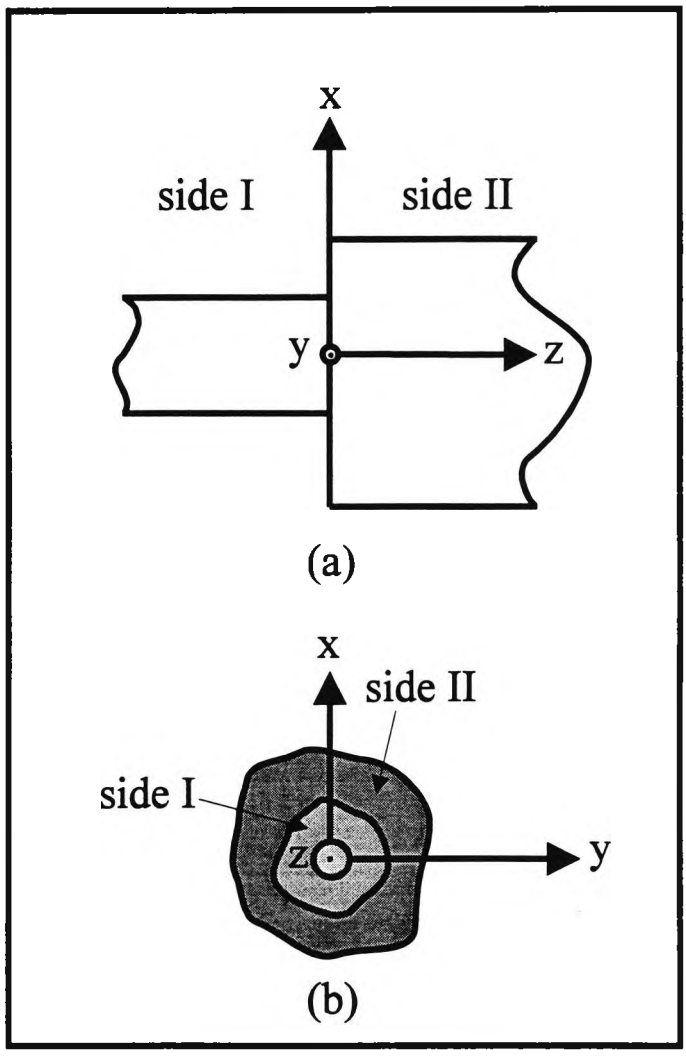

Fig. 3.3 Discontinuity at the junction of two dielectric waveguides. (a) Vertical section of the discontinuity between sides **I** and **II**. (b) Transverse cross section of the discontinuity at the junction of two sides.

The incoming wave incident on the discontinuous junction between dielectric waveguides **I** and **II** as shown in Fig. 3.3 is partly reflected, partly transmitted, and the rest radiated. Let E_t^i and H_t^i be the transverse components of the electric and magnetic fields of the incident wave, respectively. Some of the incident wave is reflected into side **I**. Besides, there will be many modes generated at the discontinuity plane to satisfy the boundary conditions. These can be guided

or radiated modes in sides **I** and **II**. The transverse components of the total electromagnetic fields E_t^I and H_t^I in side **I** and E_t^{II} and H_t^{II} in side **II** at the discontinuity plane *(z = 0)* can be expressed in terms of the eigenmodes of side **I** and side **II**, respectively, as follows:

$$E_t^I = E_t^i + \sum_{i=1}^{\infty} a_i E_{ti}^I \tag{3.1a}$$

$$H_t^I = H_t^i - \sum_{i=1}^{\infty} a_i H_{ti}^I \tag{3.1b}$$

$$E_t^{II} = \sum_{i=1}^{\infty} b_i E_{ti}^{II} \tag{3.1c}$$

$$H_t^{II} = \sum_{i=1}^{\infty} b_i H_{ti}^{II} \tag{3.1d}$$

where a_i are the amplitudes of the *ith* modes reflected from the junction with E_{ti}^I, H_{ti}^I transverse modal field components in side **I**. Similarly b_i are the amplitudes of the *ith* modes transmitted in side **II** with E_{ti}^{II}, H_{ti}^{II} transverse modal field components. Many modes are generated to satisfy the boundary conditions at the discontinuity plane and they may be propagating, radiating, or evanescent.

The LSBR method enables the calculation of a stationary solution to satisfy the continuity conditions of the tangential fields in a least squares sense by minimizing the error functional, J, given by

$$J = \int \left| E_t^I - E_t^{II} \right|^2 + \alpha \cdot Z_0^2 \left| H_t^I - H_t^{II} \right|^2 d\Omega \qquad (3.2)$$

where Z_0 is the free-space wave impedance and α is a dimensionless weighting factor. To obtain the approximate numerical solution to the problem, the infinite series expansions of equations (3.1) and (3.2) are truncated, including all the relevant propagating modes plus as many radiating and/or evanescent modes as is convenient. The minimum criterion of (3.2) reduces to the following linear equation :

$$Cx = v \qquad (3.3)$$

where C is square matrix generated from the eigenvectors and v is an array due to the incident mode. Vector $\{x\}$ is made up of all the unknown modal amplitudes. The elements of C and v are given by

$$C_{ij} = \left\langle E_{ti}, E_{tj} \right\rangle + \alpha Z^2 \left\langle H_{ti}, H_{tj} \right\rangle \qquad (3.4a)$$

$$v_i = \left\langle E_t^i, E_{ti} \right\rangle + \alpha Z^2 \left\langle H_t^i, H_{ti} \right\rangle \qquad (3.4b)$$

where $i,j = 1,...,N$ and N is the total number of modes in sides **I** and **II** and the vectors E_t and H_t are made up of all the corresponding modal fields in both sides.

Inner products involved in the above expressions are defined as

$$\left\langle x_1, x_2 \right\rangle = \int x_1 \cdot x_2^* \, ds \qquad (3.5)$$

where x_1 and x_2 are two field vectors, x_2^* is the complex conjugate of x_2 and integration is over the guide cross-section. The solution of equation (3.3) gives in $\{x\}$ the required approximate coefficients of a_i and b_i. These constitute one column of the scattering matrix, corresponding to the chosen incident mode.

3.4.2 Numerical Analysis

Nodal values of the complete **H** field for each mode for both the guides are obtained using the FE program. The **E** field over each element can be calculated from these nodal **H** fields by using Maxwell's equations. Many modal eigenvalues and eigenvectors for both sides of the discontinuity plane can be used as the input to the LSBR program. These eigenvalues and eigenvectors are generated by the vector FEM program. The LSBR program calculates the integral J and minimizes the error criterion (3.2) with respect to each value of a_i and b_i for any given incidence, by solving a homogeneous linear equation (3.3). Such a solution will give the unknown column vector $\{x\}$ consisting of the unknown reflected and transmitted coefficients of all the modes considered in the analysis. The singular value decomposition algorithm was used to solve the linear equation (3.3). For numerical efficiency, the FE nodal points in side **I** are matched with the nodal points of side **II** across the transverse plane at the interface. There is no need of extrapolation to find J as these points can be computed over each triangular element and summed over all the elements over $\sum \int_{\Delta} J_e$. Also there is no need to

generate nodal **E** fields, as nodal **H** field values can be used directly to calculate the electric field part of the integral, J, in equation (3.2).

This is the outline of the least squares boundary residual technique which is applied the work discussed in Chapter 5 to treat the discontinuity problem in directional coupler design and evaluation.

3.5 The Propagation Model

The beam propagation simulations based on the finite element method applied for the transverse domain and the use of unconditionally stable Crank-Nicholson scheme along the axial direction were also undertaken to check the results of the Least Squares Boundary method and the coupled mode approaches.

The time-dependent wave equation for pulse propagation in a nonlinear waveguide is given by (Adachihara *et al*,1990):

$$\frac{\partial^2 E}{\partial z^2} + 2jk_0\beta\left[\frac{\partial E}{\partial z} + \frac{n_i}{\beta v_i}\frac{\partial E}{\partial t}\right] + \frac{\partial^2 E}{\partial x^2} - D_p\frac{\partial^2 E}{\partial t^2} - k_0^2\left[\beta^2 - \left(n_i^2 + \delta\right)\right]E = 0 \tag{3.6}$$

where k_0 is the wavenumber of the field in the vacuum, β is the effective index, v_i is the group velocity of the field in medium i, D_p is the group velocity dispersion and δ is the total nonlinear contribution to the refractive index. Ignoring group velocity dispersion for the propagation distances under consideration and

applying the slowly varying envelope approximation to equation (3.6) leads to the time-dependent paraxial wave equation:

$$2jk_0\beta\left[\frac{\partial E}{\partial z}+\frac{n_i}{\beta v_i}\frac{\partial E}{\partial t}\right]+\frac{\partial^2 E}{\partial x^2}-k_0^2\left[\beta^2-\left(n_i^2\right)\right]E=0 \qquad (3.7)$$

The numerical simulations are carried out on the paraxial wave equation (3.7) by a combination of the finite element/Crank-Nicolson method (Hermansson *et al.*, 1990; Hayata *et al.*, 1990) and a characteristic scheme similar to that of Adachihara *et al.* (Shi and Chi, 1991; Mitchell and Moloney, 1990; Adachihara *et al.*, 1990) equation (3.7) can be expressed symbolically in the form

$$\left[\frac{\partial E}{\partial z}+\frac{n_i}{\beta v_i}\frac{\partial E}{\partial t}\right]=(L)E \qquad (3.8)$$

where L is the second-order diffraction. The total derivative on the left side of equation (3.8) is expressed in terms of a directional derivative in the (z,t) plane and integrations in the plane are taken from (z_j,t_n) to (z_{j+1},t_{n+1}). In the spirit of the split-operator technique (Hayata *et al.*, 1990) the right hand side of equation (3.8) is split into the linear and nonlinear parts solving them separately and combining the results. The linear part of equation (3.8) is first discretized using the standard Galerkin/finite-element method for the transverse direction only and the resulting matrix differential equation is finite difference to yield the following algorithm,

taking into consideration the characteristics condition $\frac{n_i}{\beta v_i}\Delta t = \Delta z$, for which Δt is calculated for any given Δz:

$$\left[A + \theta \Delta z L_{z+\Delta z,t}\right] E_{z+\Delta z,t} = \left[A + (\theta - 1)\Delta z L_{z,t}\right] E_{z,t} \tag{3.9}$$

In the Crank-Nicolson approach, $\theta = 0.5$ has been used for all the simulations in this work.

3.6 Summary

This chapter has described the important computational aspects related to the implementation of the finite element method. The approach to the use of the method was presented in the form of a flow chart. Two different methods to calculate the power transfer between two guides, namely, the least squares boundary residual approach and the propagation model approach were discussed. The application of this approach will be presented in Chapter 5, 6, 7, and 9. However, in the next Chapter, an alternative approach using coupled mode theory is considered first, reviewing the development and applications of the theory to the problem in hand.

Chapter 4

Coupled-Mode Theory

4.1 Introduction

Actual waveguides are never perfect. There are always index inhomogeneities or slight changes of the core width, which cause the modes of the waveguide to couple among each other. For example, if a pure mode is excited at the beginning of the guide, some of its power may be transferred to other guided modes, resulting in signal distortion since each guided mode travels at its own characteristic group velocity. Transfer of power to the radiation modes cause losses since the power is carried away from the core regions into the cladding which is effectively of infinite dimensions. Therefore, it is very important to know the amount of coupling that is caused by the different types of waveguide imperfections, as a knowledge of the coupling coefficients makes it possible to determine the tolerance requirements, if bounds on the allowed radiation losses or on guided mode coupling have been established. Mode coupling may even be a desirable effect. For multimode operation of waveguides it is possible, at least in principle, to reduce the pulse dispersion resulting from the different group

velocities of the modes by coupling all the guided modes among each other. The theory of mode coupling is thus of fundamental importance for the design and operation of dielectric waveguides.

A brief historical perspective of the coupled mode theory is first given, including the development and applications of the theory in microwaves in the early years and in optoelectronics and fiber optics in recent years. The coupling between the waveguide modes is examined and the more general coupled-mode equations are considered, and applications which are described by general coupled-mode equations such as codirectional coupling, contradirectional coupling and the coupling coefficient. Directional coupling, which assumes that only two waveguides are involved in the coupling is considered, followed by three different coupled-mode approaches which were used to calculate the power transfer in this work.

4.2 Historical perspective

The concept of coupled modes in electromagnetics may be first considered to have begun in the early 1950s. The application was initially to microwaves and developed gradually through the contributions of many research workers. In 1954, Pierce applied the coupled mode theory to the analysis of microwave travelling-wave tubes (Pierce, 1954). Later the work of Gould (1955) followed on the backward-wave oscillators. The coupled mode theory was then employed to treat parametric amplifiers, oscillators, and frequency converters (Louisell, 1960).

In the meanwhile, various microwave waveguides and devices were being developed. Miller (1954) first introduced the coupled mode theory to the analysis and design of microwave waveguides and passive devices. Louisell (1955) soon generated a theory to treat tapered waveguide structures, where the coupling coefficients depend on the length z. In the 1960s, the coupled mode theory was further developed to describe mode conversions due to various irregularities in microwave waveguides (Miller, 1968; 1969), and periodic waveguide structures (Tang, 1969; Huang, 1981).

A rigorous derivation of coupled mode theory was carried out by Schelkunoff (1955). He obtained a set of generalised telegraphist's equations which are a different version of the coupled mode equations, obtained directly from Maxwell's equations by expanding the unknown electromagnetic fields of a coupled system in terms of the known modes of an uncoupled system. Once the modes of the uncoupled system are defined the coupling coefficients may be determined clearly. The coupled mode equations are equivalent to Maxwell's equations as long as a complete set is assumed for the mode expansion. For most applications, however, only a limited number of modes (usually two) is used in the expansion. Therefore, the coupled mode theory remains an approximate, yet valuable and often fairly accurate mathematical description of electromagnetic oscillation and wave propagation in a coupled system. Haus showed in 1958 that the coupled mode theory could be derived from a variational principle set up for the propagation constant of the coupled system (Haus, 1958). Due to the stationary

nature of the variational principle, the errors made in an incomplete expansion do not lead to a dramatic deterioration of the accuracy for the propagation constants calculated from the use of the coupled mode theory. If the fields of the coupled system are approximated as a linear superposition of the fields of the uncoupled systems, then the optimum result obtainable for the propagation constants originates from the coupled mode equations.

The coupled mode theory for optical waveguides was developed by Marcuse (1971; 1973), Snyder (1970; 1972), Yariv and Taylor (1973), and Kogelnik (1969; 1975), from the early 1970s. It has been successfully applied to the modelling and analysis of various guided-wave optoelectronic and fiber optical devices, such as optical directional couplers made of thin films and channel waveguides (Taylor, 1973; Kogelnik, 1975; Noda, 1981; Haus, 1981). It has also been used to study the wave coupling phenomena in nonlinear media such as harmonic generation in bulk materials (Armstrong *et al.*, 1962) and nonlinear pulse or soliton propagation (Crosignani *et al.*, 1981; 1982).

The conventional coupled mode theory assumed that the modes of the uncoupled systems are orthogonal to each other. This may be true if the modes belong to the same reference structures. In studying the mode coupling in coupled systems, however, the modes of the isolated systems are often chosen as the basis for the mode expansion and these modes may not be orthogonal. The orthogonal coupled mode theory (OCMT) is not correct for the description of the mode-coupling process in this case. The effect of nonorthogonality between waveguide

modes on cross-talk in optical couplers was first recognised by Chen and Wang (1984) and then studied by Haus and Whitaker (1985) in a proposal to eliminate the cross-talk due to this effect. Later on, several formulations of the nonorthogonal coupled mode theory (NCMT) were developed by Hardy and Streifer (1985), Haus, Huang, Kawakami, and Whitaker (1987), and Chuang (1987). The new nonorthogonal coupled mode theory (NCMT) is shown to yield more accurate dispersion characteristics and field patterns for the modes of the coupled waveguides. It also calls for a modification of the description of the power exchange between the waveguides.

There were some discrepancies among the different formulations at the early stage of the development. Some were superficial and soon resolved by reformulation (Streifer *et al.*, 1987). Snyder, Ankiewicz, and Altintas (1987) showed that the nonorthogonal formulations could lead to erroneous results for the coupling length of the TM modes of parallel slabs when the index discontinuity is large. The origin of the error is apparent in this case since the waveguide modes used as the trial solution in the coupled mode theory are subject to serious error when the index steps are large. They have also demonstrated, in the same example, that the conventional orthogonal coupled mode theory based on the same trial solution gives excellent prediction about the coupling length, as was earlier resolved by Haus, Huang, and Snyder (1989).

Despite the controversies, there has been an intense level of research activity in the past few years in developing and applying the nonorthogonal

coupled mode theory in the areas of optoelectronics and fiber optics. Vassallo (1987), Marcatili (1986), Syms (Syms and Peall, 1988), Huang (1989) developed simplified scalar versions that may be applied to weakly guiding structures and a modified vector version for the strongly guided structures.

4.3 Coupling between waveguide modes

4.3.1 The Coupled-Mode Equations

Many of the experimental situations of guided wave optics and especially those which involve the exchange of power between modes can be treated by means of the coupled-mode approach. As mentioned earlier, this formalism, introduced originally by Pierce (1954), describes the total propagating disturbance in a structure as a sum of (usually two) unperturbed modes of the system whose amplitudes vary with axial distance, z, due to some coupling between them. It has produced useful results when the z variation is slow, and has been applied to the description of different guided-wave phenomena (Yariv, 1973). In the following section some of the main features of this formalism will be discussed.

Consider two electromagnetic modes with, in general, different frequencies whose complex amplitudes are A and B. These are taken as the eigenmodes of the unperturbed medium so that they represent propagating disturbances

$$\left.\begin{aligned} a(z,t) &= Ae^{j(\omega_a t-\beta_a z)} \\ b(z,t) &= Be^{j(\omega_b t\pm\beta_b z)} \end{aligned}\right\} \qquad (4.1)$$

where A and B are the complex normalized amplitudes which are independent of z in the unperturbed structure .

In the presence of a perturbation, power is exchanged between modes a and b. The complex amplitudes A and B in this case are no longer constant but depend on z. They can be shown to obey relations of the type

$$\left.\begin{aligned} \frac{dA}{dz} &= K_{ab} B e^{-j\Delta z} \\ \frac{dB}{dz} &= K_{ba} A e^{+j\Delta z} \end{aligned}\right\} \qquad (4.2)$$

The constant, Δ, is equal to the difference in the propagation constants of the driven waves and the driving polarizations. The phase mismatch constant, Δ, merits some discussion. It is clear from the structure of (4.2) that a cumulative sustained exchange of power between modes a and b requires that $\Delta = 0$. Otherwise the values of dA/dz, for example, from different parts of the propagation path interfere destructively. In most of the problems of interest, the process of power exchange can be visualised as follows. Travelling mode b interacts with the perturbation to yield a travelling polarization wave. This wave in turn drives mode a. Simultaneously, mode a interacts with the perturbation to drive mode b.

The coupling coefficients K_{ab} and K_{ba} are determined by the physical situation under consideration and will be discussed in section 4.3.2.

However, before proceeding with specific experimental situations, some general conclusions which apply to the large number of phenomena which are described by equations of the general form of (4.2) are discussed.

4.3.2 Codirectional Coupling

First, the case where modes a and b carry electromagnetic power in the same direction is considered. It is extremely convenient to define A and B in such a way that $|A(z)|^2$ and $|B(z)|^2$ correspond to the power carried by mode a and mode b, respectively. The conservation of total power is thus expressed as

$$\frac{d}{dz}\left(|A|^2+|B|^2\right) = 0 \tag{4.3}$$

which, using (4.2), is satisfied when

$$K_{ab} = -K_{ba}^{*} \tag{4.4}$$

If the boundary conditions are such that a single mode, say b, is incident at $z = 0$ on the perturbed region, $z > 0$, the following applies:

$$\left.\begin{aligned} b(0) &= B_0 \\ a(0) &= 0 \end{aligned}\right\} \tag{4.5}$$

Subject to these conditions, the solutions of (4.2) become

$$A(z) = B_0 \frac{2K_{ab}}{\left(4K^2 + \Delta^2\right)^{1/2}} e^{-(j\Delta z/2)} \sin\left[\frac{1}{2}\left(4K^2 + \Delta^2\right)^{1/2} z\right] \tag{4.6a}$$

$$B(z) = B_0 e^{(j\Delta z/2)} \left\{\cos\left[\frac{1}{2}\left(4K^2 + \Delta^2\right)^{1/2} z\right] - j\frac{\Delta}{\left(4K^2 + \Delta^2\right)^{1/2}} \sin\left[\frac{1}{2}\left(4K^2 + \Delta^2\right)^{1/2} z\right]\right\} \tag{4.6b}$$

where $K^2 \equiv |K_{ab}|^2$.

Under phase-matched condition ($\Delta = 0$), a complete spatially periodic power transfer between modes a and b takes place with a period, π/K, in this situation,

$$\left.\begin{aligned} a(z,t) &= B_0 \frac{K_{ab}}{K} e^{j(\omega_a t - \beta_a z)} \sin(Kz) \\ b(z,t) &= B_0 e^{j(\omega_b t - \beta_b z)} \cos(Kz) \end{aligned}\right\} \tag{4.7}$$

4.3.3 Contradirectional Coupling

In this case the propagation in the unperturbed medium is described by

$$\left.\begin{aligned} a &= A e^{j(\omega_a t + \beta_a z)} \\ b &= B e^{j(\omega_b t - \beta_b z)} \end{aligned}\right\} \tag{4.8}$$

where A and B are constant. Mode a corresponds to a left (-z) travelling wave while b travels to the right. A time-space periodic perturbation can lead to power

exchange between the modes. Conservation of total power may now be expressed as

$$\frac{d}{dz}\left(|A|^2 - |B|^2\right) = 0 \tag{4.9}$$

which is satisfied by (4.2) if we take

$$K_{ab} = K_{ba}^* \tag{4.10}$$

so that

$$\left.\begin{aligned} \frac{dA}{dz} &= K_{ab} B e^{-j\Delta z} \\ \frac{dB}{dz} &= K_{ab}^* A e^{j\Delta z} \end{aligned}\right\} \tag{4.11}$$

In this case, mode b is taken with an amplitude B_0 to be incident at $z = 0$ on the perturbation region which occupies the space between $z = 0$ and $z = L$. Since mode a is generated by the perturbation, this yields $a(L) = 0$. With these boundary conditions, the solution of (4.11) is given by

$$A(z) = B_0 \frac{2jK_{ab}e^{-j(\Delta z/2)}}{-\Delta \sinh\frac{SL}{2} + jS\cosh\frac{SL}{2}} \sinh\left[\frac{S}{2}(z - L)\right] \tag{4.12}$$

$$B(z) = B_0 \frac{e^{j(\Delta z/2)}}{-\Delta \sinh\frac{SL}{2} + jS\cosh\frac{SL}{2}} \left\{ \Delta \sinh\left[\frac{S}{2}(z-L)\right] + jS\cosh\left[\frac{S}{2}(z-L)\right] \right\} \tag{4.13}$$

where

$S = \sqrt{4K^2 - \Delta^2}$, and $K \equiv |K_{ab}|$.

Under phase-matching conditions ($\Delta = 0$) we have

$$\left.\begin{aligned} A(z) &= B_0\left(\frac{K_{ab}}{K}\right)\frac{\sinh[K(z-L)]}{\cosh(KL)} \\ B(z) &= B_0\frac{\cosh[K(z-L)]}{\cosh(KL)} \end{aligned}\right\} \tag{4.14}$$

4.3.4 The Coupling Coefficient

The general behaviour of the two coupled modes is described by (4.6), (4.12) and (4.13) for the case of codirectional and contradirectional coupling, respectively. The form of these equations is independent of the numerical magnitude of the coupling coefficient, K. The latter, however, determines the interaction strength or, in practice, the distance over which a given fractional power exchange between the two modes takes place.

Consider the coupling between, say, a TE mode

$$a^{(\pm)}(x,z,t) = A^{(\pm)}(z)e^{j(\omega_a t \mp \beta_a z)}\,\mathcal{E}_y^{(a)}(x) \tag{4.15}$$

and a forward-travelling TM mode

$$b^{(+)}(x,z,t) = B^{(+)}(z)e^{j(\omega_b t-\beta_b z)}\,\mathcal{H}_y^{(b)}(x) \tag{4.16}$$

where A and B are the power-normalised mode amplitudes. The (+) and (-) superscripts refer to forward and backward waves respectively. Consider the dielectric waveguide sketched in Fig. 4.1.

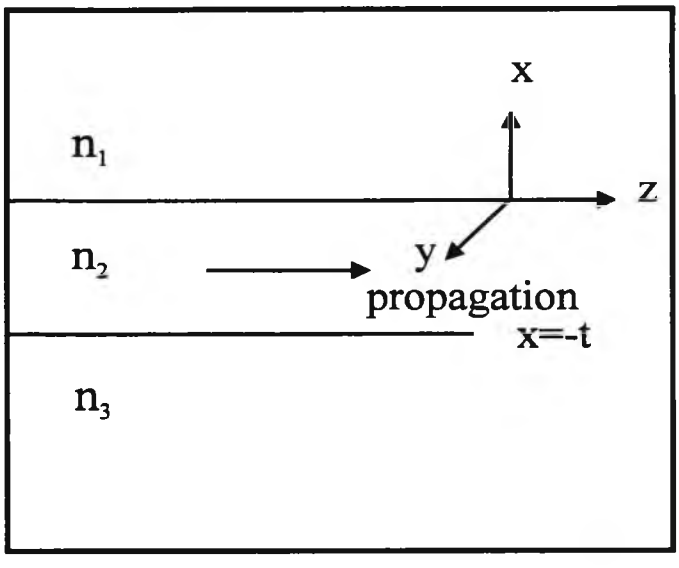

Fig. 4.1 Schematic of a planar dielectric waveguide.

It consists of a film of thickness, t, and index of refraction, n_2, sandwiched between media with indices, n_1 and n_3. Taking $\partial/\partial y = 0$, this guide can, in the general case, support a finite number of confined TE modes with field components E_y, H_x, and H_z and TM modes with components H_y, E_x, E_z. The transverse function $\mathcal{E}_y(x)$ is taken as

$$\mathcal{E}_y = \begin{cases} C\ \exp(-qx), & 0 \le x < \infty \\ C\left[\cos(hx) - (q/h)\sin(hx)\right], & -t \le x \le 0 \\ C\left[\cos(ht) + (q/h)\sin(ht)\right]\ \exp\left[p(x+t)\right], & -\infty < x \le -t \end{cases} \tag{4.17}$$

where

$$h = \left(n_2^2 k^2 - \beta^2\right)^{1/2}$$
$$q = \left(\beta^2 - n_1^2 k^2\right)^{1/2}$$
$$p = \left(\beta^2 - n_3^2 k^2\right)^{1/2}$$
$$k = \frac{\omega}{c}$$

and the transverse function $\mathcal{H}_y(x)$ is taken as

$$\mathrm{H}_y(x) = \begin{cases} -\dfrac{h}{\overline{q}} C e^{-qx}, & 0 \le x < \infty \\ C\left[-\dfrac{h}{\overline{q}}\cos(hx) + \sin(hx)\right], & -t < x < 0 \\ -C\left[\dfrac{h}{\overline{q}}\cos(ht) + \sin(ht)\right] e^{p(x+t)}, & -\infty < x \le -t \end{cases} \tag{4.18}$$

where

$$\overline{q} = \frac{n_2^2}{n_1^2} q$$

The wave equation for the perturbed and unperturbed case are

$$\nabla^2 E_y(r,t) = \mu\varepsilon \frac{\partial^2 E_y}{\partial t^2} + \mu \frac{\partial^2}{\partial t^2}\left[P_{pert}(r,t)\right]_y \tag{4.19a}$$

$$\nabla^2 E_y(r,t) = \mu\varepsilon \frac{\partial^2 E_y}{\partial t^2} \tag{4.19b}$$

where P_{pert} represents the deviation in the medium polarization responsible for the mode coupling. The wave equation for the perturbed case follows directly from Maxwell's equation if $\mathbf{D} = \varepsilon_0\mathbf{E}+\mathbf{P}$ is taken into consideration. Formal, but straightforward considerations show that the coupling between the two modes may be described by

$$\frac{dA^{(-)}}{dz} e^{j(\omega_a t+\beta_a z)} - \frac{dA^{(+)}}{dz} e^{j(\omega_a t-\beta_a z)} = -\frac{j}{4\omega_a}\frac{\partial^2}{\partial t^2}\int_{-\infty}^{\infty}\left[P_{pert}(r,t)\right]_y \mathcal{E}_y^{(a)}(x)\,dx \tag{4.20}$$

where, in this case, $P_{pert}(r,t)$ is a polarization arising from the interaction of field of the TM mode, $b^+(x,z,t)$, and the medium perturbation responsible for the coupling of the two, otherwise independent, modes. This perturbation can be due, as an example, to a travelling sound wave, mechanical corrugations, an induced electrooptic birefringence, or a magnetooptic Faraday rotation. Now, synchronous exchange of power (*i.e.*, one which does not fluctuate in time or space) requires that the exponents on both side of (4.20) be equal. Since this will not occur in general for both $A^{(-)}$ and $A^{(+)}$, a coupling will take place from the forward TM mode to either $A^{(-)}$ or $A^{(+)}$. This last statement can be expressed analytically, by comparing (4.20) to (4.2) which gives

$$K_{ab}^{(\pm)} e^{j\Delta^{(\pm)}z} = \pm\frac{je^{-j(\omega_a t\mp\beta_a z)}}{4\omega_a B^+}\frac{\partial^2}{\partial t^2}\int_{-\infty}^{\infty}\left[P_{pert}(r,t)\right]_y \mathcal{E}_y^{(a)}(x)\,dx \tag{4.21}$$

In the cases of interest in this work $|\Delta^+| >> |\Delta^-|$ or vice versa, and the coupling is limited to the pair of modes for which Δ is small. When equation (4.21) is applied, as will be done in the following sections, it will be found that $P_{pert}(r,t)$ is proportional to $B^+(z)e^{j\omega_a t}$ so that K_{ab} is a constant.

4.4 Directional Coupling

Exchange of power between guided modes of parallel waveguides is known as directional coupling. In an optoelectronic system, waveguide directional couplers perform a number of useful functions in thin-film devices, including power division, modulation, switching, and frequency and polarization selection.

The power can be completely transferred from one waveguide to the other when two coupled waveguides have equal propagation constants (the synchronous case). There is only a fraction of the power initially propagating in one waveguide which can be transferred to the other when the propagation constants are unequal (asynchronous case).

Waveguide coupling can be treated theoretically by using coupled mode theory. Consider the case of the two planar waveguides as shown in Fig. 4.2. The refractive index distributions for the two guides in the absence of coupling are given by $n_a(x)$ and $n_b(x)$. The transverse electric field distribution for a particular guided mode of waveguide, a, and a particular mode of waveguide, b, will be

denoted by $\mathcal{E}_y^{(a)}$ and $\mathcal{E}_y^{(b)}$, and the propagation constants by β_a and β_b. The field for the coupled-guide structure for propagation in the positive z direction may be approximated by

$$E_y = A(z)\,\mathcal{E}_y^{(a)}(x)\,e^{j(\omega t-\beta_a z)} + B(z)\,\mathcal{E}_y^{(b)}(x)\,e^{j(\omega t-\beta_b z)} \tag{4.22}$$

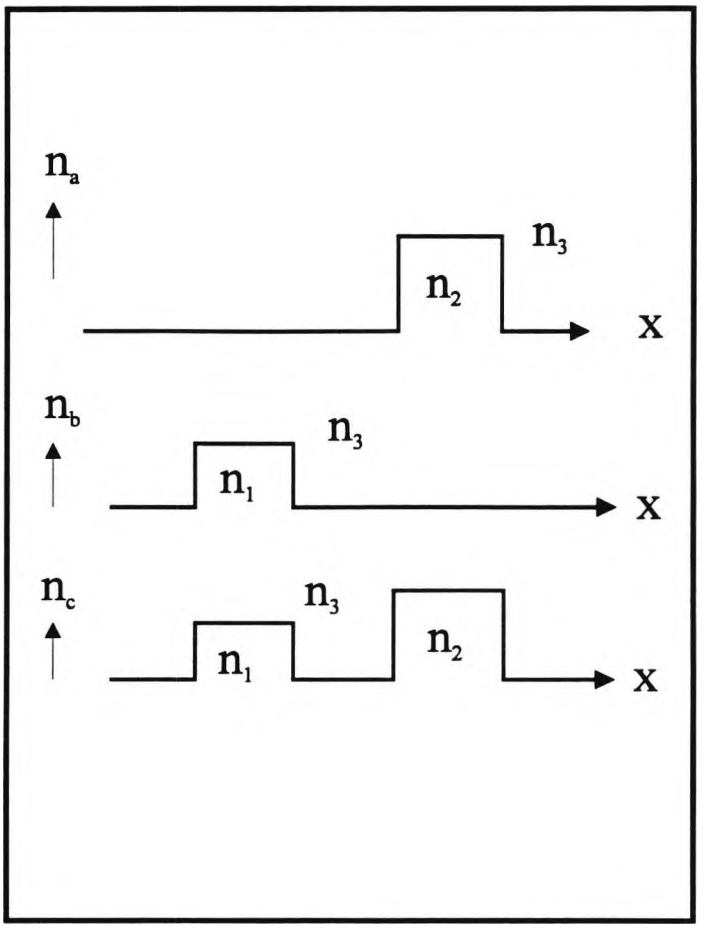

Fig 4.2 Spatial variation of refractive index for uncoupled waveguides $n_a(x)$ and $n_b(x)$, and for a parallel coupled waveguide structure $n_c(x)$.

The perturbation polarization responsible for the coupling may be calculated by substituting (4.22) into (4.19), neglecting the variation of A and B. The result is

$$P_{pert} = -e^{j\omega t}\varepsilon_0\left[\mathcal{E}_y^{(a)}A(z)\left(n_c^2 - n_a^2\right)e^{-j\beta_a z} + \mathcal{E}_y^{(b)}B(z)\left(n_c^2 - n_b^2\right)e^{-j\beta_b z}\right] \tag{4.23}$$

where $n_c(x)$ is the refractive index for the two-guide structure.

Substituting (4.23) into (4.20) and integrating over x yields

$$\left.\begin{aligned}\frac{dA}{dz} &= K_{ab}Be^{-j\Delta z} + M_a A\\ \frac{dB}{dz} &= K_{ab}Ae^{j\Delta z} + M_b B\end{aligned}\right\} \tag{4.24}$$

where

$$\left.\begin{aligned}\Delta &= \beta_a - \beta_b\\ K_{ab} &= -\frac{j\varepsilon_0\omega}{4}\int_{-\infty}^{\infty}\left(n_c^2 - n_a^2\right)\mathcal{E}_y^{(a)}\mathcal{E}_y^{(b)}\,dx\\ M_{(a,b)} &= -\frac{j\varepsilon_0\omega}{4}\int_{-\infty}^{\infty}\left(n_c^2 - n_{(a,b)}^2\right)\left(\mathcal{E}_y^{(a,b)}\right)^2 dx\end{aligned}\right\} \tag{4.25}$$

The terms M_a and M_b represent small corrections to β_a and β_b, so (4.24) reduces to the familiar form of (4.2), with $\Delta = \beta_a - \beta_b - j\left(M_a - M_b\right)$. The solution is given by (4.6). If a power, P_0, is initially coupled into guide b at $z = 0$, the interguide distribution for $z > 0$ may be given by

$$\left.\begin{aligned} P_a &= P_0 \frac{4K^2}{4K^2+\Delta^2}\sin^2\left[\frac{\left(4K^2+\Delta^2\right)^{1/2} z}{2}\right] \\ P_b &= P_0\left\{\frac{\Delta^2}{4K^2+\Delta^2}+\frac{4K^2}{4K^2+\Delta^2}\cos^2\left[\frac{\left(4K^2+\Delta^2\right)^{1/2} z}{2}\right]\right\} \end{aligned}\right\} \tag{4.26}$$

Complete power transfer occurs in a distance $L = \pi/2K$ in the synchronous case ($\Delta = 0$). In the asynchronous case ($\Delta \neq 0$), both the coupling length and the maximum power transfer are less than in the synchronous case.

The coupling between waveguides with different propagation constants $\left(\beta^{(a)} \neq \beta^{(b)}\right)$ can be improved by a periodic perturbation in the refractive index. The most efficient coupling by a sinusoidal perturbation requires that $\Delta = 0$, where

$$\Delta = \beta_a \pm \beta_b \pm \frac{2\pi}{\Lambda} \tag{4.27}$$

and Λ is the period of the perturbation, measured in the z direction. Both codirectional and contradirectional power transfer are possible.

The preceding discussion assumes that only two waveguides are involved in the coupling, but coupled-mode theory can also be applied to problems involving more than two waveguides. In the case of an array of equally spaced, synchronous waveguides, the coupled-mode relations are given by:

$$\frac{dA_n}{dz} = K\left(A_{n-1} + A_{n+1}\right) \tag{4.28}$$

where K may be obtained from (4.25), and A_n represents the mode amplitude for the nth waveguide. If all of the incident power is initially in the zeroth guide for z = 0, the solution to (4.28) is then given by

$$A_n(z) = A_0(0)(-j)^n J_n(2jKz) \tag{4.29}$$

for $z > 0$, where J_n is the Bessel function of order n.

4.5 Three different Coupled-Mode approaches

4.5.1 Introduction

Theoretical improvements in the understanding of strongly coupled waveguides have only been attempted very recently (Hardy and Streifer, 1985; Chuang, 1987). A simple and approximate version of the coupled-mode equations for parallel dielectric waveguides has also been presented by Marcatili (1986) to account for the asymmetric properties of waveguides using a newly found relation between the coupling coefficients and the overlap integral of two-coupled waveguides. A few conditions are assumed in that paper :

1) A scalar formulation of the fields is considered.

2) The refractive index perturbation is very small, such that second-order terms can be ignored.

$$\left.\begin{aligned} n^2 &= n_0^2\left[1+\Delta_a(x,y)+\Delta_b(x,y)\right]^2 \\ n^2 &\approx n_0^2\left[1+2\Delta_a(x,y)+2\Delta_b(x,y)\right] \end{aligned}\right\} \tag{4.30}$$

Thus the new relation between the two coupling coefficients in the work of Marcatili (1986) is only approximate.

3) The overlap integral C is assumed to be small (weakly coupled) and is not included in the coupled-mode equations because the coupled-mode equations in the work of Marcatili (1986) are almost the same as those for the conventional theory without including the overlap integrals in the four coupling parameters, γ_a, γ_b, K_{ab}, and K_{ba}.

Chuang has applied the theory developed in several papers (Hardy and Streifer, 1985; 1986; 1986a; Haus *et al.*, 1987; Chuang, 1987; 1987a) and showed that all the above conditions are not required. It has been shown that an exact analytical relation governing the coupling coefficients, the overlap integrals, and the propagation constants derived in the paper from Chuang (1987) using a generalised reciprocity theorem can be combined with the formulation of Marcatili and will give very good numerical results, even for strongly coupled waveguides. It has been pointed out in the work of Hardy (Hardy and Streifer, 1985) that the four parameters γ_a, γ_b, K_{ab}, and K_{ba} should include the overlap integrals to obtain the correct propagation constants of the supermodes. Since only β_a, β_b of the individual waveguides and K_{ab}, K_{ba} of the conventional coupling coefficients are used in the coupled-mode equations in the work of Marcatili (1986), that theory will not yield accurate numerical results and may violate energy conservation significantly, unless the overlap integral $C << 1$, which is assumed by Marcatili (1986).

Three very similar formulations of strongly coupled waveguides have been presented in recent publications (Hardy and Streifer, 1985; Haus *et al.*, 1987; Chuang, 1987). The formulation by Haus *et al.* (1987) is limited to the lossless system and has a small difference in the z-component of the electric field for the trial functions in the variational approach. The formulation of Hardy and Streifer (1985) does not satisfy energy conservation and the reciprocity theorem and still contains a small error, while the theory of Chuang, (1987) (which was derived in a much simpler way) satisfies these laws analytically. Independently, a reformulation of the work of Hardy (Hardy and Streifer, 1985) has been made (Streifer *et al.*, 1987) recently and is identical to that of Chuang (1987) after the modifications.

The formulations from Hardy and Streifer, Marcatili and Chuang have been used in this work to calculate the power transfer and some parameters such as C_{ab}, C_{ba}, K_{ab}, K_{ba}, β_1 and β_2 in different structures in this thesis. A comparison, is then made of those results. Those formulations are shown in the following section.

4.5.2 The formulations from Chuang for Two Coupled Waveguides

Starting with the coupled-mode equations

$$\frac{dU}{dz} = j\gamma_a U + jK_{ab}V \tag{4.31a}$$

$$\frac{dV}{dz} = j\gamma_b V + jK_{ba}U \tag{4.31b}$$

where

$$\gamma_a = \frac{\beta_a + \left(K_{11} - \overline{C}_{ab} K_{21}\right)}{\left(1 - \overline{C}_{ab}^2\right)} \tag{4.32a}$$

$$\gamma_b = \frac{\beta_b + \left(K_{22} - \overline{C}_{ab} K_{12}\right)}{\left(1 - \overline{C}_{ab}^2\right)} \tag{4.32b}$$

$$K_{ab} = \frac{\left(K_{12} - K_{22}\overline{C}_{ab}\right)}{\left(1 - \overline{C}_{ab}^2\right)} \tag{4.32c}$$

$$K_{ba} = \frac{\left(K_{21} - K_{11}\overline{C}_{ab}\right)}{\left(1 - \overline{C}_{ab}^2\right)} \tag{4.32d}$$

where the subscript 1 refers to waveguide *a* or 1, and 2 refers to waveguide *b* or 2, whichever is convenient.

$\overline{C}_{ab}$ and K_{pq} (p, q = 1,2 or a, b) are defined as

$$C_{pq} = \frac{1}{2}\int_{-\infty}^{\infty}\int E_t^{(q)} \times H_t^{(p)} \cdot \hat{z}\, dxdy \tag{4.33}$$

$$\overline{C}_{pq} = \frac{1}{2}\left(C_{pq} + C_{qp}\right) = \overline{C}_{qp} \tag{4.34}$$

$$K_{pq} = \frac{\omega}{4}\iint \Delta\varepsilon^{(q)}\left[E_t^{(p)} \cdot E_t^{(q)} - \frac{\varepsilon^{(p)}}{\varepsilon} E_z^{(p)} E_z^{(q)}\right] dxdy \tag{4.35}$$

where $\varepsilon(x,y)$ is the permittivity function of the multiwaveguide system and $\varepsilon^{(q)}(x,y)$ is the permitivity function of a single waveguide, q, defined as

$$\Delta\varepsilon^{(q)} = \varepsilon(x,y) - \varepsilon^{(q)}(x,y) \tag{4.36}$$

In the theory of Marcatili (1986),

1) $\overline{C}_{ab}$ is assumed to be zero in the above four parameters,

2) K_{11} and K_{22} are ignored, and

3) K_{12} and K_{21} are defined only for scalar fields (pure TE case).

Thus, that formulation is almost the same as that for the conventional theory (Yariv, 1973) and will lead to significant errors if $\overline{C}_{ab}$ becomes larger than, say, 10 percent (where C_{aa} and C_{bb} are normalised to be 1).

The asynchronism factor in terms of the more correct parameters γ_a, γ_b, K_{ab}, and K_{ba} in (4.32a)-(4.32d) have been defined, where

$$\delta = \frac{\gamma_b - \gamma_a}{2\sqrt{K_{ab}K_{ba}}} \tag{4.37}$$

Given the initial excitation at $z = 0$ of a two-coupled waveguide, $a(0) = 1$, $b(0) = 0$, the following is obtained:

$$U(z) = \left[\cos\ \psi z - j\frac{\Delta}{\psi}\sin\ \psi z\right] e^{j\phi z} \tag{4.38a}$$

$$V(z) = \frac{jK_{ba}}{\psi}\ \sin\ \psi z\, e^{j\phi z} \tag{4.38b}$$

where

$$\phi = \frac{\gamma_b + \gamma_a}{2} \tag{4.39a}$$

$$\psi = \sqrt{\Delta^2 + K_{ab}K_{ba}} \tag{4.39b}$$

$$\Delta = \frac{\gamma_b - \gamma_a}{2} \tag{4.39c}$$

The two eigenvalues γ_1, γ_2 and eigenvectors are well known:

$$\gamma_1 = \phi + \psi \tag{4.40a}$$

$$\gamma_2 = \phi - \psi \tag{4.40b}$$

It is also easy to show that

$$\delta = \frac{1}{2\bar{c}}\left[\sqrt{\frac{K_{ba}}{K_{ab}}} - \sqrt{\frac{K_{ab}}{K_{ba}}}\right] \tag{4.41}$$

where

$$\bar{c} = \overline{C}_{ab} = \overline{C}_{ba}$$

The solutions (4.38a) and (4.38b) can be written as

$$U(z) = \left\{\cos\left[\sqrt{K_{ab}K_{ba}}\, z\left(1+\delta^2\right)^{1/2}\right] - j\frac{\delta}{\left(1+\delta^2\right)^{1/2}}\cdot\sin\left[\sqrt{K_{ab}K_{ba}}\, z\left(1+\delta^2\right)^{1/2}\right]\right\}e^{j\phi z} \tag{4.42a}$$

$$V(z) = j\frac{e^{\sinh^{-1}\bar{c}\delta}}{\sqrt{1+\delta^2}}\sin\left[\sqrt{K_{ab}K_{ba}}\, z\left(1+\delta^2\right)^{1/2}\right]e^{j\phi z} \tag{4.42b}$$

The output power P_a in waveguide a when waveguide b terminates at $z = l$ is obtained using

$$E_t(x,y,z=l) \cong U(l)E_t^{(a)}(x,y) + V(l)E_t^{(b)}(x,y) \tag{4.43a}$$

$$E_t(x,y,z=l) \cong \sum_{n=1}^{\infty} u_n^{(a)} E_t^{(a)n}(x,y) \tag{4.43b}$$

$$H_t(x,y,z=l) \cong U(l)H_t^{(a)}(x,y) + V(l)H_t^{(b)}(x,y) \tag{4.44a}$$

$$H_t(x,y,z=l) \cong \sum_{n=1}^{\infty} v_n^{(a)} H_t^{(a)n}(x,y) \tag{4.44b}$$

where the expansion in (4.43a) or (4.44a) is in terms of individual waveguide modes and in (4.43b) or (4.44b) is in terms of all the guided and radiation modes of waveguide a alone, since they form a complete set. Multiplying (4.43) by $H_t^{(a)}$ and integrating over the cross section, the following is obtained

$$u_1^{(a)} = U(l) + C_{ab}V(l) \tag{4.45}$$

Similarly,

$$v_1^{(a)} = U(l) + C_{ba}V(l) \tag{4.46}$$

These boundary conditions at $z = 0$ and $z = l$ follow very closely those of Marcatili (1986). The guided power due to the first mode, β_a, in waveguide a is, thus,

$$P_a = \frac{1}{2}\mathrm{Re}\left[u_1^{(a)}v_1^{(a)*}\frac{1}{2}\iint E_t^{(a)1} \times H_t^{(a)1} \cdot \hat{z}\, dxdy\right] \tag{4.47a}$$

$$P_a = 1 - \left(\frac{1 - C_{ab}C_{ba}}{1+\delta^2}\right) e^{2\sinh^{-1}\bar{c}\delta} \cdot \sin^2\left[\sqrt{K_{ab}K_{ba}}\, l\left(1+\delta^2\right)^{1/2}\right] \tag{4.47b}$$

using equations (4.42), (4.45), and (4.46). A similar procedure for the output power in waveguide b when waveguide a is terminated at $z = l$ leads to

$$P_b = \mathrm{Re}\left[\left(C_{ba}U + V\right)\left(C_{ab}^*U^* + V^*\right)\right] \tag{4.48a}$$

$$P_b = C_{ab}C_{ba} + \frac{1 - C_{ab}C_{ba}}{1+\delta^2}\sin^2\left(\sqrt{K_{ab}K_{ba}}\, l\left(1+\delta^2\right)^{1/2}\right) \tag{4.48b}$$

These results are very similar to those of Marcatili (1986) except that the parameters are defined in terms of the more accurate parameters γ_a, γ_b, K_{ab}, and K_{ba}.

4.5.3 The formulations from Hardy and Streifer for Two Coupled Waveguides

The propagation constants, γ_a and γ_b, are given by

$$\gamma_a = \frac{\beta_a + \left[K_{11} - C_{ab}K_{21} + C_{ab}C_{ba}(\beta_a - \beta_b)\right]}{(1 - C_{ab}C_{ba})} \tag{4.49a}$$

and

$$\gamma_b = \frac{\beta_b + \left[K_{22} - C_{ba}K_{12} + C_{ab}C_{ba}(\beta_b - \beta_a)\right]}{(1 - C_{ab}C_{ba})} \tag{4.49b}$$

where the corrections to the individual waveguide mode propagation constants, β_a and β_b describe the effects of the modal interactions. The coupling coefficients are

$$K_{ab} = \frac{\left\{K_{12} + C_{ab}\left[\beta_a - \beta_b - K_{22}\right]\right\}}{(1 - C_{ab}C_{ba})} \tag{4.50a}$$

and

$$K_{ba} = \frac{\left\{K_{21} + C_{ba}\left[\beta_b - \beta_a - K_{11}\right]\right\}}{(1 - C_{ab}C_{ba})} \tag{4.50b}$$

In (4.49a)-(4.50b), the coefficients, C_{ab} and C_{ba} describe the individual waveguide mode overlap, i.e.,

$$C_{pq} = 2\hat{z} \cdot \int_{-\infty}^{\infty}\int \left[E_t^{(q)} \times H_t^{(p)}\right] dxdy, \qquad p,q = a,b \tag{4.51}.$$

The individual modes may be normalised such that

$$C_{aa} = C_{bb} = 1 \tag{4.52}$$

The constants K_{pq} $(p,q = 1,2)$ depend on the perturbations to the individual waveguides and are defined by

$$K_{pq} = \omega \int\int \Delta\varepsilon^{(p)} \left[E_t^{(p)} \cdot E_t^{(q)} - \frac{\varepsilon^{(q)}}{\varepsilon_0 n^2} E_z^{(p)} E_z^{(q)} \right] dxdy, \qquad p,q = 1,2 \tag{4.53}$$

where $\varepsilon^{(p)}$, $p = 1,2$ refer to the individual waveguides and $\Delta\varepsilon^{(p)}$, $p = 1,2$ are the perturbations to the respective guides. Note that the integrals in equation (4.53) extend only over the regions in which the perturbations occur. For example, in a simple case, the region of waveguide b is that over which the perturbation is applied to waveguide a, and vice versa. By contrast, the integrals in (4.51) extend over all space. More complicated waveguiding structures may be decomposed into two individual guides, as follows

$$\varepsilon^{(1)}(x,y) + \Delta\varepsilon^{(1)}(x,y) = \varepsilon_0 n^2(x,y) \tag{4.54a}$$

and

$$\varepsilon^{(2)}(x,y) + \Delta\varepsilon^{(2)}(x,y) = \varepsilon_0 n^2(x,y) \tag{4.54b}$$

where $\varepsilon^{(1)}(x,y)$ and $\varepsilon^{(2)}(x,y)$ each represent the individual waveguides singly embedded in the surrounding medium. Note that

$$\varepsilon^{(1)}(x,y) + \varepsilon^{(2)}(x,y) \neq \varepsilon(x,y) = \varepsilon_0 n^2(x,y),$$

since each function contains the same surroundings. Moreover, most generally $\varepsilon_0 n^2(x,y)$ need not even equal the mathematical union of $\varepsilon^{(1)}(x,y)$ and $\varepsilon^{(2)}(x,y)$,

because an additional index perturbation not encompassed by either waveguide also could be included.

Considering two parallel lossless guides with $U \equiv 0$ and $V = V_0$ at $z = 0$, it is not necessary to address the question of how that initial connection is established, but that issue must be considered in any analysis, regardless of the equations used to describe the propagation and coupling along the length where the guides are parallel. Upon solving equation (4.31) subject to these initial conditions, the following is obtained

$$V(z) = V_0\left[\cos(\psi z)+\frac{j\Delta}{\psi}\sin(\psi z)\right]e^{j\phi z} \tag{4.55a}$$

and

$$U(z) = V_0\frac{jK_{ab}}{\psi}\sin(\psi z)e^{j\phi z} \tag{4.55b}$$

It can be observed that when $\psi z = \frac{\pi}{2}$, $|U|$ is maximum. If waveguide, b, could be terminated at that point, the modal amplitude and power in a can be estimated. Thus by multiplying the entire field by $H_t^{(a)}$ and integrating the result, $U+C_{ab}V$ can be obtained. Based on this estimate, the power remaining in waveguide a is given by

$$P_a = \frac{1}{4}\left|U+C_{ab}V\right|^2 = \frac{1}{4}\frac{|V_0|^2}{\psi^2}\left|K_{ab}+C_{ab}\Delta\right|^2 \tag{4.56}$$

and this result is independent of the formula used to evaluate K_{ab}.

Instead, however, the coupling process can be considered to begin with $U = V_0$ and $V = 0$ at $z = 0$. If, after propagating $\psi z = \pi/2$, waveguide a can be terminated then, as above, the modal amplitude in waveguide b would be $V+C_{ba}U$. Consequently, the power remaining in waveguide b may be estimated to be

$$P_b = \frac{1}{4}\left|V + C_{ba}U\right|^2 = \frac{1}{4}\frac{|V_0|^2}{\psi^2}\left|K_{ba} - C_{ba}\Delta\right|^2 \tag{4.57}$$

In order to satisfy reciprocity in a lossless waveguide system, P_a and P_b as given by equation (4.56) and (4.57), should be equal.

4.5.4 The formulations from Marcatili for Two Coupled Waveguides

The overlap integral C_{ab} and C_{ba} may be defined as

$$C_{pq} = \int E_p E_q dxdy, \qquad p,q = a,b \tag{4.58}$$

The coupling coefficient K_{ab} and K_{ba} can also be defined as

$$K_{ab} = \frac{k\int (n_a - n_s)E_a E_b dxdy - kC\int (n_a - n_s)E_b E_b dxdy}{(1-C^2)} \tag{4.59a}$$

$$K_{ba} = \frac{k\int (n_b - n_s)E_a E_b dxdy - kC\int (n_b - n_s)E_a E_a dxdy}{(1-C^2)} \tag{4.59b}$$

where the wave number, $k = \frac{2\pi}{\lambda}$, n_s is refractive index in the substrate and in this case $C_{ab} = C_{ba} = C$.

The power outputs from both devices are

$$P_a = 1 - \frac{1-C^2}{1+\delta^2} e^{-2\sinh^{-1} C\delta} \sin^2 \frac{\pi}{2}\sqrt{1+\delta^2} \tag{4.60a}$$

$$P_b = C^2 + \frac{1-C^2}{1+\delta^2} \sin^2 \frac{\pi}{2}\sqrt{1+\delta^2} \tag{4.60b}$$

and the two eigenvalues are well known :

$$\gamma_{1,2} = \frac{\beta_a + \beta_b}{2} \pm \sqrt{K_{ab} K_{ba}}\sqrt{1+\delta^2} \tag{4.61}$$

4.6 Summary

The history and development of the coupled-mode theory were considered in summary in this Chapter. The conventional coupled-mode theory assumed that the modes of the uncoupled systems are orthogonal to each other. However, the orthogonal coupled-mode theory is not correct for the description of the mode-coupling process in the mode expansion. In subsequent work, several formulations of the nonorthogonal coupled mode theory were developed by several groups, but there have been some discrepancies among the different formulations at the early stage of the development. Despite the controversies, there has been an intense level of research activity in the past few years in developing and applying the

nonorthogonal coupled mode theory in the areas of optoelectronics and fiber optics. In this Chapter, the general coupled-mode theory was also considered, to lead to improving of coupled-mode theory. However, the three different coupled-mode approaches namely, the Hardy and Streifer approach, the Marcatili approach and the Chuang approach were taken into consideration in their application in different directional coupler structures. The comparison of results obtained on several waveguides using the three different approaches will be presented in Chapters 5, 6 and Chapter 7.

Chapter 5

Strongly Coupled Dielectric Waveguides

5.1 Introduction

Directional couplers are important for many applications in optical communications and integrated optics (Lee, 1986; Hunsperger, 1984). In its simplest form, a directional coupler consists of two parallel dielectric waveguides in close proximity to each other (Marcuse, 1989). Under suitable conditions, a light wave launched into one of the waveguides can couple completely into the opposite guide. However, once the light has crossed over, the wave can also couple back into the first guide, so that power is exchanged continuously, as often as the length of the device permits. However, complete exchange of light power is only possible between modes that have equal phase velocities or, equivalently, equal propagation constants. To be more precise, the propagation constants must be equal for each guide in isolation for complete power transfer. Equality of the propagation constants, also called phase synchronism, occurs naturally when the two waveguides are identical and the use of this leads to what is termed a synchronous

directional coupler. In that case, all the guided modes (if there are more than one) of both guides are in phase synchronism and can couple one to the other at all wavelengths. However, two dissimilar waveguides can also have modes that are in phase synchronism, a condition that can exist only for certain specific wavelengths.

Directional couplers can be used as power dividers. In principle, since complete exchange of power is possible for a synchronous directional coupler, any arbitrary power splitting ratio can be achieved by proper adjustment of the length of the directional coupler. In this chapter, the effects of the adjustment of the length of the directional coupler both in terms of the separation distance between two waveguides and the width of a guide will be shown. Another important use of directional couplers - light switching and modulating (Alferness, 1982; Auracher *et al.*, 1984; Neter, 1984; Alferness and Veselka, 1985)-requires that the propagation constants can be influenced by external means. For example, if one or both waveguides consists of electro-optic materials exhibiting the Pockels effect, the refractive index and hence the propagation constants of the guided modes can be modified by externally applied electric fields. This makes it possible to influence the phase synchronism between the two modes of the coupled waveguides, permitting a modulation of the coupling efficiency. Thus, it is possible to switch (or modulate) light from one waveguide to the other at speeds that are only limited by the length of the device (Veselka and Korotky, 1986). The results of an electro-optic directional coupler switch are shown in Chapter 6.

Finally, directional couplers can be utilized to design optical wavelength filters (Taylor, 1973; Alferness and Veselka, 1985). For couplers made of identical waveguides, this application is made possible by the fact that the coupling strength depends on the wavelength. The coupling coefficients K_{ab} and K_{ba} are identical at a particular wavelength. Thus, if a directional coupler permits complete exchange of power at a certain wavelength, it becomes less effective at shorter as well as at longer wavelengths so that every directional coupler is also a wavelength filter. However, the achievable bandwidth is not satisfactory. The filter becomes narrower if the two waveguides are as dissimilar as possible, achieving phase synchronism only in a narrow wavelength range. The result of the simulation of an optical filter employing a synchronous and a nonsynchronous directional coupler, has also been shown in Chapter 7.

The accurate calculation of the coupling parameters is of considerable interest, in order to study the loss of synchronism in electro-optic modulators and switches or in optical filters in the use of nonidentical sections to reduce bandwidth. In most of the practical directional coupler-based devices, the individual waveguides use two-dimensional confinement and can be of arbitrary cross-section with anisotropic, nonlinear, lossy or active materials. However, our concern here has been restricted to slab waveguides in order to make a comparison with other published work. The finite element method (Rahman *et al.*, 1991) has already been established as one of the most powerful methods available to characterize a wide range of practical waveguides. This chapter mainly deals with

specific parallel waveguides, where the power coupling efficiency between two optical waveguides is presented using the finite element method, along with the results of improved coupled mode approaches (Hardy and Streifer, 1985; Marcatili, 1986; Chuang, 1987) and the least squares boundary residual method (Rahman and Davies, 1988; 1988a).

5.2 The Finite Element Method and Least Squares Boundary Residual Method approaches

It is possible to find the power transfer between two guides starting from the individual modes of the isolated guides or from the supermodes of the complete coupled structure. In this work, both such approaches are used, after obtaining accurate eigenvalues and eigenvectors of the individual guides and the coupled structures.

Since the finite element method (FEM) can provide accurate solutions for the supermodes of the coupled system, an alternative to the coupled mode approach, the Least Squares Boundary Residual (LSBR) method has been applied to directional coupler problems. This procedure may be used to find the power carried by the even and odd supermodes for a given incident power in guide "*a*" or "*b*". Here it is assumed that a single isolated waveguide section, section **I**, is butt coupled to the directional coupler section, section **II**, as shown in Fig 5.1. The main objective is to calculate the amplitudes of the even and odd modes b_1, b_2 respectively in section **II**. The LSBR approach is better than the use of the

traditional overlap integral methods as many modes can be considered to satisfy the field continuity at the discontinuity junction plane. This approach is also more satisfactory than the point matching methods because the error integral is evaluated over the discontinuity interface, rather than just field matching at some specific points.

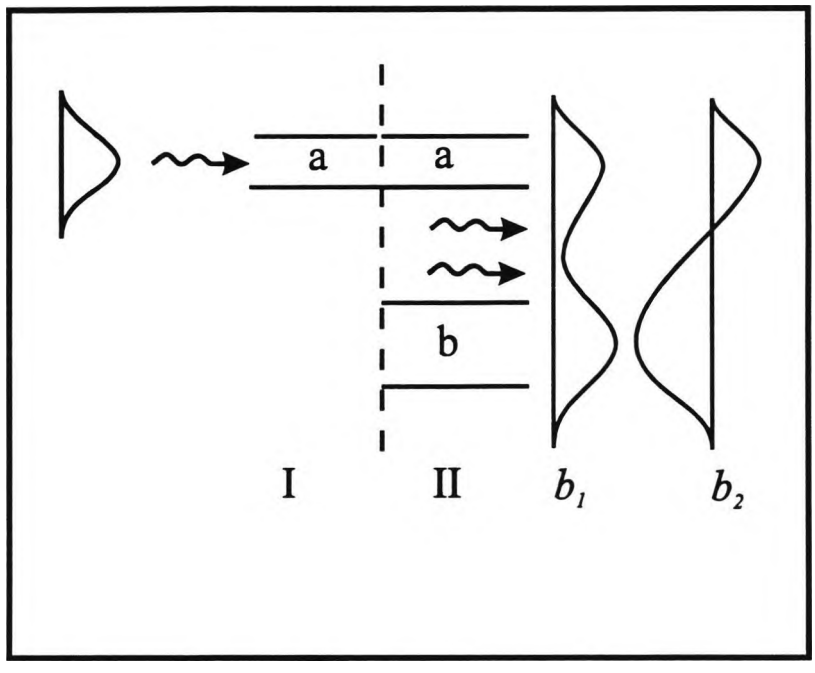

Fig. 5.1 Butt coupling of an isolated guide to the directional coupler section.

A directional coupler consists of two adjacent waveguides arranged so that the tail of the field supported by one waveguide overlaps the other waveguide. This overlap causes a coupling between the two waveguides. If the incident wave of total power, P_o, is launched into one waveguide such as guide a, it will transfer it to waveguide b over the coupling length L_c, and then transfer back again. The wave

propagates in the two waveguides with the propagation constants β_a and β_b, respectively. If the coupler is asymmetric (*i.e.*, the two waveguides have different geometries and/or refractive indices) there will be a propagation constant difference between the modes,

$$2\delta = (\beta_a - \beta_b) \tag{5.1}$$

Under the approximation that the coupling is weak (*i.e.*, the coupling coefficient K is small) and that δ is small, the coupling can be described by the following formula (Yariv, 1976)

$$P_a = P_o \frac{K^2}{K^2 + \delta^2} \sin^2\left[\left(K^2 + \delta^2\right)^{1/2} \cdot l\right] \tag{5.2}$$

where P_a is the output power of waveguide a and l is the physical length of the coupling region. Obviously, complete power transfer requires that $\delta = 0$, *i.e.*, that the light has the same propagation constant in both waveguides. All the power will then be found in waveguide b if the coupler length, l, is equal to an odd multiple of L_C ($L_C = \pi/(2K)$). For electro-optic modulators or filters with a narrow bandwidth directional coupler, couplers with a high degree of asymmetry or strong coupling must be considered. The treatment in two familiar texts (Taylor, 1973) and (Yariv, 1976) which are based on perturbation technique is not applicable in this case. A method proposed by Suematsu and Kishino (Suematsu and Kishino, 1977) is, however, employed. The case of the TE mode is treated here, but the case of the TM mode can be easily dealt with in a similar way. The procedure is as follows.

A two-parallel-slab-waveguide system is considered, which consists of five dielectric layers, that is, there are two waveguiding layers or cores and three other regions with lower refractive indices that separate and clad the two waveguiding layers. These layers are assumed to be lossless. The refractive index distribution varies along the transverse y-axis and is independent of the transverse x and the longitudinal z axes. This two-parallel-waveguide system supports the two fundamental waveguide modes $H_e(y,z)$, $H_o(y,z)$, that is, even and odd modes which have slightly different propagation constants β_e and β_o, respectively, and are orthonormal with respect to the Poynting power. First the finite element method is used to find the lowest-order even and odd supermodes. From the related eigenvalue equations, the propagation constants for the two modes can be obtained. The field distribution in the two waveguides can be described as a superposition of the two supermodes. Provided that the input waveguide is single mode, higher order supermodes can generally be neglected since their coupling to the input mode is weak at the wavelengths of interest. The two supermodes interfere and since they propagate with slightly different velocities, optical power transfer occurs from one waveguide to the other along the propagation direction. In the absence of higher-order modes, the travelling wave can be expressed in terms of

$$E(y,z) = b_1 E_e(y) e^{-j\beta_e z} + b_2 E_o(y) e^{-j\beta_o z} \tag{5.3}$$

$$H(y,z) = b_1 H_e(y) e^{-j\beta_e z} + b_2 H_o(y) e^{-j\beta_o z} \tag{5.4}$$

where b_1 and b_2 are the amplitudes of the normalized even and odd lowest order supermodes with field distributions H_e and H_o and propagation constants β_e and β_o, respectively. In this work, the supermode coefficients, b_1 and b_2 are solved by using the least squares boundary residual method. To discuss the coupling between two parallel waveguides, their boundary is defined as the middle plane, for the sake of simplicity. Since the two modes travel at different phase velocities, they alternately add and cancel with respect to each other. Therefore, the guide wave given by equation (5.3) and equation (5.4), which is a combination of these modes, exchanges power periodically. It is assumed that the starting point of the longitudinal axis, $z = 0$, is the point where the maximum power is observed in waveguide a. The power can be gradually transferred to waveguide b as it propagates. However, the small amount of power which is observed in waveguide b at $z = 0$, is not transferred to waveguide a. Thus, that small amount of power may be called the uncoupled factor at waveguide b. On the other hand, at $z = L_c$, the coupling length, the power transfer from waveguide a to b becomes maximum, but a small fractional amount of power will remain in waveguide a.

The wave is normalized by

$$\int_{-\infty}^{\infty} E(y,z)\, H^*(y,z)dy = |b_1|^2 + |b_2|^2 = 1 \qquad (5.5)$$

The power density at any point is given by the amplitude of the Poynting vector :

$$\begin{aligned} P(y,z) &= \mathrm{Re}\left|\overline{E}\times\overline{H}\right| = \mathrm{Re}\left[E(y,z)H^{*}(y,z)\right] \\ &= b_1^2 E_e(y)H_e^{*}(y)+b_2^2 E_o(y)H_o^{*}(y)+b_1 b_2 \cdot \\ &\quad \left[E_e(y)H_o^{*}(y)+E_o(y)H_e^{*}(y)\right]\cdot\cos\left[(\beta_e-\beta_o)z\right] \end{aligned} \tag{5.6}$$

By integrating over each side of $y = 0$, the power carried by each waveguide can be expressed as a function of the propagation distance, z.

The power fraction in guide b is thus given by

$$\begin{aligned} P_b(z) &= \int_{-\infty}^{0} P(y,z)\,dx \\ &= b_1^2(1-\xi_{ee})+b_2^2(1-\xi_{oo})-b_1 b_2(\xi_{eo}+\xi_{oe})\cdot\cos\left[(\beta_e-\beta_o)z\right] \end{aligned} \tag{5.7}$$

where ξ_{ee}, ξ_{oo}, ξ_{eo}, and ξ_{oe} are defined as $(i, j = e, o)$:

$$\xi_{ij} = \int_{0}^{\infty} E_j(y)H_i^{*}(y)\,dy \tag{5.8}$$

At $z = 0$ the power distribution in the guides has a profile given by the launching conditions. For optimal launching into guide a, the power fraction in guide b should have a minimum value, or uncoupled factor.

From equations (5.7) and (5.8), there are now four equations which may be written as:

$$P_a(z=0) = b_1^2\xi_{ee}+b_2^2\xi_{oo}+b_1 b_2(\xi_{eo}+\xi_{oe}) \tag{5.9}$$

$$P_a(z=z) = b_1^2\xi_{ee} + b_2^2\xi_{oo} + b_1b_2(\xi_{eo} + \xi_{oe})\cdot\cos\left[(\beta_e - \beta_o)z\right] \quad (5.10)$$

$$P_b(z=0) = b_1^2(1-\xi_{ee}) + b_2^2(1-\xi_{oo}) - b_1b_2(\xi_{eo} + \xi_{oe}) \quad (5.11)$$

$$P_b(z=z) = b_1^2(1-\xi_{ee}) + b_2^2(1-\xi_{oo}) - b_1b_2(\xi_{eo} + \xi_{oe})\cdot\cos\left[(\beta_e - \beta_o)z\right] \quad (5.12)$$

Using these equations the power transfer efficiency from the supermode of the complete coupled structure can be calculated.

5.3 Slab Waveguide Coupler

5.3.1 A general description of the coupler

At first, the accuracy of the finite element method as a means to obtain propagation constants for the individual modes and supermodes is illustrated. To reduce the coupling length, the separation distance, τ_3, can be reduced to increase the mode coupling and subsequently shorten the overall device length. However, this will introduce cross-talk due to incomplete power transfer between the guides, even when the guides may be identical. First a synchronous directional coupler problem (Chen and Wang, 1984) is considered to test our numerical procedures. In the first example, $n_a = n_b = 3.44$, $n_c = n_s = 3.436$, $\tau_a = \tau_b = 2.0$ μm, and the optical wavelength is considered to be 1.06 μm. This device is shown diagramatically in Fig. 5.2.

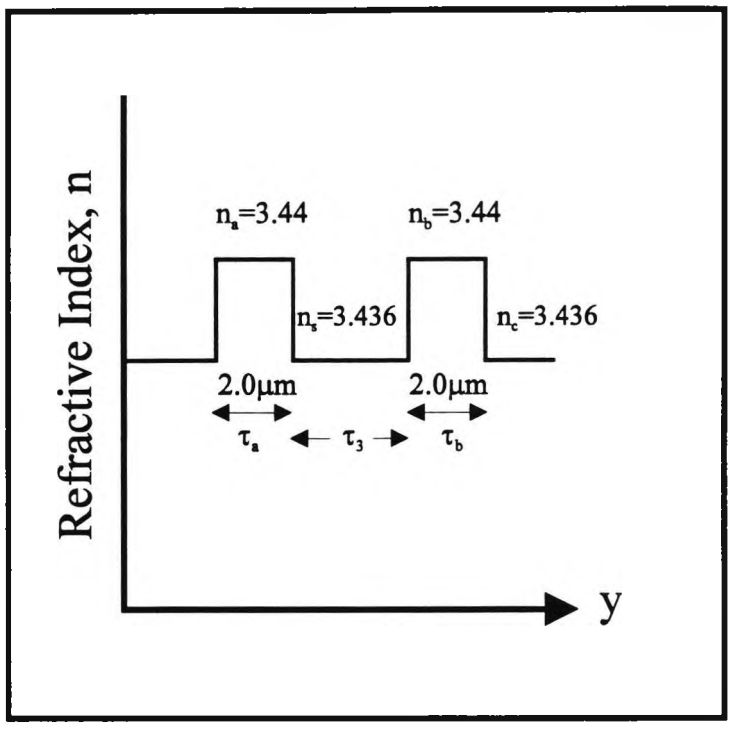

Fig. 5.2 Schematic diagram of synchronous directional coupler.

The directional coupler to be dealt with in the second example (shown in Fig. 5.3), analyzed by Hardy and Streifer (1985), is considered. Two slab waveguides "*a*" and "*b*" with film thicknesses τ_a and τ_b are separated by τ_3 (of μm dimensions). The refractive indices for the guides *a* and *b*, the separation and the cladding region are n_a, n_b, n_s and n_c respectively and the operating wavelength is 0.8 μm. Generally, our interest is limited to geometries in which the modal fields of the entire structure are well represented by a superposition of the fundamental individual waveguide modes so that the fields $\{E_t, H_t\}$ under consideration are those for which higher order modes are small in comparison with the other terms.

So, the higher order modal interaction is ignored in this work and only the coupling between the fundamental modes of the cores is considered.

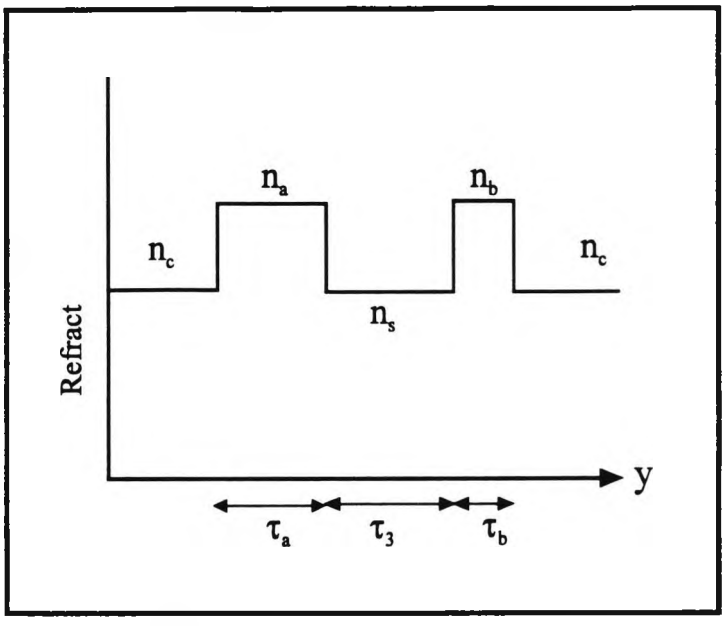

Fig. 5.3 Schematic diagram of two parallel coupled optical waveguides.

5.3.2 Solutions for identical coupled slab waveguide.

Results for the E_x field profiles for even and odd TE supermodes, the variation of the coupling length, L_c, the cross-talk for the first example (shown in Fig. 5.2), will be shown.

Fig. 5.4 shows the E_x field profiles for the even and odd TE supermodes for a synchronous directional coupler when τ_a and τ_b are identical (2.0 μm) and the separation distance, τ_3 = 5.0 μm. It can be seen that the modal profiles are symmetrical since the individual guides are identical.

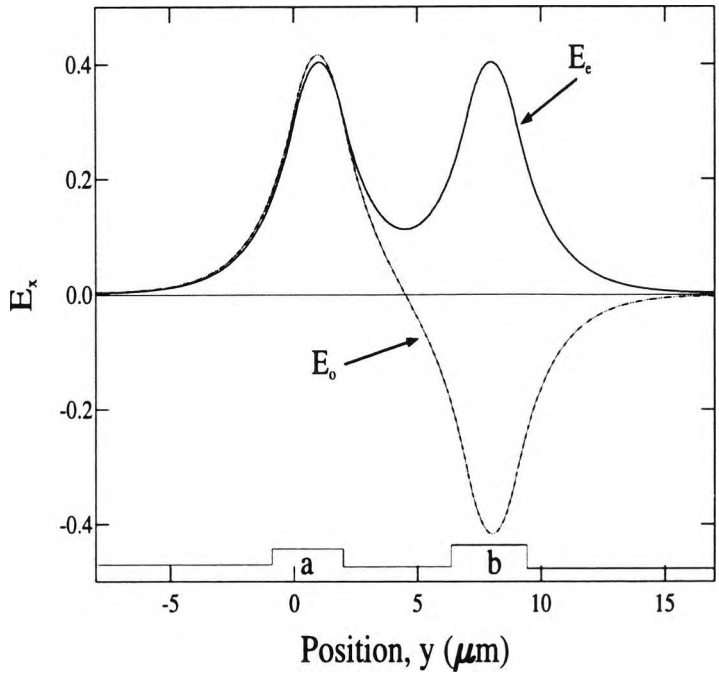

Fig. 5.4 E_x field profiles for the even- and odd-like TE supermodes.

Fig. 5.5 shows the variation of the coupling length, L_c, with the separation distance, τ_3. It can be seen that the coupling length, L_c becomes larger with increasing τ_3 and follows an exponential law, so that the resulting coupling length, L_c vs τ_3 plot is linear on a log-linear scale. It can also be noticed from this figure that the analytical result and the FEM result are indistinguishable one from another.

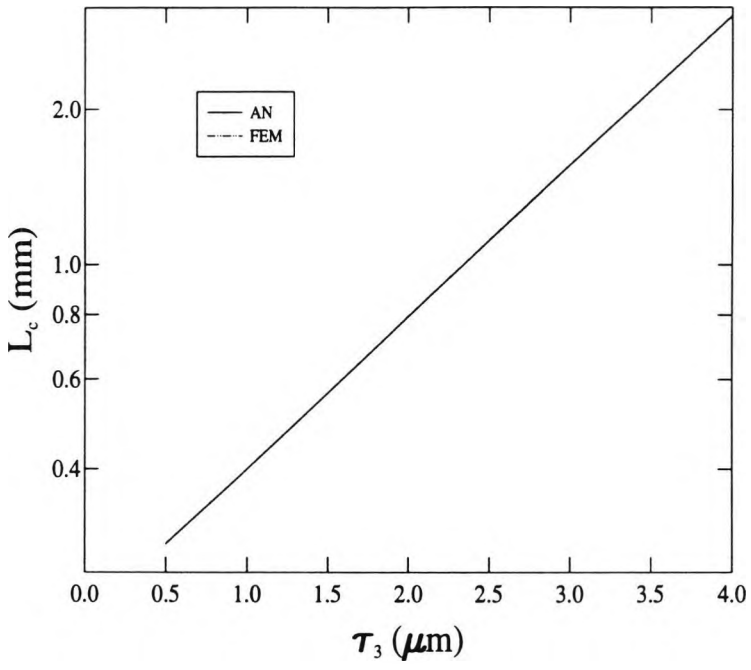

Fig. 5.5 Variation of the coupling length with the separation distance.

To find the power transfer efficiency and cross-talk, using the coupled mode approaches, the overlap integrals and coupling coefficients need to be calculated. To illustrate the procedure and the steps taken, some intermediate results are presented for the first example with coupled identical waveguides, which is easier than in the second example, which is for the coupled nonidentical waveguides. Fig. 5.6 shows the variation of K_{ab} and K_{ba} with the separation between the two waveguides, τ_3, when the thicknesses of the guide *a* and *b* are fixed at 2.0 μm. In this figure, K_{ab} and K_{ba} are almost identical when the separation becomes larger. It can also be observed that K_{ab} and K_{ba} reduce monotonically as τ_3 increases. The

coupling coefficients K_{ab} and K_{ba} may be calculated by using the following equation (Hardy and Streifer, 1985).

$$K_{ab} = \frac{\left\{\tilde{K}_{ab} + C_{ab}\left[\beta^{(a)} - \beta^{(b)} - \tilde{K}_{bb}\right]\right\}}{\left(1 - C_{ab}C_{ba}\right)} \tag{5.13}$$

$$K_{ba} = \frac{\left\{\tilde{K}_{ba} + C_{ba}\left[\beta^{(b)} - \beta^{(a)} - \tilde{K}_{aa}\right]\right\}}{\left(1 - C_{ab}C_{ba}\right)} \tag{5.14}$$

where

$$\tilde{K}_{ab} = \omega \int_{-\infty}^{+\infty}\int \Delta\varepsilon^{(a)}\left[E_t^{(a)} \cdot E_t^{(b)} - \frac{\varepsilon^{(b)}}{\varepsilon_o n^2} E_z^{(a)} E_z^{(b)}\right] dxdy \tag{5.15}$$

$$\tilde{K}_{ba} = \omega \int_{-\infty}^{+\infty}\int \Delta\varepsilon^{(b)}\left[E_t^{(b)} \cdot E_t^{(a)} - \frac{\varepsilon^{(a)}}{\varepsilon_o n^2} E_z^{(b)} E_Z^{(a)}\right] dxdy \tag{5.16}$$

Fig. 5.7 shows the cross-talk in dB with the separation distance, τ_3, using the coupled mode approach (CH) (Chuang, 1987) and the Least Squares Boundary Residual method (LSBR) approach. In this example, results from both the approaches agree reasonably with those from the work of Chen and Wang (1984). It is clear that the extinction ratio decreases exponentially as the waveguide separation increases. When the separation, τ_3, was greater than 5.0 μm, the extinction ratio was less than -22.1 dB for all three different approaches. However, the shorter the coupling length is, the worse the cross-talk gets. This is due to

unequal coupling of the input wave to the even and odd eigen mode in the coupling region.

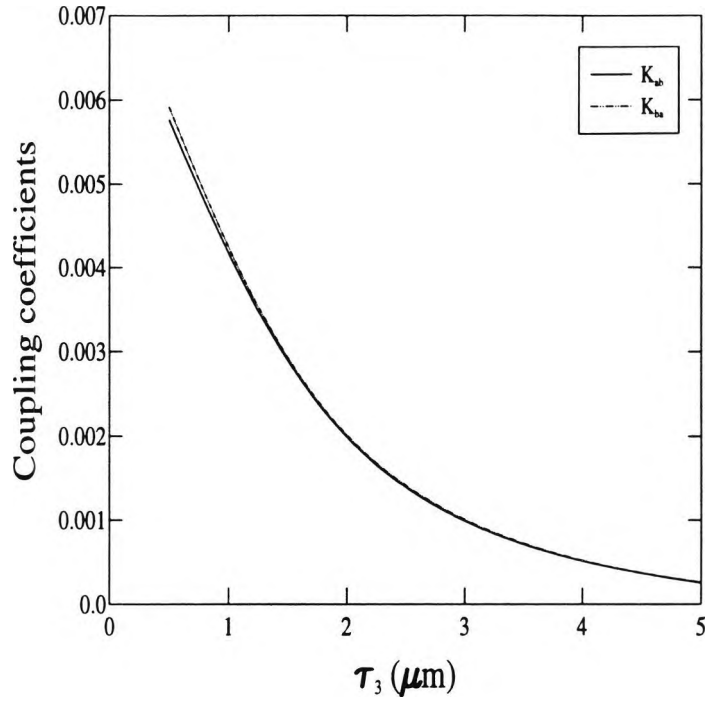

Fig. 5.6 Variation of coupling coefficients with the separation between two waveguides, τ_3.

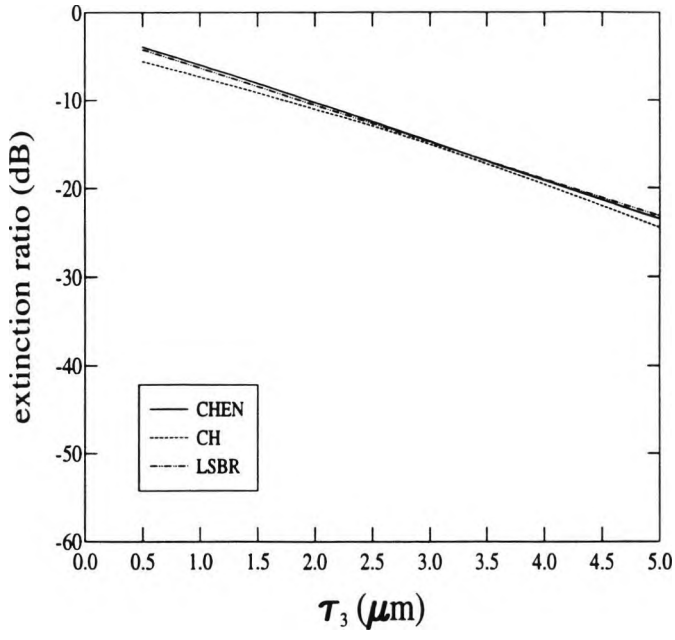

Fig. 5.7 Cross-talk between the guides with the separation distance for an identical coupled waveguides.

5.3.3 Solutions for nonidentical coupled slab waveguide.

In this example, two waveguides with identical refractive indices, $n_a = n_b =$ 3.6 and the cladding refractive index, $n_s = n_c = 3.4$ are considered. In this case τ_a and τ_3 are fixed at 0.15 μm and 0.4 μm respectively, but τ_b varies from 0.1 μm to 0.2 μm. Here β_b is the propagation constant for the isolated guide *b* and β_e and β_o are propagation constants for the even and odd supermodes of the coupled guides. The analytical solutions (AN) may be obtained by finding roots of the transcendental equation due to the field matching at the dielectric interfaces. The finite element (FEM) solutions are obtained by using 4000 mesh divisions. It takes

about 10 seconds to find the modal solutions in this way on a SUN Sparcstation 2 for this mesh refinement. Table 5.1 shows the comparison of the finite element solutions with the analytical solutions for the individual TE mode of the isolated guide "*b*" and the even and odd TE supermodes of the coupled structure. It shows the excellent agreement of the finite element results obtained with the analytical results and if required, the accuracy of the results can be further improved by using an even finer mesh.

τ_b	β_b		β_e		β_o	
in μm	AN	FEM	AN	FEM	AN	FEM
0.10	26.97534	26.97534	27.20137	27.20137	26.93143	26.93143
0.12	27.06138	27.06138	27.20992	27.20992	27.01436	27.01436
0.15	27.18799	27.18798	27.24361	27.24360	27.11346	27.11346
0.18	27.30535	27.30534	27.32241	27.32241	27.15637	27.15636
0.20	27.37685	27.37685	27.38579	27.38578	27.16669	27.16668

Table 5.1 The comparison of finite element solutions (FEM) with analytical solution (AN) for β_b, β_e and β_o.

Fig. 5.8 shows the E_x field profiles for the even and odd- TE supermodes for a synchronous directional coupler when $\tau_a = \tau_b = 0.15$ μm, with the separation distance, $\tau_3 = 0.4$ μm. It can be observed that the modal profiles are symmetrical since the individual guides are identical.

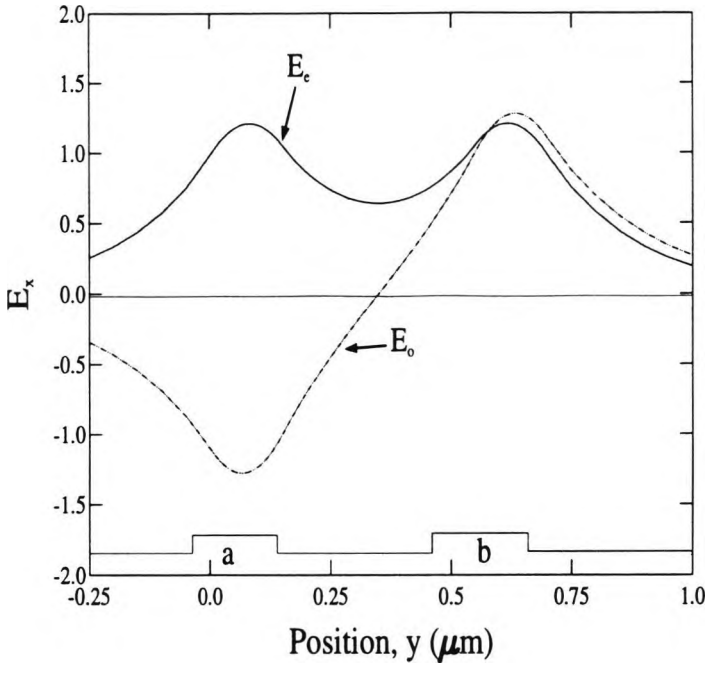

Fig. 5.8 E_x field profiles for the even- and odd- like TE supermodes for an identical coupled waveguide.

Fig. 5.9 shows the E_x field profiles for the even- and odd-like TE supermodes for a nonsynchronous directional coupler when τ_a and τ_b are 0.15 μm and 0.1 μm respectively, with the separation distance, τ_3 = 0.4 μm. It can be observed that the modal profiles are not symmetrical since the individual guides are not identical. The first supermode is the even-like mode with most of the power confined in the guide "*a*" whereas the second supermode is the odd-like mode with most of the power confined in the guide "*b*". This occurs because the dominant mode in guide "*a*" has a higher propagation constant than the mode in guide "*b*" (as $\tau_a > \tau_b$) so the first supermode with higher propagation constant resembles more

the mode E_a when the individual modes are not phase matched. The power intensity profiles obtained from these field profiles match accurately with the exact profiles shown in Fig. 2 of the results of Hardy and Streifer (1985).

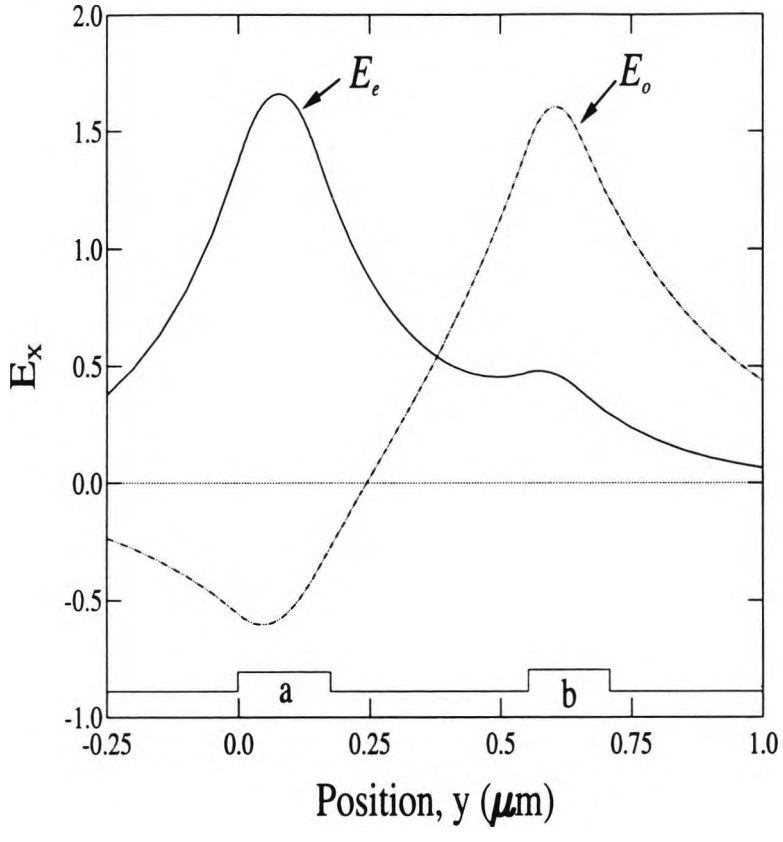

Fig. 5.9 E_x field profiles for the even- and odd- like TE supermodes for nonidentical coupled waveguide.

The coupling length of the coupled waveguides can be accurately calculated from the propagation constant difference of the first two supermodes. In the finite element method, the propagation constants of the two supermodes are obtained

directly, whereas using the coupled mode theory, these can also be estimated from the individual modes of the two isolated guides by using different coupled mode approaches.

Fig. 5.10 shows the variation of the propagation constants of the two supermodes with the second guide thickness, τ_b. The finite element results (FEM) and analytical results (AN) are identical and cannot be distinguished in this figure. Results using the Hardy and Streifer (HS) approach (1985) agreed better with the analytical and the FEM results. Results using the Marcatili (MA) approach (1986) are consistently higher value than the actual eigenvalues. The propagation constants of individual modes β_a and β_b are also shown. Results using the Chuang (CH) approach (1987) are also satisfactory except when τ_b = 0.10 μm, resulting in β_e being smaller than β_a, which cannot be correct. The propagation constant of the even supermode should be higher than that of the first isolated mode and the propagation constant of the odd supermode should be lower than that of the second isolated mode.

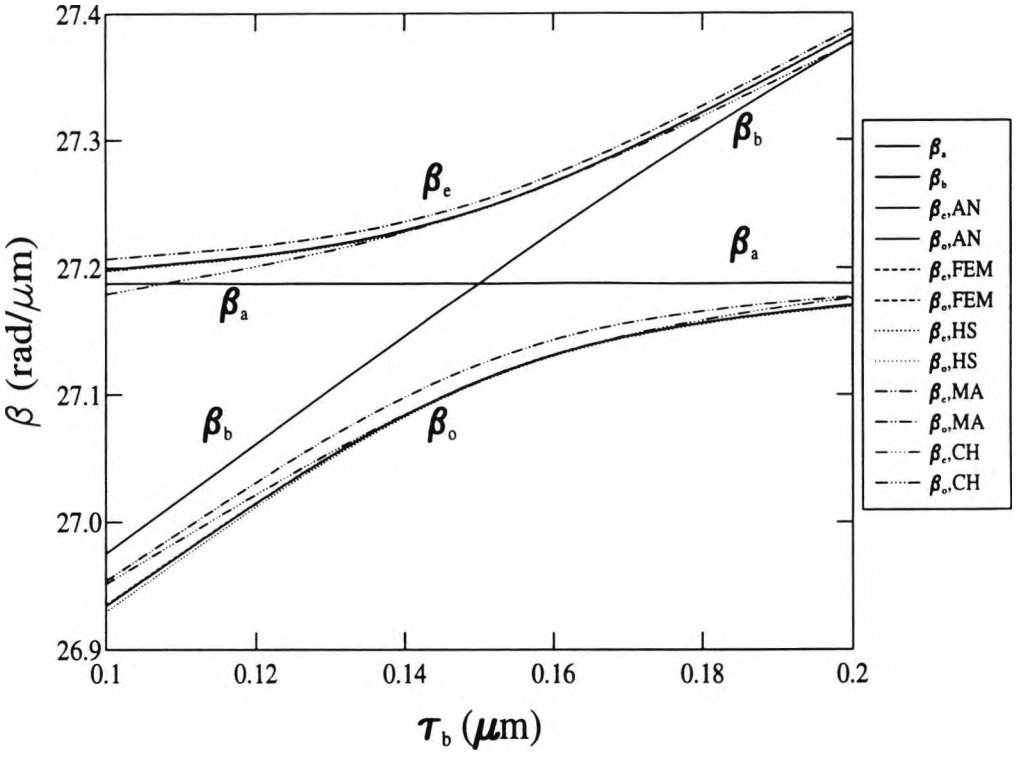

Fig. 5.10 Variation of the calculated supermode propagation constants with the second guide thickness, τ_b.

Fig. 5.11 shows the coupling length variation with the second guide width, τ_b, when τ_a = 0.15 μm for different separation distances, τ_3. It has been shown in Table 5.1 that the analytical (AN) and the finite element results (FEM) agree extremely well even when the guides are strongly coupled and they cannot be distinguished one from another, whereas the calculation of the propagation constants of the supermodes by using the coupled mode approaches may be satisfactory but not very accurate, as shown in Fig. 5.10. The coupled mode (CH)

approaches (Chuang, 1987) agree well for the weakly coupled conditions but in general they overestimate the coupling length when the guides are not synchronous, as shown for $\tau_3 = 0.4\ \mu m$. This is due to the fact that the coupled mode approach suffers from nonorthogonality between the modes of different waveguides when the guides are not identical. It should also be noted that when $\tau_a = \tau_b$, the coupling length varies exponentially with the separation distance, τ_3, but when τ_a is not equal to τ_b, the coupling length depends strongly on the factor $|\beta_a - \beta_b|$.

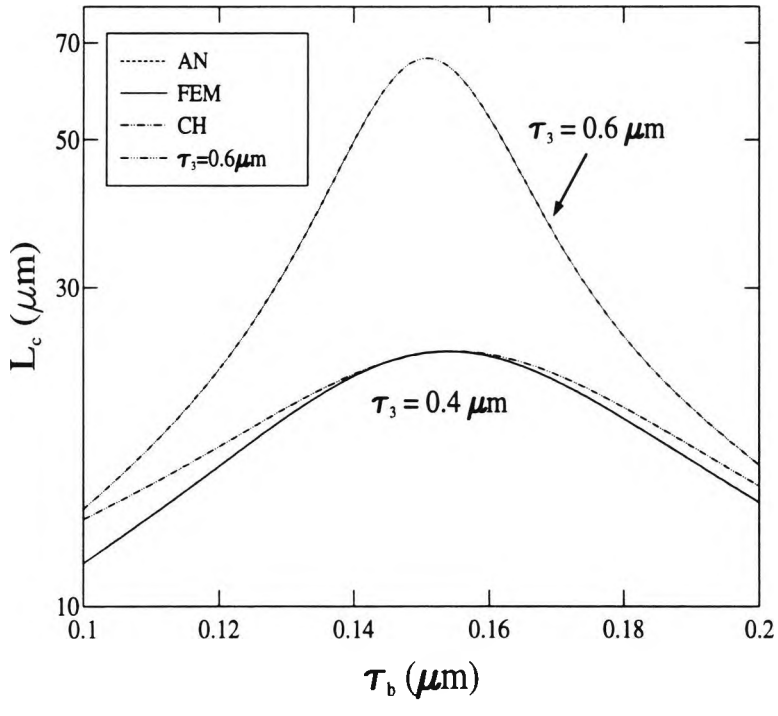

Fig. 5.11 Variation of coupling length with the second guide thickness, τ_b for different separation between the guides, τ_3 (Analytical AN solution overlaps FEM solution).

Fig. 5.12 shows the variation of the coupling length with the separation distance, τ_3, for different approaches. It can be seen that the coupling length increases with separation τ_3 and follows an exponential law. It can also be observed that the analytical (AN) solution and FEM solution are identical. However, the results from Marcatili have overestimated whereas the results from HS and CH have underestimated the values obtained using the previous methods.

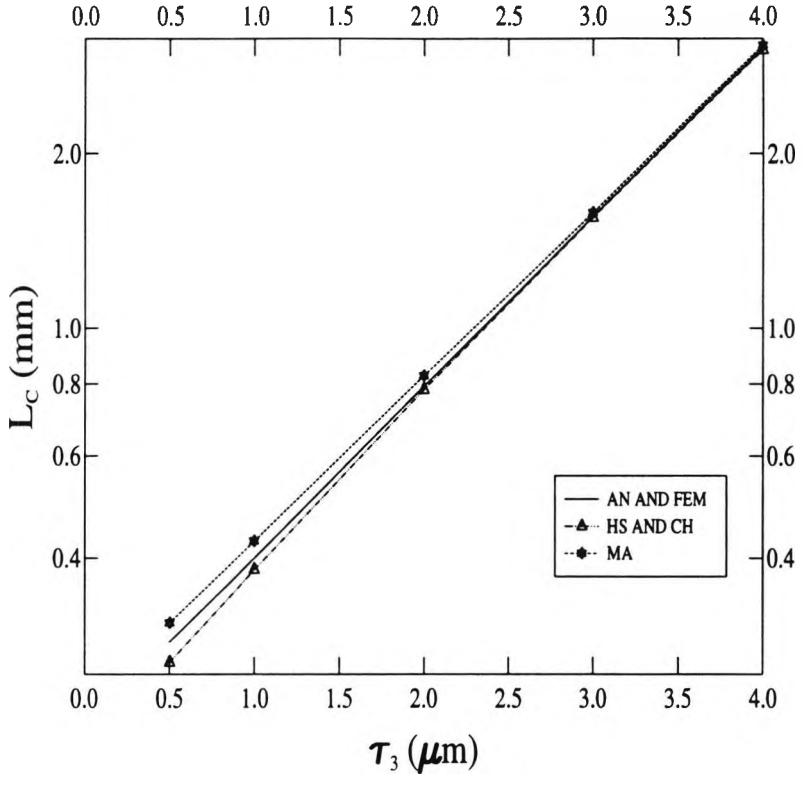

Fig. 5.12 Variation of coupling length with the separation distance, τ_3 for different approaches (the AN solution overlaps the FEM solution).

Fig. 5.13 shows the variation of C_{ab} and C_{ba} with the thickness of the guide b, τ_b, when the thickness of guide a and τ_3 are fixed at 0.15 μm and 0.4 μm respectively. It can be observed from this figure that C_{ab} and C_{ba} are identical at τ_b = 0.15 μm and slightly different when the two waveguides are nonidentical.

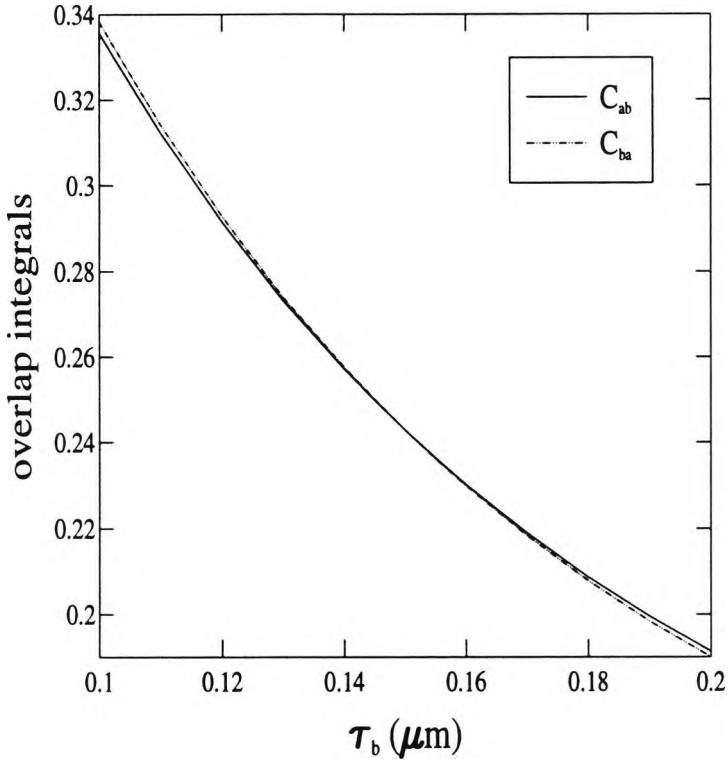

Fig. 5.13 Variation of the overlap integral C_{ab} and C_{ba} with the thickness of guide b.

Fig. 5.14 shows the variation of K_{ab} and K_{ba}, $\tilde{K}_{ab}$ and $\tilde{K}_{ba}$ with the thickness of guide b, τ_b, when the thickness of guide a and τ_3 are fixed at 0.15 μm and 0.4 μm respectively. In this figure, K_{ab} and K_{ba} are compared with the approximate coupling coefficients $\tilde{K}_{ba}$ and $\tilde{K}_{ab}$. K_{ab} reduces monotonically as τ_b increases, where as K_{ba} increases. It can be observed that the coupling coefficients are identical when $\tau_a = \tau_b$, but when the guides are not identical, the coupling coefficients can differ widely. Our results agree well with those of Hardy and Streifer (1985).

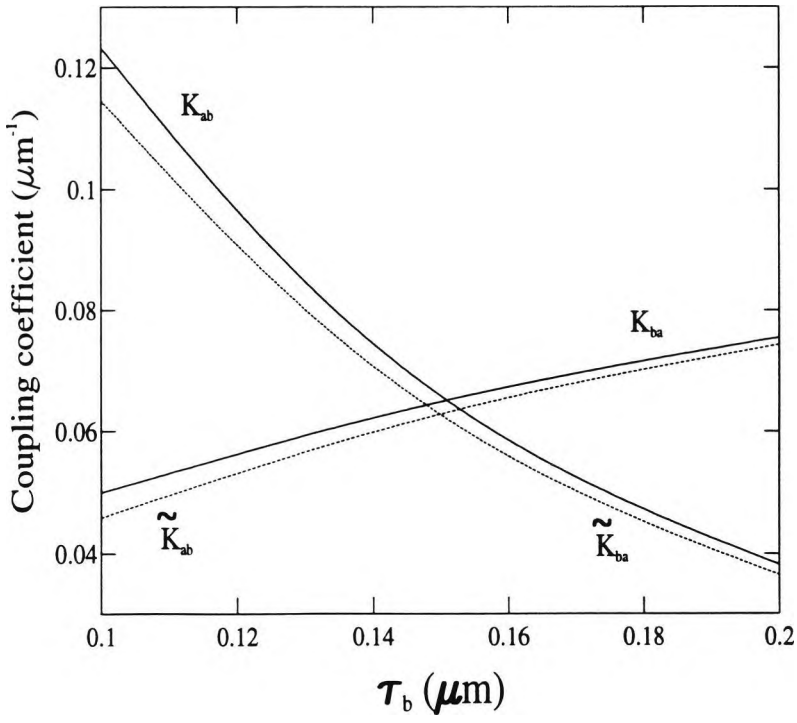

Fig. 5.14 Variation of coupling coefficients with the second guide thickness, τ_b.

One of the major emphases of this thesis has been the calculation of the power transfer efficiency between the two optical waveguides. It has been mentioned earlier that the power transfer ratio can be obtained by starting from the individual modes of the isolated guides or from the supermodes of the complete coupled structure. Results are shown later in which both approaches are used, after obtaining accurate eigenvalues and eigenvectors of the individual guides and the coupled guides.

To do so, first the amplitudes of the even and odd supermode field coefficients are calculated using the LSBR approach as discussed in section 5.2. Fig. 5.15 shows the variation of coefficients b_1 and b_2 with a second guide thickness, τ_b. When guide a is wider than guide b, ($\tau_b < \tau_a$), the amplitude of the odd-like supermode (b_2) is higher than that of the even-like supermode (b_1). Similarly, when guide b is wider than guide a ($\tau_b > \tau_a$) an even-like supermode carries more power than the odd-like supermode. It can be noted that when τ_b = 0.15 μm, although the guides are identical, the two supermodes carry unequal power, where b_1 is equal to 0.786 and b_2 is equal to 0.617. This is due to the strong coupling between the isolated modes and their inequality is responsible for a less than 100% power transfer between the guides. However, it has been shown by the authors that for weakly coupled identical guides, $b_1 \approx b_2 \approx \frac{1}{\sqrt{2}}$ and each supermode will carry half of the incident power in section **I**.

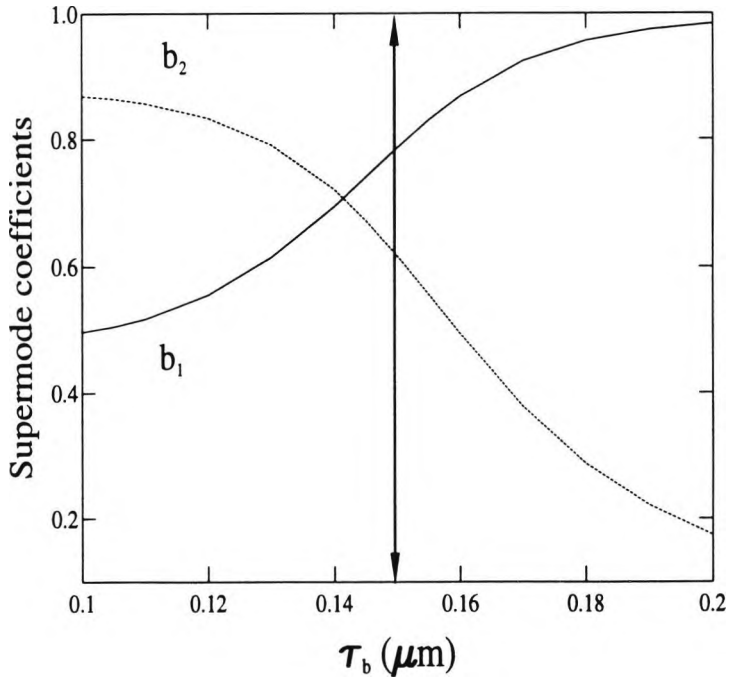

Fig. 5.15 Variation of supermode amplitude coefficients, b_1 and b_2 with the second guide thickness, τ_b.

Fig. 5.16 shows the variation of the maximum power transfer efficiency with τ_b using three different approaches. In this case the total length of the device has been adjusted to be equal to the coupling length for different values of the widths of the guide, b. Contrary to the result of the use of the coupled mode approaches, the LSBR result shows the maximum power transfer between the guides when τ_b is slightly smaller than 0.15 μm. However, it has been shown by the authors by using

the LSBR approach that maximum power transfer between the guides takes place when $\tau_b = \tau_a$, only if the guides are weakly coupled.

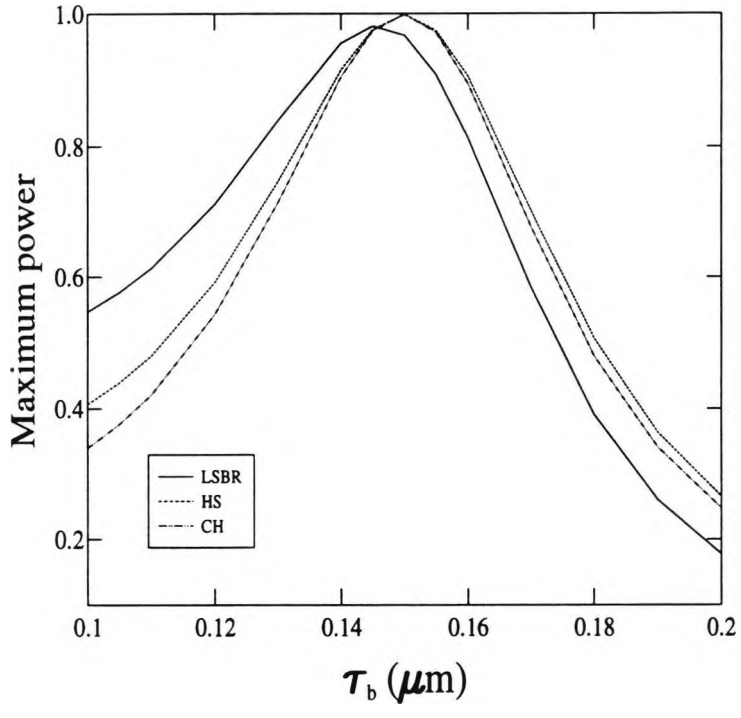

Fig. 5.16 The maximum power transfer efficiency between the guides with the second guide thickness, τ_b.

Fig. 5.17 shows the variation of the power transfer efficiency with τ_b using the coupled mode (CH) (Chuang, 1987) and LSBR approaches. In this case, the total length of the device is fixed at L_c for τ_b = 0.15 μm, where both the effect of the lack of phase synchronism and the change of the coupling length have been considered. This condition simulates the loss of synchronism due to fabrication

tolerances or to external effects. Here, the power transfer efficiency is significantly lower than the maximum power transfer, as shown in Fig. 5.16. This reduced power transfer is due to the additional effect of the coupling length mismatching as the value of L_c changes with τ_b, whereas the device length is kept fixed.

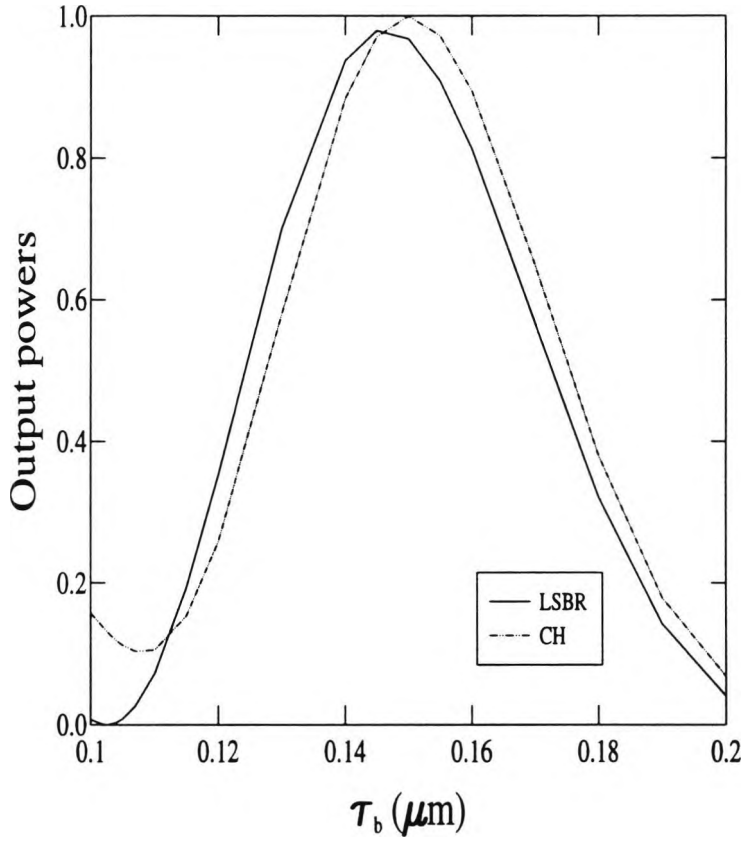

Fig. 5.17 The power transfer efficiency between the guides with the second guide thickness, τ_b for a fixed length directional coupler devices.

Table 5.2 shows the effect of mesh division for different approaches. The result, P_r, which represents different values of power in guide *a* and *b* for HS is seen to improve with increasing mesh division. However, the result from Marcatili and that of Chuang does not show such an improvement whereas the LSBR result is seen to be independent of mesh division.

L_c changed										
t_b	mesh	HS		MA		CH		LSBR		
		P_b	P_r	P_b	P_t	P_b	P_t	P_a	P_a+P_b	$(b_1+b_2)^2$
0.10	1x500	0.40321	0.0022	0.15781	1.140	0.34246	1.264			
	1x1000	0.40520	0.0008	0.15810	1.141	0.30391	1.239			
	1x2000	0.40607	0.0002	0.15824	1.141	0.30289	1.239	0.38968	1.000	1.001
	1x4000	0.40659	0.0002	0.15832	1.141	0.33961	1.263			
0.12	1x500	0.58631	0.0065	0.46244	1.237	0.54975	1.286			
	1x2000							0.58311	1.000	1.003
	1x4000	0.59194	0.0004			0.54281	1.285			
0.15	1x500	0.99250	0.015	0.99983	1.053	0.99960	1.050			
	1x1000	0.99623	0.0076	0.99996	1.056	0.99985	1.055			
	1x2000	0.99811	0.0038	0.99999	1.057	0.99992	1.057	0.99558	1.000	0.99924
	1x4000	0.99906	0.0018	1.00000	1.058	0.99993	1.058			
0.20	1x500	0.26605	0.0046	0.03869	1.034	0.24454	1.0660			
	1x2000							0.24595	1.000	0.998
	1x4000	0.26632	0.0009			0.24834	1.069			

Table 5.2 The power transfer efficiency with mesh division ($P_r = P_a - P_b$, $P_t = P_a + P_b$).

5.4 Summary

The extinction ratio for an identical directional coupler using different approaches has been presented and good agreement with the work of Chen has been seen. Results for the overlap integral, C_{ab} and C_{ba}, and the coupling coefficients, K_{ab} and K_{ba}, for planar waveguide were presented to verify the different approaches and they are seen to agree very well with those of Hardy and Streifer. The power transfer efficiency between the two waveguides was also

calculated by using the three different coupled mode approaches and the least squares boundary residual approach. All the results were seen to agree well. However, to develop further the verification and applicability of the method and to develop these approaches, a further application in directional couplers in an electro-optic switch and an optical filter will be shown in Chapter 6 and Chapter 7.

Chapter 6

Electro-Optic Directional Coupler Switch

6.1 Introduction

In chapter 5 the solution of the coupled-mode equations for strongly coupled dielectric waveguides has been described. In this chapter, the result of an investigation of electro-optic directional coupler will be shown. A knowledge of coupling between optical waveguides is important for many directional coupler-based devices, such as those, made from electro-optic materials, which are the basis of several important guided-wave devices including switches and modulators. The refractive index of the waveguide material changes due to the applied modulating field, as shown schematically in Fig. 6.1 which in turn affects the propagation constants of the two individual guides, the phase matching between them and the coupling length. When the refractive indices of the two guides are not identical, then the power transfer efficiency deteriorates, due to the lack of phase matching between the guides. All these effects, combined together, change the total power

transfer from one guide to another as a function of the applied potential, for applications to switches and modulators.

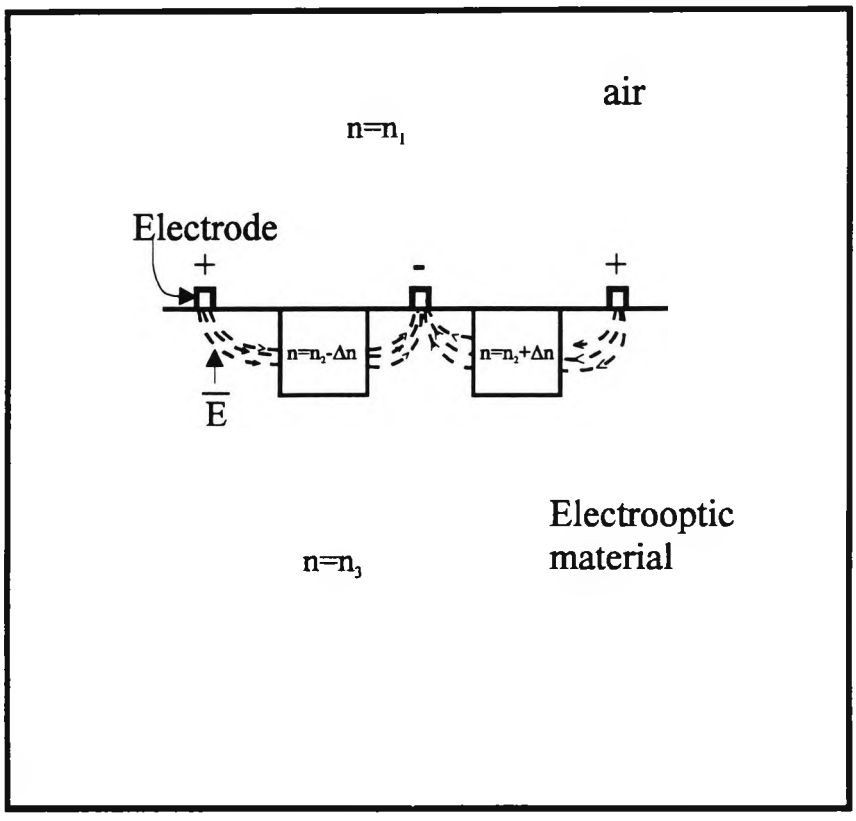

Fig. 6.1 The applied field increases the refractive index of one waveguide and decreases that of the other.

The use of the finite element method can provide an excellent means to obtain accurate modal field profiles and propagation constants for all the modes of each individual guide or for all the supermodes for a coupled structure consisting of two or more waveguides. Once the modal properties of the isolated and supermodes are known, the power transfer efficiency between the guides can be calculated by using the coupled mode approaches. Since the finite element method can provide accurate solutions for the supermodes of the coupled system, as a

complimentary approach, the Least Squares Boundary Residual (LSBR) method has also been applied in this Chapter to characterize such directional coupler devices. Beam propagation simulations based on the versatile finite element method for the transverse domain and the unconditionally stable Crank-Nicholson scheme were also undertaken to compare with the results by using the other methods.

6.2. Solution for Electro-Optic Directional Coupler Switch

In this example, a titanium-diffused $LiNb0_3$ electro-optic directional coupler switch is considered together with its simplified equivalent planar structure, as shown in Fig. 6.2. The unperturbed guides are 2 μm wide and with a refractive index value of 2.2, when no modulation is applied. The separation region between the guides is *s* μm wide with a refractive index in this region, and as well as in the two cladding regions, of value 2.19. The operating wavelength is 1.06 μm. In this work it is assumed that when a positive modulation field is applied, the refractive index in the left guide is increased by $\Delta n/2$ and decreased by an equal amount in the right guide, due to the opposite sign of the electric field, and the guides lose their identity. Although the refractive index change due to the electro-optic effect, Δn_i, can be tensor and proportional to the modulating field components, the variational formulation given by equation (2.13) can handle this, but in this planar example only an isotropic refractive index change is considered, to compare our results with published work.

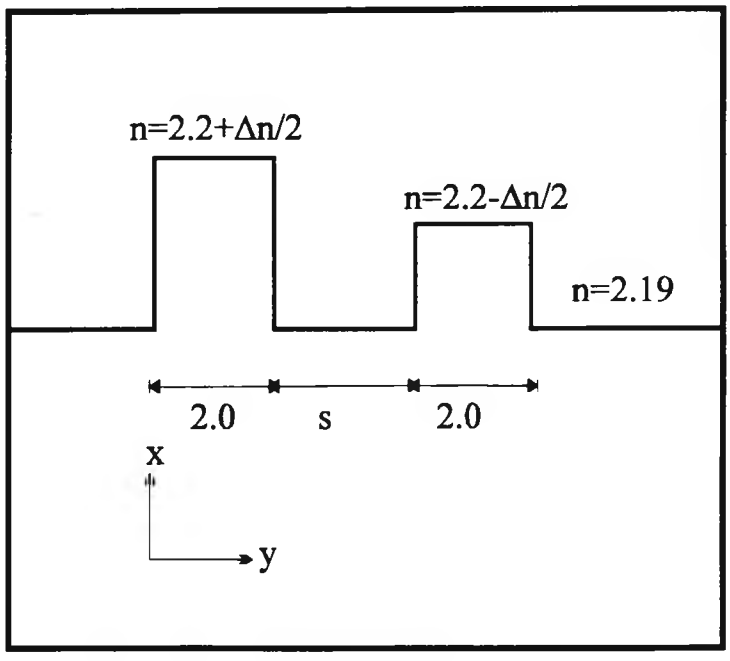

Fig. 6.2 Schematic diagram of the structure representing an electro-optic directional coupler switch.

The electric modal field profiles for the first TE supermode are shown in Fig. 6.3a for $\Delta n = 0$ and 0.002 when the guide separation, *s*, is 1.9 μm. When no modulation is applied, $\Delta n = 0$, the two guides are identical and the even and odd supermodes are symmetrical and antisymmetrical respectively. The even supermode for identical coupled guides is shown by solid line for $s = 1.9$ μm. However, when a modulation is applied, it can be observed that the first supermode is the deformed even-like mode with more power confined in the left guide which has a higher refractive index than the right guide as shown by dotted line. In Fig. 6.3(b), the field profiles for the second supermodes are shown when $\Delta n = 0$ and $\Delta n = 0.002$. It can observed that the second odd-like supermode is more confined in the right guide when $\Delta n = 0.002$, which is shown in Fig. 6.3(b). This deformation is more prominent when the guide separation, *s*, is increased ($s = 2.5$ μm) as shown in Fig.

6.4. The even supermode for identical coupled guides for different separations, s, is also shown in Fig. 6.5. It can be observed that due to increased separation between the two guides for s = 2.5 μm, the field intensity is lower at the centre of the couple structure.

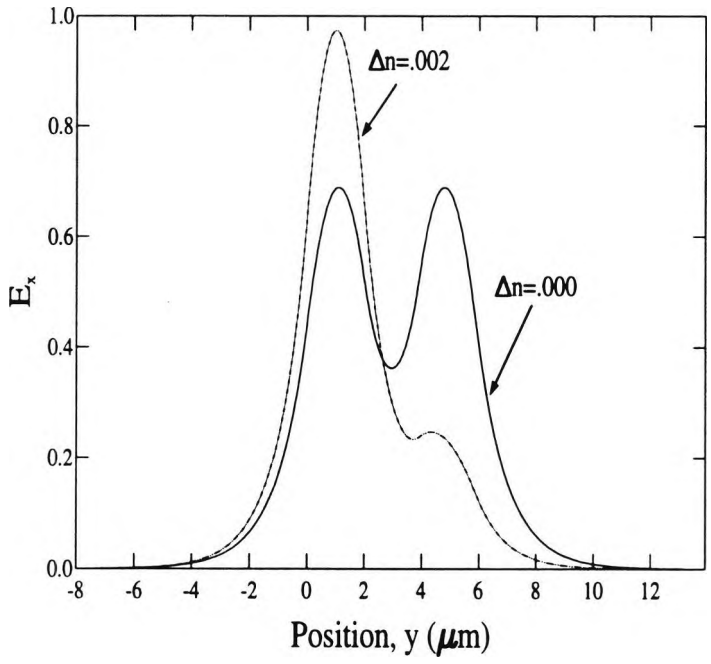

Fig. 6.3a The first TE supermode field profiles for Δn = 0, and 0.002.

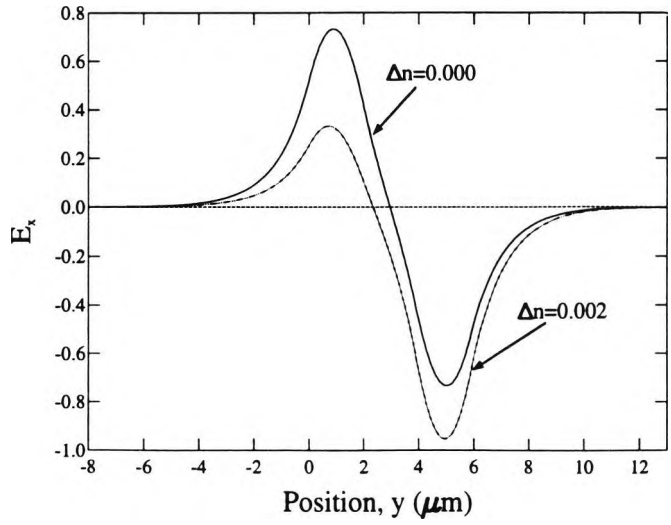

Fig. 6.3b The second TE supermode field profiles for Δn = 0, and 0.002.

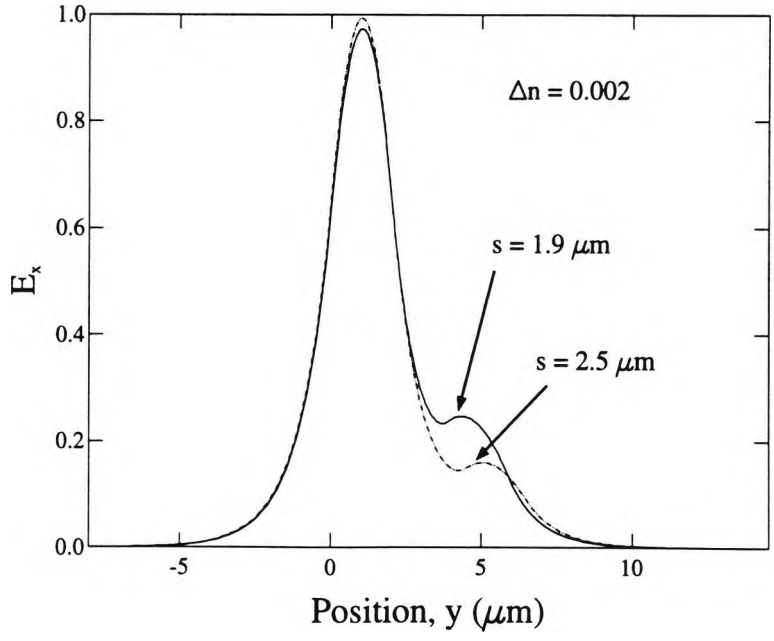

Fig. 6.4 The first TE supermode field profiles for Δn = 0.002 for different separations.

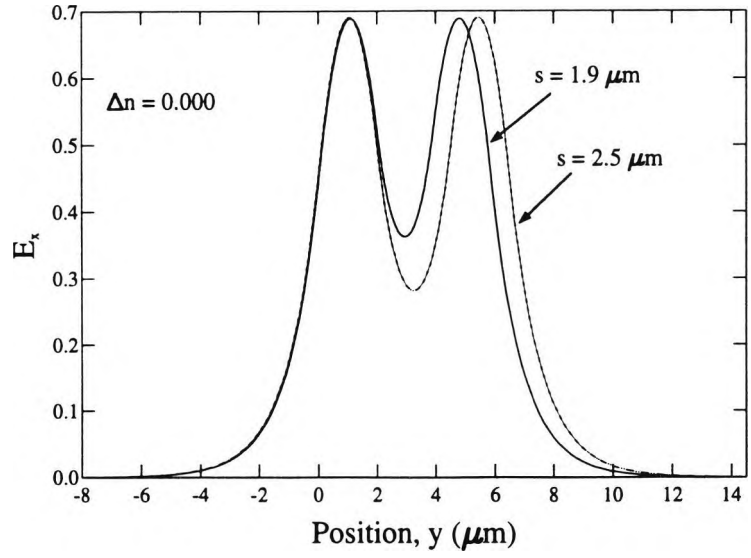

Fig. 6.5 The first TE supermode field profiles for $\Delta n = 0$ for different separations.

The coupling length decreases with the applied modulation, since the propagation constant difference, $\Delta\beta$, between the two isolated waveguide modes increases. Propagation constants of two supermodes can also be calculated from the unperturbed modes of the two isolated guides using the coupled mode approach. Fig. 6.6 shows that the coupling length variations with Δn using the analytical method [AN], the finite element method [FEM] and using the coupled mode approach [CH]. The analytical results and the finite element results are identical and cannot be distinguished one from another. The results using the coupled mode approach (Chuang, 1987) [CH] shows slight disagreement. It can be observed that

the coupling length is 296 μm when $\Delta n = 0.002$, compared to 583 μm at $\Delta n = 0$. It can also be mentioned that the coupling length varies exponentially with separation, *s*, when the two waveguides are identical at $\Delta n = 0$. However, for the larger value of Δn, the coupling length is not sensitive to the separation, *s*. This situation is due to the fact that in this case the coupling length affects mainly by the difference between the propagation constants of isolated guides *a* and *b*, *i.e.*, $|\beta_a - \beta_b|$.

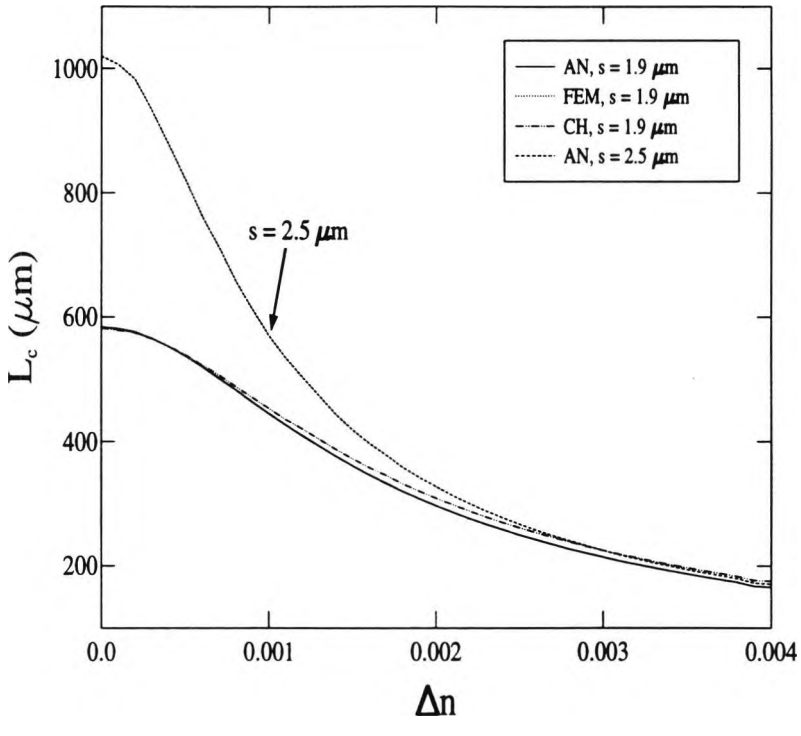

Fig. 6.6 Variation of the coupling length with Δn, using different procedures.

Next, the overlap integral, C_{ab} and C_{ba} and the coupling coefficients, K_{ab} and K_{ba} are calculated by using the coupled mode approach. Fig. 6.7 shows the variation of the coupling coefficients , K_{ab}, K_{ba} and the overlap integral, C_{ab}, C_{ba} by applying the coupled mode approach (Chuang, 1987). It can be noticed at $\Delta n = 0$, $K_{ab} = K_{ba}$, whereas when Δn increases, K_{ab} increases and K_{ba} decreases. It may also be observed that C_{ab} and C_{ba} both increase with $|\Delta n|$ and C_{ab} and C_{ba} are nearly identical.

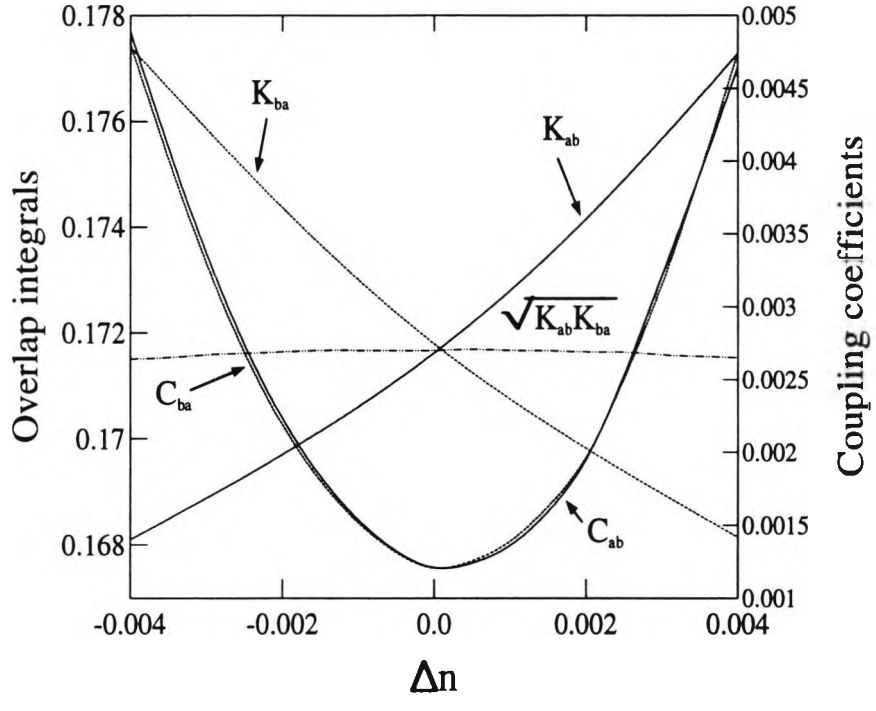

Fig. 6.7 The variation of the overlap integral and coupling coefficients with Δn.

The least-squares boundary residual method also has been applied to obtain the coefficients of the two supermodes excited at the directional coupler interface, stemming from the fundamental mode in guide *b*. Fig. 6.8 shows the variation of the supermode coefficients with Δn for different separations between the two guides, *s*. It can be observed that when Δn = 0 and the separation distance is large, $b_1 \equiv b_2 \equiv$ 0.707, which proves that the cross-talk will be insignificant. It can be seen that the coefficient of the even supermode, b_1, decreases with Δn whereas that of the odd supermode, b_2, increases. It can be also noticed that at a large separation, such as *s* = 6.0 μm, b_1 and b_2 are identical at Δn = 0 but $b_1 \rightarrow 0$ and $b_2 \rightarrow 1.0$ rapidly as Δn increases.

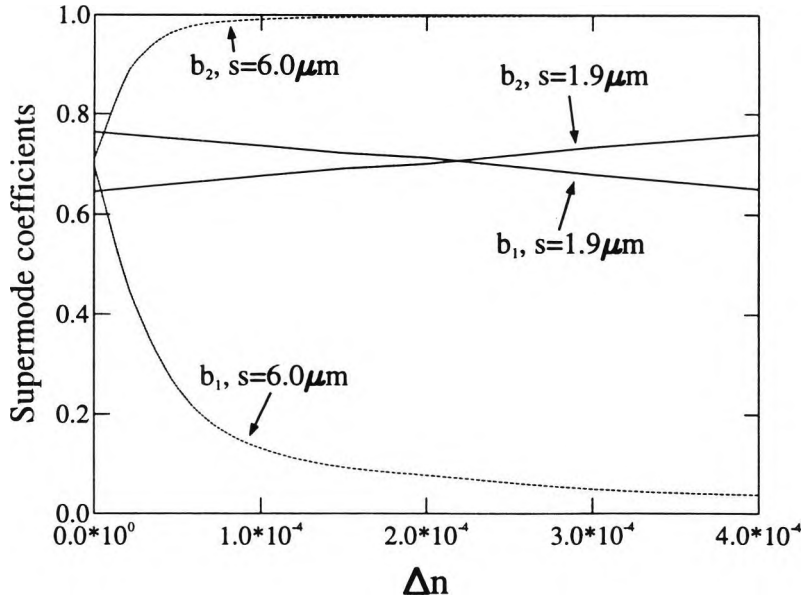

Fig. 6.8 The variation of the supermode coefficients with Δn.

Table 6.1 shows the coefficient of the even supermode, b_1, and the odd supermode, b_2, with different values of the separation, s, when $\Delta n = 0$. It can be seen that the coefficients of the even supermode and the odd supermode become equal when the two waveguides are weakly coupled.

separation, s (μm)	b_1	b_2
1.9	0.76388	0.64497
2.5	0.74470	0.66728
4.0	0.71959	0.69440
6.0	0.70969	0.70449

Table 6.1 The supermode coefficients, b_1, b_2 with different value of separation, s, for $\Delta n = 0$.

Next, the finite element based propagation method is used to follow the evolution to mode coupling from one waveguide to another. Fig. 6.9(a) shows the evolution of the optical wave propagation along the axial direction when $\Delta n = 0$, and in this case the guides are identical. The initial power was launched in guide b, and at a distance equal to the coupling length, L_{co}, most of the power has been

transferred to guide *a*. Fig. 6.9(b) shows the evolution of the optical wave propagation along the axial direction when $\Delta n = 0.0015$ and in this case the guides are not identical. It can be observed that at the coupling length, L_c, which is smaller than L_{co}, only part of the incident power in guide *b* has been transferred to guide *a*, and beyond this length, the power from guide *a* transfers back to guide *b*.

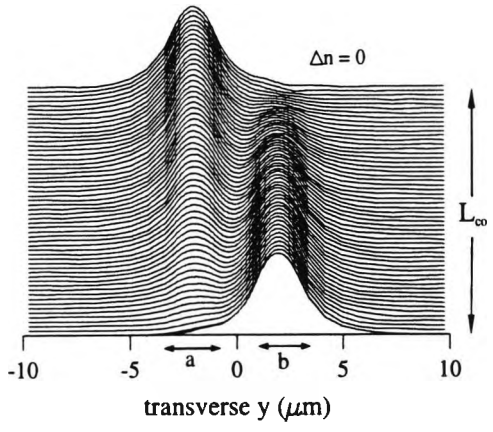

(a)

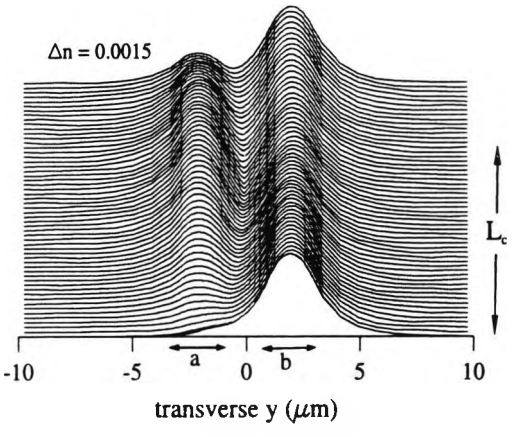

(b)

Fig. 6.9 Propagation of optical power along the axial direction when (a) $\Delta n = 0$. (b) $\Delta n = 0.0015$.

Fig. 6.10 shows the variation of the maximum power transferred from guide *b* to guide *a* with the change of refractive index difference, Δn, between the guides. This is the maximum power that can be transferred in each case by adjusting the device length to be exactly equal to its coupling length for given Δn. It can be seen that results obtained using the LSBR and the finite element propagation method agree very well but the results from the coupled mode approaches (CH) (Chuang, 1987) and (HS) (Hardy, 1985) underestimate the maximum power transfer.

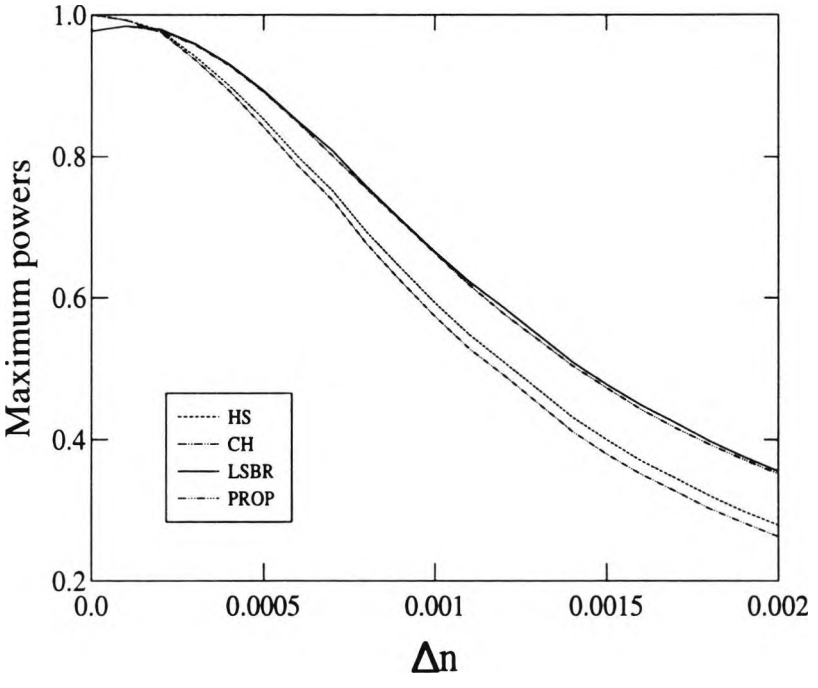

Fig. 6.10 Maximum power transfer between two coupled waveguides.

Fig. 6.11 shows the variation of the output power transfer from guide *b* to guide *a* with the change of refractive index, Δn, between the guides, when the device length is kept fixed at $L = L_{co}$ = 583 μm, which is the coupling length when no modulation is applied. Results obtained using the LSBR approach show that the power efficiency becomes nearly equal to unity, only when the guides are weakly coupled. It can be seen that the results agree reasonably well for all the approaches used. Here, the power transfer efficiency is significantly lower than the maximum power transfer, as shown in Fig. 6.10. This reduced power transfer is due to the additional effect of the coupling length mismatching as the value of L_c changes with Δn, whereas the device length is kept fixed.

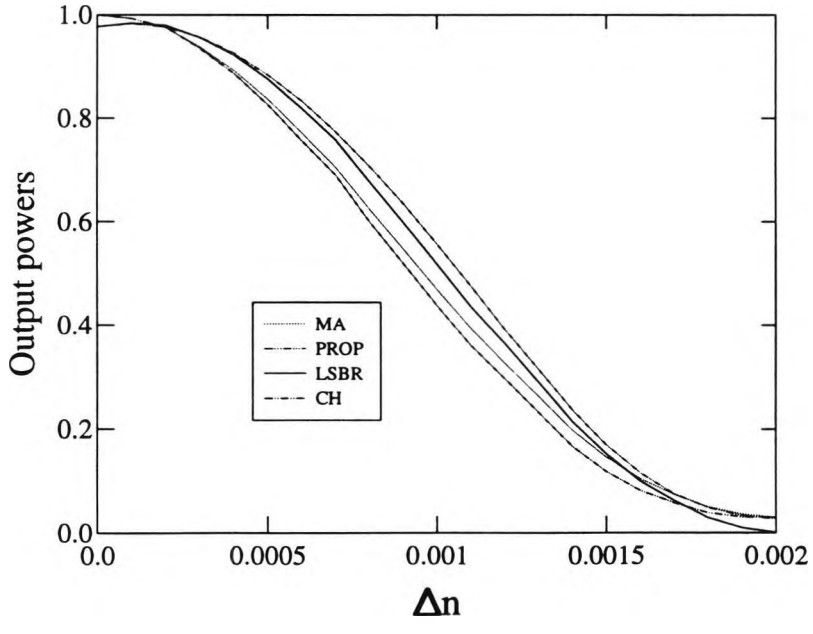

Fig. 6.11 Variation of the coupled output power in guide *a* with the refractive index change Δn.

Fig. 6.12 shows the power transfer efficiency between the guides under three different situations. The first, which is approximate and termed *A*, neglects the phase mismatch ($\Delta\beta$) but considers only the effect of the coupling length (L_c) change due to the applied modulation. It can be seen that almost 100% power transfer occurs from guide *a* to guide *b* when $\Delta n = 0$. However, as Δn increases to 0.002, the power transfer from guide *a* to guide *b* is very small. This is due to the fact that at this situation the coupling length is nearly half of the coupling length at $\Delta n = 0$, so the power moves back to guide *a* as the total device length is now twice the coupling length for $\Delta n = 0.002$. In the second approximate case, *B*, the maximum power transfer is calculated when the device length is adjusted to be identical to the coupling length for all values of Δn. In this case, only the effect of phase mismatching between the two isolated guides is considered. It can be observed that almost 100% power transfer occurs from guide *a* to guide *b* when $\Delta n = 0$ but again less power transfer is possible as Δn increases. In case *C*, as in the practical situation, the device length is fixed at $L=L_{co}$, L_{co} being the coupling length when no modulation is applied and also, in this case, the effect of phase mismatching is considered. The power transfer from guide *a* to *b* is always less than the maximum power transfer, as shown by curve *B*. Our result agrees very well with the results of Chuang (1987).

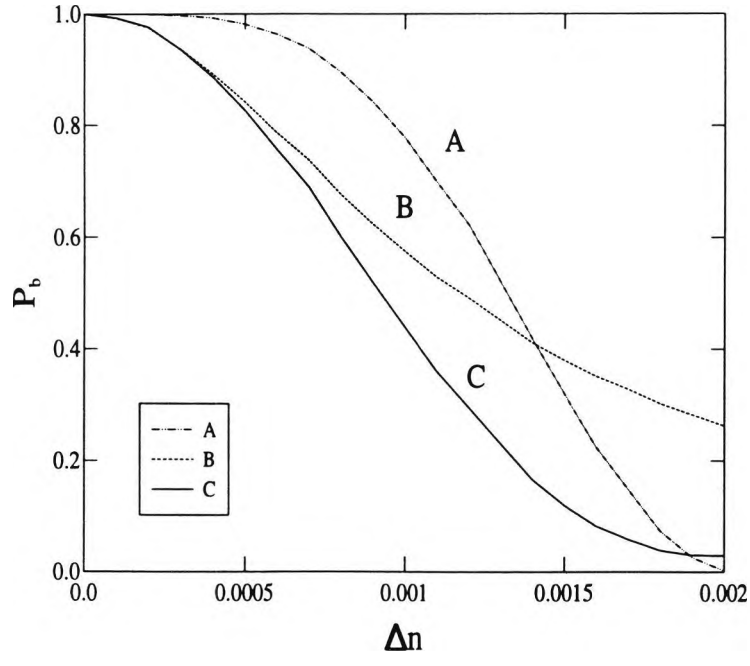

Fig. 6.12 Variation of power transfer for three different situations.

Fig. 6.13 illustrates the faster switching properties when the separation length, *s*, is increased when both coupling length and phase mismatching is considered. This is due to the fact that two isolated modes lose their synchronism faster because of reduced modal interactions. However, it should also noted that with a larger waveguide separation, *s*, the device length will be longer and fabrication tolerances may be more critical.

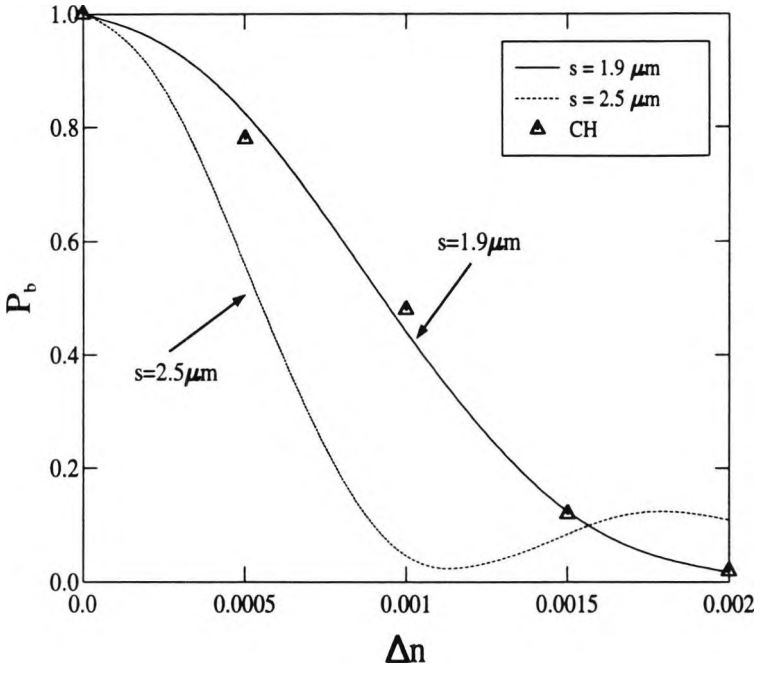

Fig. 6.13 Variation of power transfer for two separation distances between the guides.

Table 6.2 shows the power transfer efficiency with mesh division. In this case P_r is the difference of P_a and P_b, and P_t is the total of P_a and P_b and the coupling length, L_c is varied for each Δn. In order to satisfy reciprocity in a lossless waveguide system, P_a and P_b as given by equations (4.56) and (4.57) should be equal and P_t should be equal to 1.0 to satisfy energy conservation. It can be seen that the result from HS improves with mesh division but the result from CH and for the two mesh divisions used the LSBR result are seen to be independent of mesh

division. However, the results of all approaches converge with the use of a finer mesh. It can be also observed that P_b decreases with a higher value of Δn.

Δn	mesh	HS		CH		LSBR		
		P_b	P_r	P_b	P_t	P_a	P_a+P_b	b_1+b_2
0.0000	1*1000	0.99308	0.014	0.99941	1.021			
	1*2000	0.99653	0.007	0.99983	1.024	0.99146	1.000	0.99950
	1*4000	0.99827	0.003	0.99992	1.026	0.99147	1.000	0.99950
	Aitken	0.99979	0.0003	0.99994	1.028			
0.0005	1*1000	0.84607	0.011	0.85510	1.137			
	1*2000	0.84932	0.005	0.84845	1.138	0.84512	1.000	0.99972
	1*4000	0.85095	0.002	0.84507	1.139	0.84513	1.000	0.99971
	Aitken	0.85259	0.0004	0.84158	1.140			
0.0010	1*1000	0.58826	0.008	0.58662	1.168			
	1*2000	0.59066	0.004	0.58028	1.168	0.58891	1.000	0.99975
	1*4000	0.59187	0.002	0.57709	1.168	0.58893	1.000	0.99975
	Aitken	0.59310	0.00004	0.57386	1.168			
0.0020	1*1000	0.27732	0.003	0.26745	1.135			
	1*2000	0.27851	0.001	0.26498	1.134	0.27859	1.000	0.99949
	1*4000	0.27907	0.0004	0.26378	1.134	0.27862	1.000	0.99949
	Aitken	0.27957	0.00035	0.26265	1.134			

Table 6.2 The power transfer efficiency with mesh division

6.3 Summary

Results for the coupling length, L_c, the power transfer, P_a, P_b, are presented for planar waveguide to compare the applicability of the different approaches considered. Our results agree very well with those of Chuang. The formulation of Hardy and Streifer (1985) does not satisfy energy conservation and the reciprocity theorem and still contains a number of small errors, while the theory of Chuang (1987) which was derived in a much simpler way, satisfies these laws analytically.

Independently, a reformulation of the work of Hardy (1985) has been made (Streifer, 1987) recently and is identical to that of Chuang after the modifications. However, the main advantages of these approaches is their applicability for 2-D confinement structures. Some results in the application of these techniques to an optical filter directional coupler will be shown in Chapter 7.

Chapter 7

An Optical Filter using a Synchronous and Nonsynchronous Directional Coupler

7.1. Introduction

In this chapter, work is presented on the characterization of an optical filter using a synchronous and nonsynchronous directional coupler. The photonic communication systems operating at 1.30 or 1.55 μm are particularly important due to the zero fibre dispersion or extremely low loss at these wavelengths respectively. The semiconductor material system, particularly $In_{1-x}Ga_xAs_yP_{1-y}$ is suitable for the construction of a wide range of photonic components at these wavelengths. In this chapter, a novel wavelength-selective integrated optical directional coupler using *InGaAsP* waveguide embedded in *InP* is characterized. Due to the flexibility of the *InGaAsP-InP* material system, the wavelength and the bandwidth can be freely chosen in the design and electronic tuning is also possible. Very narrow bandwidths may be obtained which extend the potential applications to include wavelength-

stabilized semiconductor lasers, wavelength-modulation decoders, etc (Broberg *et al.*, 1986).

The accurate calculation of coupling parameters is of considerable interest, more specifically for strongly coupled nonidentical guides, as may be used in the design of wavelength filters. These devices with narrow bandwidth, using nonsymmetrical structures, are important for wavelength-division multiplexing in photonic devices. In the next section, the results of such identical and nonidentical directional coupler waveguides will be shown.

7.2 Directional couplers consisting of identical waveguides

In this chapter, two directional coupler examples, one identical case and the other a nonidentical case are studied in terms of their coupling length and power transfer coefficient variation with wavelength. Two slab waveguides "*a*" and "*b*" with film widths *a* and *b* are separated by a distance, *s*. The refractive indices for the guides *a* and *b*, the separation region and the cladding region are given by n_a, n_b, n_s, and n_c respectively. The materials that make up the waveguides considered here are $In_{1-x}Ga_xAs_yP_{1-y}$ for the guiding layers and *InP* for the cladding and separation layers. The refractive indices n_a and n_b for the two guiding layers, when lattice matched to *InP*, are calculated by using the formulae given by Broberg and Lindgren (1984) as shown below :

$$n = \left[1 + \frac{E_d}{E_0} + \frac{E_d E^2}{E_0^3} + \frac{\eta E^4}{\pi} \ln\left(\frac{2E_0^2 - E_g^2 - E^2}{E_g^2 - E^2}\right)\right]^{1/2} \tag{7.1}$$

where

$$\eta = \frac{\pi E_d}{2E_0^3\left(E_0^2 - E_g^2\right)} \tag{7.2}$$

$$E_0 = 0.595\,x^2(1-y) + 1.626\,xy - 1.891\,y + 0.524\,x + 3.391 \tag{7.3}$$

$$E_d = (12.36\,x - 12.71)\,y + 7.54\,x + 28.91 \tag{7.4}$$

$$E = \frac{1.240}{\lambda} \tag{7.5}$$

$$E_g(eV) = 1.35 - 0.72\,y + 0.12\,y^2 \tag{7.6}$$

$$\lambda_g(\mu m) = \frac{1.240}{E_g(eV)} \tag{7.7}$$

Fig. 7.1 shows the variation of refractive index in the guide, n_g, with the value of arsenic concentration, y. It can be seen that refractive index increases with the value of y.

The wavelength dependent refractive index of *InP* in the cladding and the separation layers is determined by the formula given by Glembocki and Piller (1985) as shown in equation 7.8.

$$n^2 = A + \frac{B\lambda^2}{\left(\lambda^2 - C^2\right)} \tag{7.8}$$

where λ is in angstroms and the constants for room temperature are $A = 7.255$, $B = 2.316$, and $C^2 = 0.3922 \times 10^8$.

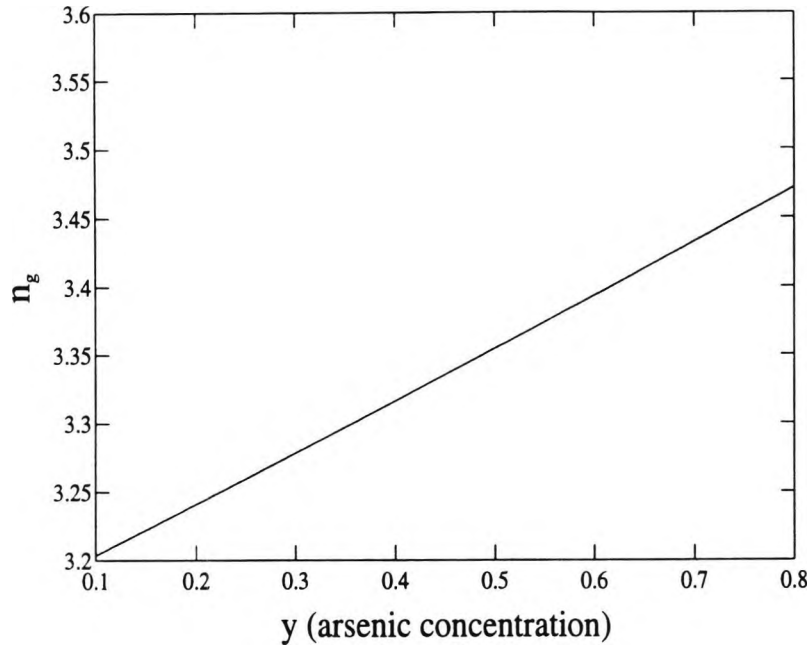

Fig. 7.1 Variation of refractive index, n_g with value of arsenic concentration, y.

Fig. 7.2 shows the variation of refractive index in guide a, b, n_a, n_b, and the separation layers, n_s with wavelength, λ for the values of y in guide a and b are 0.25 and 0.15 respectively. The refractive indices of guides a and b decrease with the wavelength, but their rates of change are different as shown in Fig. 7.2.

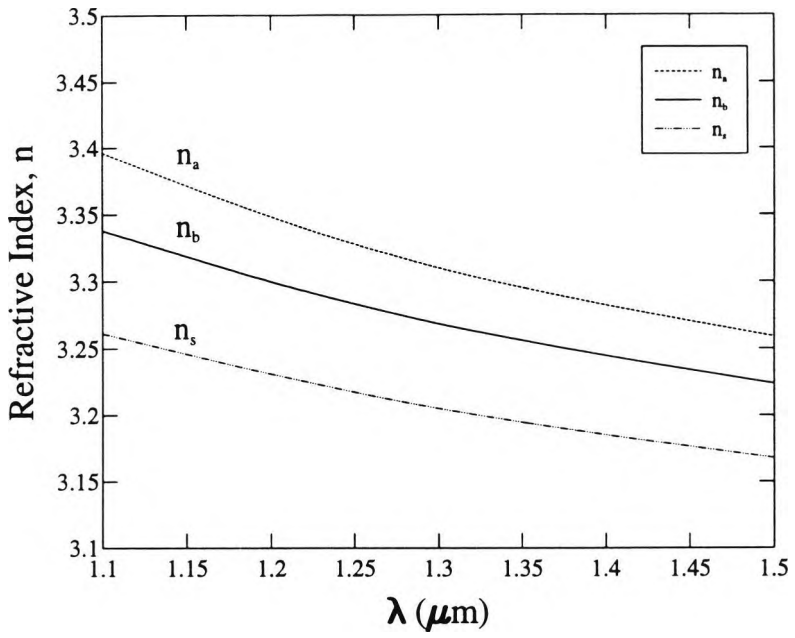

Fig. 7.2 Variation of refractive index, n with λ.

In this structure, the coupling between the two identical waveguides with their dimensions, $a = b = 1.6$ μm and the arsenic concentration, $y = 0.15$ are considered. In this example, two waveguides have identical refractive indices and these values decrease with wavelength. Here, two guides are phase matched at all wavelengths and maximum power is transferable whenever the interaction length is equal to the coupling length.

Fig. 7.3 shows the variation of the coupling length with the operating wavelength. The normalized guide dimensions decrease with the wavelength and also the refractive index differences between the guides and claddings decrease, these effects together reducing the modal confinement of two individual modes.

This reduced modal confinement increases the coupling coefficient, so the coupling length decreases with the wavelength. It can also be observed that the coupling length increases with the separation of the waveguides, because the modal interaction also decreases.

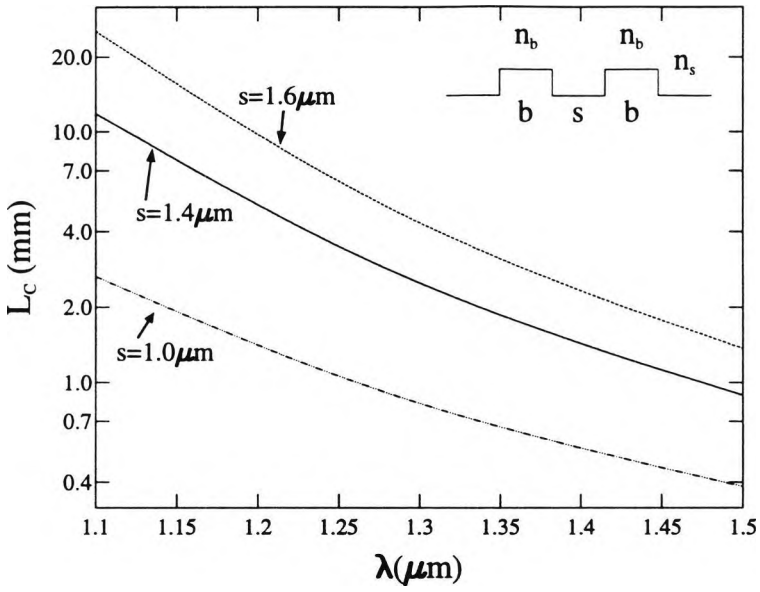

Fig. 7.3 Variation of the coupling length with the operating wavelength for coupled identical waveguides.

If the effective interaction length of the directional coupler is equal to the coupling length at 1.3 μm, then maximum power transfer is possible from one guide to another at this wavelength. However, for other wavelengths, the power transfer will be reduced, as the wavelength-dependent coupling length is not equal to the device length. Fig. 7.4 shows the maximum power transfer between the two guides with wavelength, for different waveguide separations, *s*. This figure shows that the

maximum power is transferable when the wavelength is equal to 1.3 μm, the designed wavelength. When the wavelength decreases, the maximum power transfer decreases monotonically. However, when the operating wavelength increases, the power transfer decreases and reaches zero when the wavelength-dependent coupling length becomes twice the coupling length at 1.3 μm, and after that it again increases. It can also be observed that the power transfer curve is slightly sharper when the separation between the guides is larger, although the tuning property is still very poor for the optical filter using coupled identical waveguides.

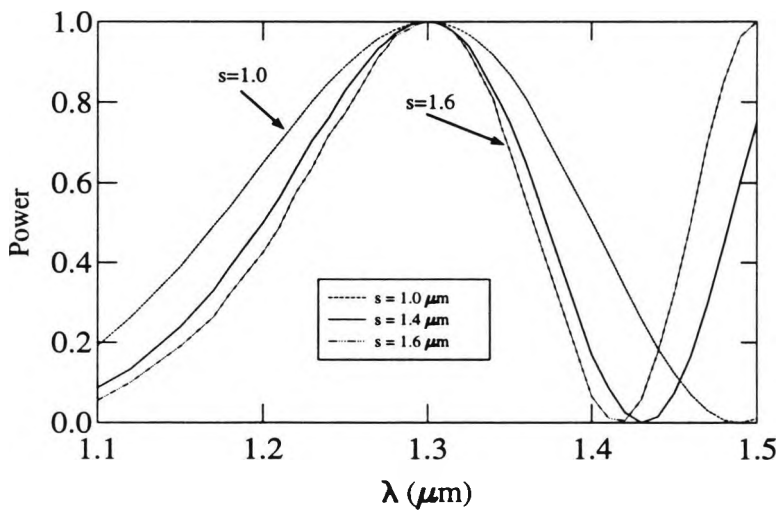

Fig. 7.4 Variation of the power transfer efficiency with the operating wavelength for coupled identical waveguides.

7.3 Directional Couplers consisting of a nonidentical waveguides

In the second example, two nonidentical guides, both index matched to *InP*, but with widths 1.6 μm and 0.53 μm and arsenic concentrations (y) of 0.15 and 0.25 respectively, are considered.

Fig. 7.5 shows the variation of β_a/β_b with the operating wavelengths, λ. It can be observed that β_a and β_b are equal at a wavelength λ = 1.30 μm. For this dimension and material combination, the two isolated guides are phase matched at a wavelength of 1.3 μm. Alternatively phase matching can be achieved at any given wavelength by adjusting waveguide parameters.

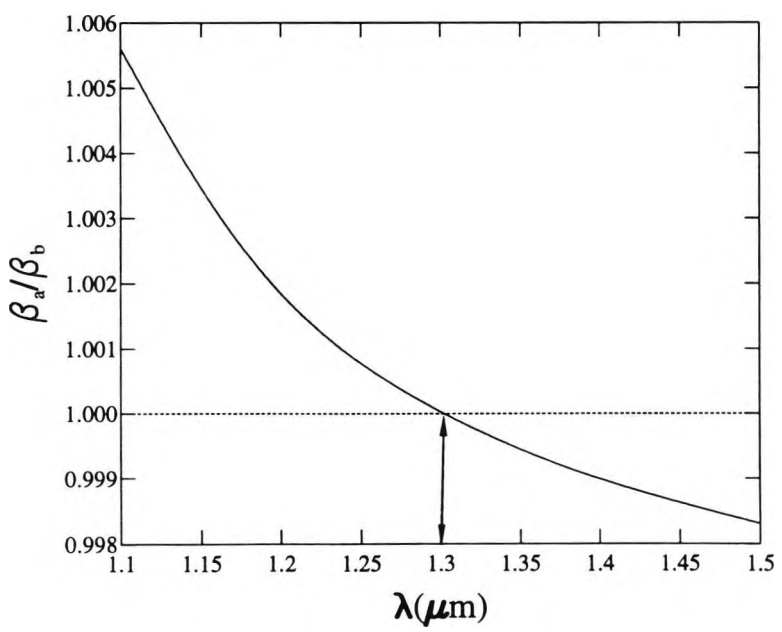

Fig. 7.5 Variation of β_a/β_b with different wavelength.

For a planar structure, analytical solutions are possible, in order to obtain the propagation constants for the even and odd supermodes β_1 and β_2 by applying field continuity at the dielectric interfaces. The finite element (FE) solutions agree very well with the analytical solutions. It can be noted here that an analytical solution cannot be obtained for a waveguide in 2-D confinement because of hybrid-mode analysis is required to satisfy the boundary conditions, but the FEM can provides accurate modal solutions for isolated guides and for coupled structures for a wide range of such practical waveguides. Starting from β_a and β_b, the propagation constants of the isolated modes, the even and odd supermodes β_1 and β_2, may be also calculated using coupled mode approximation.

Table 7.1 shows a comparison of the finite element solutions with the three different appproaches for the even and odd **TE** supermodes of the coupled structures. Here β_1 and β_2 are propagation constants for the even and odd supermodes of the coupled guides. The FEM solution is obtained by using a 1x4000 mesh division of the structure. It takes about 5 seconds to find a modal solution on Sun-Sparcstation 2 for this mesh refinement. Table 7.1 shows excellent agreement of the FEM and coupled mode approach results and if required, the accuracy can be further improved by using an even finer mesh.

λ in μm	FEM		HS		MA		CH	
	β_1	β_2	β_1	β_2	β_1	β_2	β_1	β_2
1.28	16.01373	16.00814	16.01373	16.00814	16.01373	16.00816	16.01373	16.00815
1.29	15.87338	15.86958	15.87337	15.86958	15.87338	15.86959	15.87337	15.86958
1.30	15.73609	15.73326	15.73609	15.73325	15.73610	15.73327	15.73609	15.73325
1.31	15.60200	15.59873	15.60200	15.59872	15.60202	15.59873	15.60200	15.59872
1.32	15.47080	15.46627	15.47080	15.46626	15.47082	15.46627	15.47080	15.46626

Table 7.1 Propagation constants of supermodes.

Fig. 7.6 shows the E_x field profiles for the even-like **TE** supermodes for a nonidentical directional coupler when *a* and *b* are 0.53 μm and 1.6 μm respectively, with the separation distance, s = 1.4 μm. When λ = 1.30 μm, the two isolated guides are phase matched. It can be observed that in this case the power is equally divided in two guided regions but the supermode is not symmetrical because of the asymmetrical geometry of two guides. However, when λ = 1.26 μm, it can be observed that the modal profiles are highly asymmetrical, and the first supermode is the even-like mode with most of the power confined in the guide *a*. This is because the dominant isolated mode in guide *a* has a higher propagation constant than the isolated mode in guide *b* so the first supermode with a higher propagation constant resembles more the mode E_a, when not phase matched. By contrast, the second supermode (odd-like) carries more power in guide *b*, as shown in Fig. 7.7. On the other hand, when λ = 1.34 μm, the propagation constant of the dominant mode in guide *b* is higher than the propagation constant of the similar isolated mode in guide

a, and hence the first supermode has most of the power confined in the waveguide region *b* and the second supermode carries more power in guide *a*.

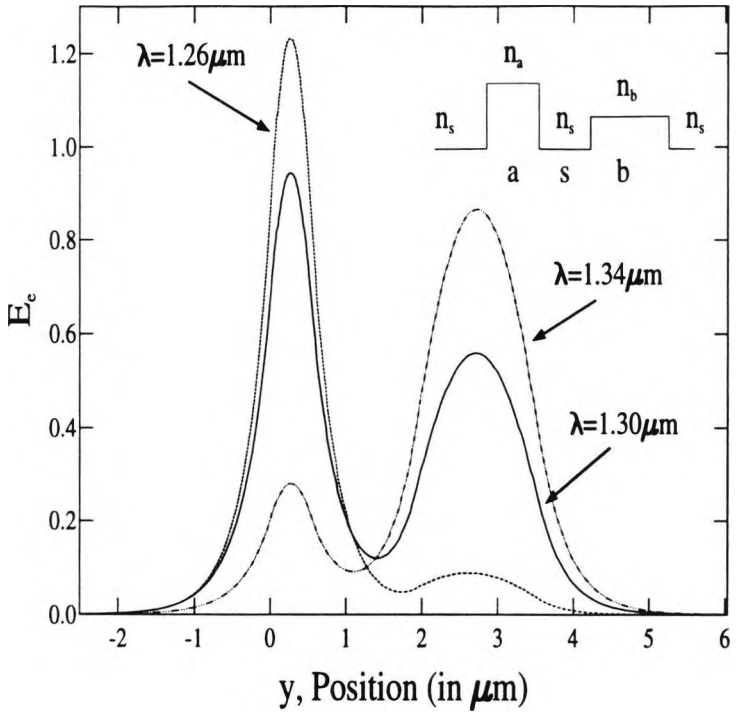

Fig. 7.6 E_x field profiles for the even-like TE supermodes.

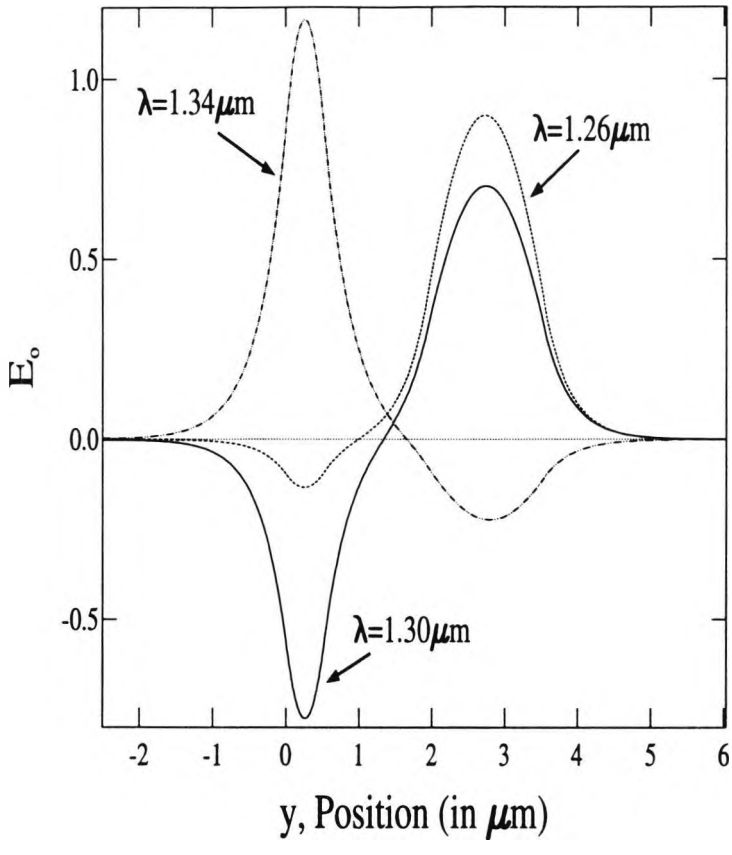

Fig. 7.7 E_x field profiles for the odd-like TE supermodes.

Fig. 7.8 shows the variation of the effective refractive index for even-like and odd-like modes with wavelength. It can be seen that the effective refractive indices decrease with wavelength. It can also be observed that the effective refractive index for the even-like mode is higher than that of odd-like mode due to the higher propagation constant. It can be observed that their phase difference is minimum at $\lambda = 1.3$ μm.

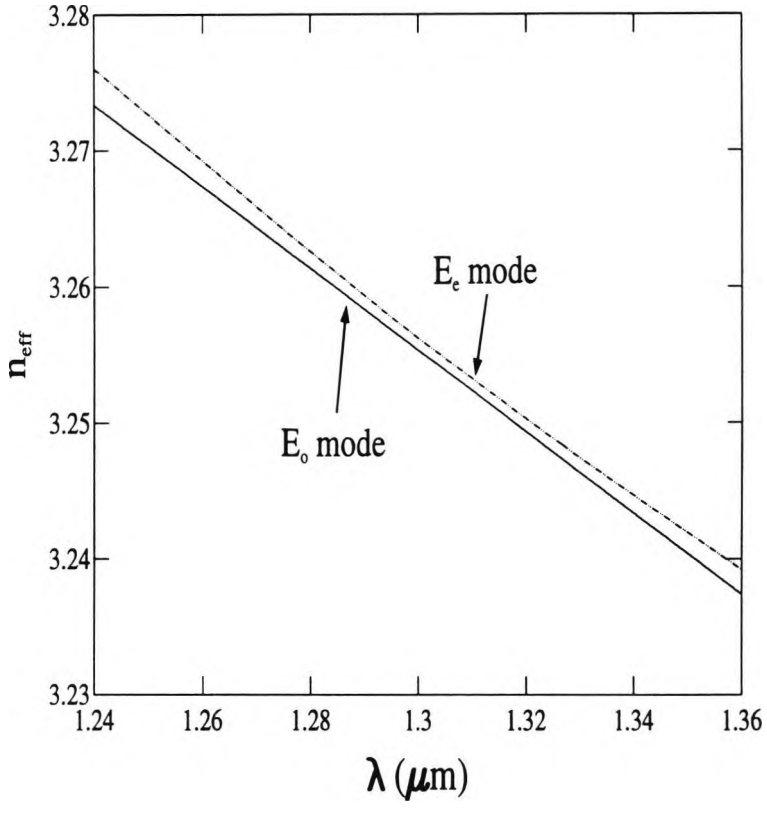

Fig. 7.8 Variation of effective refractive indices for even-like mode and odd-like mode with wavelength, λ.

Fig. 7.9 shows the variation of the coupling length with the operating frequency for this structure. It can be observed that the coupling length is a maximum at a wavelength of 1.3 μm and it decreases for other wavelengths. Further, the coupling length is higher for larger waveguide separations with sharp resonant features. When the wavelength is far away from the resonance value, the

coupling length is not sensitive to the waveguide separation, *s*. In this situation the coupling length depends mostly on the factor $|\beta_a - \beta_b|$. It can also be noted that coupling lengths are smaller for all other nonphase matching wavelengths for similar waveguide separations.

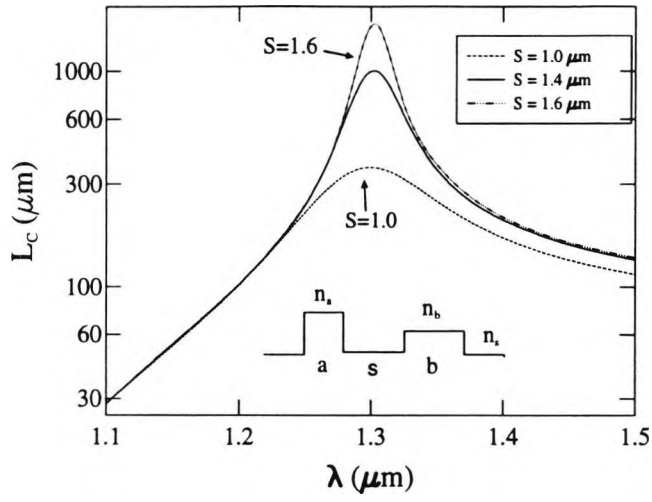

Fig. 7.9 Variation of the coupling length with the operating wavelength for coupled nonidentical waveguides.

Fig. 7.10 shows the power transfer efficiency for this same structure with the operating wavelength, by simply considering the change in the coupling length. Here, the power transfer also reduces when the wavelength is not the designed value, which is 1.3 μm, but it can be observed that nonsymmetrical couplers have a much smaller bandwidth. It should be noted that the horizontal axis of Fig. 7.9 is

expanded in comparison to Fig. 7.4. The effect of varying the separation distance is also very prominent for this example.

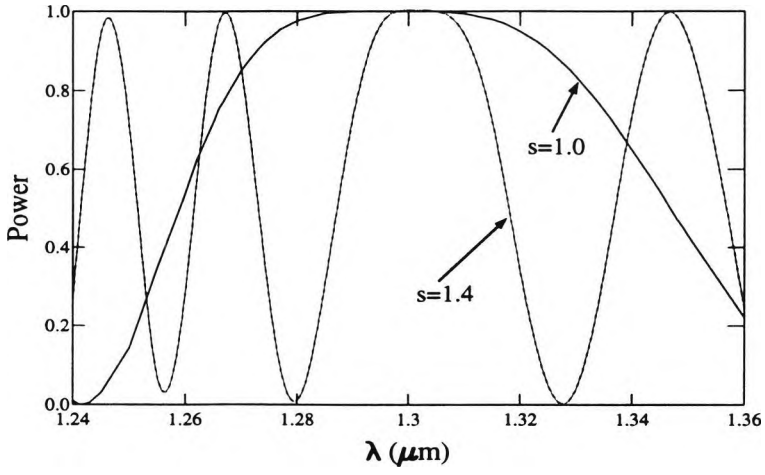

Fig. 7.10 Variation of the power transfer efficiency with the operating wavelength for coupled nonidentical waveguides by considering only the mismatching of the coupling lengths.

Next, the maximum power transfer between the two waveguides is calculated by using coupled mode theory (Hardy and Streifer, 1985). In this case, the effects of phase mismatching (Δ) and modal overlap (C_{ab}) are taken into account. Even when the device length is adjusted to make it equal to the coupling length for each wavelength, all the power cannot be transferred from one guide to the other due to a mismatch in their phase velocities. The coupling coefficient K_{ab} is the coupling per unit length from guide b to a, whereas the coupling coefficient K_{ba} is the coupling per unit length from guide a to b. Fig. 7.11 shows the variation of

the coupling coefficient K_{ab} and the coupling coefficient K_{ba} with the wavelength, λ, when the waveguide separation, s = 1.4 μm. It can be observed that K_{ab} and K_{ba} increase with wavelength and they have identical values when λ = 1.30 μm.

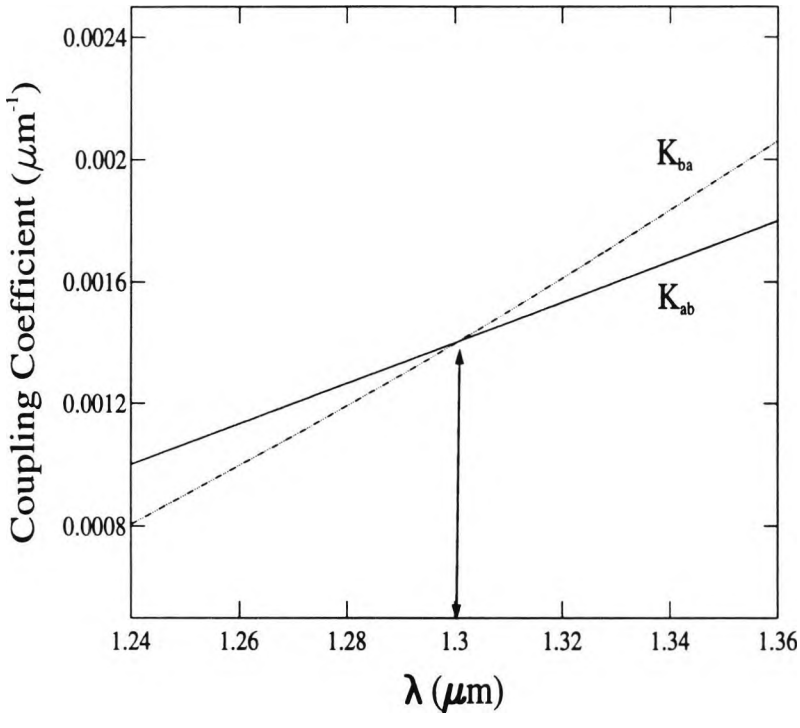

Fig. 7.11 Variation of the coupling coefficients with the operating wavelength.

The power transfer efficiency may be calculated by using the three different coupled mode approaches. Given the initial excitation at z = 0 of two coupled waveguides, P_a (z = 0) = 1 and P_b (z = 0) = 0, P_{bm} is the maximum output power in guide b. This is given as $P^{(b)}$ in equation (15) by Hardy and Streifer (1985) and as P_b in equation (26) by Chuang (1987)

Fig. 7.12 shows the variation of P_b with mesh divisions for λ = 1.31 μm and s = 1.4 μm using three different approaches. In this experiment, the λ = 1.31 μm has been selected to test a case where power remained in both the guides are significant. It can be seen that all three methods result in power converges, but at different values. The results of Hardy and Streifer (HS) agree better with those of Chuang (CH) when the mesh increases whereas the results of Marcatili show a larger deviation.

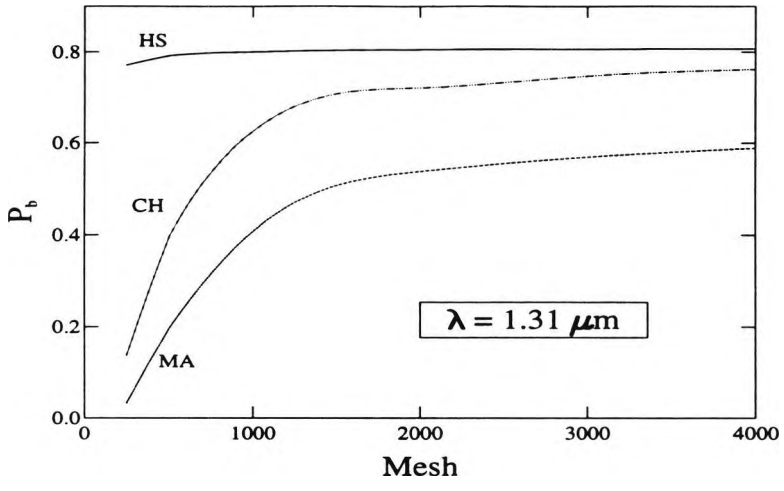

Fig. 7.12 Variation of the power transfer efficiency with mesh.

Instead, however, if the initial excitation is in guide b, (P_a (z=0) = 0 and P_b (z=0) =1), then P_{am} is the maximum power in guide a, given as $P^{(a)}$ in equation (14) by Hardy and Streifer and as P_a in equation (25) by Chuang. In order to satisfy reciprocity in a lossless waveguide system, P_{am} and P_{bm} should be equal.

Fig. 7.13 shows the variation of the different values of the power transfer efficiency P_a and P_b for the Hardy and Streifer (HS) situation with the mesh density. It can be observed that the error reduces as the mesh increases. For all the values of wavelengths, it has been found that the reciprocal error reduces monotonically with the total mesh division.

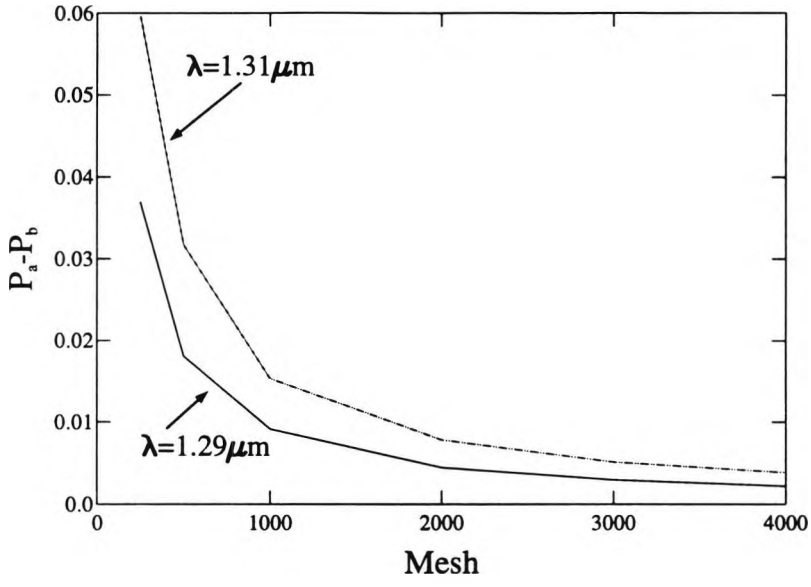

Fig. 7.13 Variation of the power difference of P_a and P_b with mesh.

Considerable disagreement between the results of the three procedures can be observed, even when a very fine mesh has been used.

Fig. 7.14 shows the maximum power transfer between the guides when the device dimension is adjusted for each wavelength, that is, in this case the lack of

power transfer due to phase mismatching only is considered. Results are also presented when the length of the device is not adjusted with the wavelength, as in the practical case, and further, phase mismatching is taken into account using the coupled mode approach.

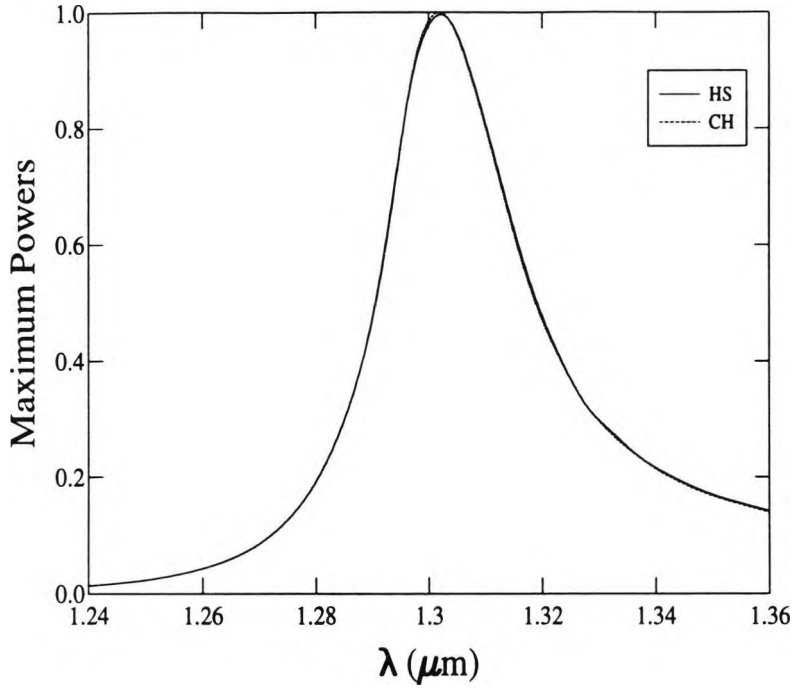

Fig.7.14 Variation of the power transfer efficiency with the operating wavelength for coupled nonidentical waveguides by considering only the phase velocity mismatching.

Fig. 7.15 shows the variation of β_a/β_b for the TM mode for several different wavelengths, λ. It can be observed that β_a and β_b are equal at a wavelength λ = 1.2627 μm. For this situation, the two isolated guides are phase matched at a

wavelength of 1.2627 μm, clearly illustrating polarization dependent properties for this structure.

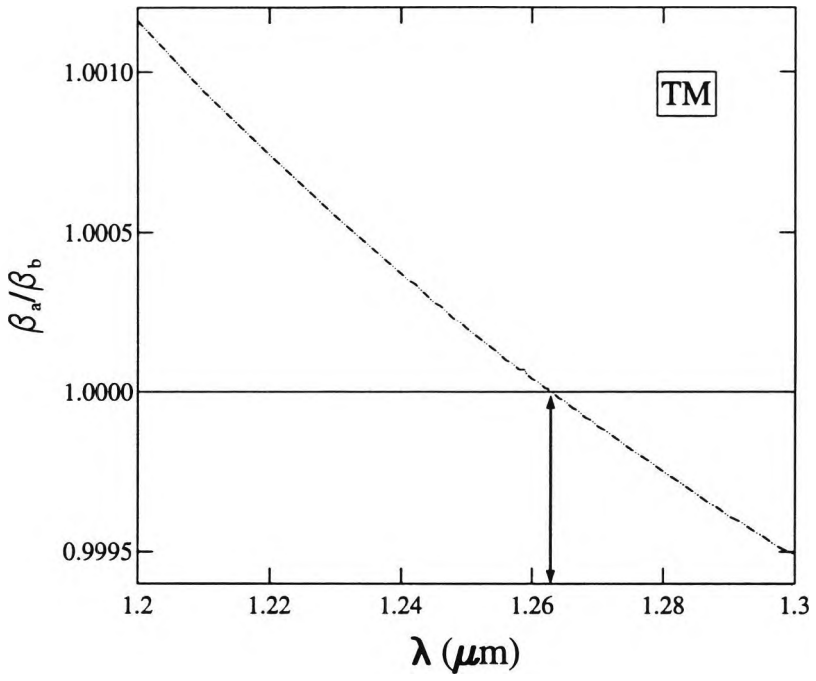

Fig. 7.15 Variation of β_a / β_b for TM mode with different wavelength.

Fig. 7.16 shows the power transfer between the two waveguides with the operating wavelength using the CH and the LSBR approaches. In this case, the total length of the device is fixed at a value L_{co}, (where L_{co} is the coupling length at $\lambda = 1.3$ μm), when both the effect of the lack of phase synchronism and the change of the coupling length have been considered. It clearly shows a filter characteristic with very sharp wavelength tuning. The results obtained agree well with those of Huang *et al.* (Huang *et al.*, 1992), who used the finite-difference based beam

propagation method (FDBPM) in their analysis. It can be noted that for TM modes there is a significant shift of the tuning wavelength, due to the vector nature of the electromagnetic waves. Additionally, a degradation of the extinction ratio for the TM mode is also observed due to the polarization dependence of the coupling length.

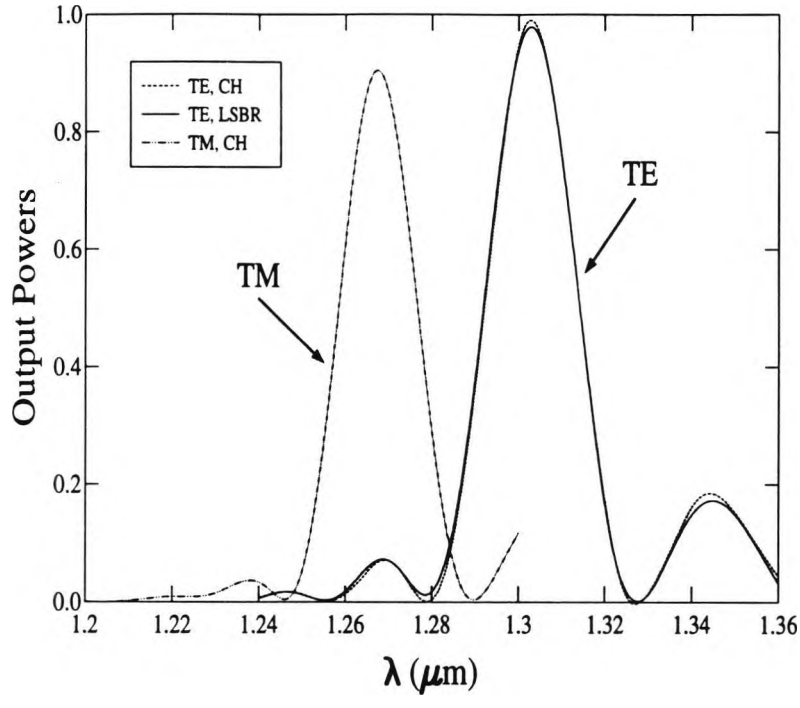

Fig. 7.16 The polarization dependence of the directional coupler filter.

7.4 Summary

The results presented in this section for optical filters using identical and nonidentical directional couplers show the comparison between the coupled mode approaches and the least squares boundary residual approach. The result of Chuang agree better with those of the least squares boundary residual approach. A polarization dependency is also shown for this structure. These agreements show the capability of the finite element method, even when it was applied to a planar waveguide, but its main advantages will be seen in the case of a 2-D confinement directional coupler which will be discussed in Chapter 8 and Chapter 9 where other simpler methods are not satisfactory. Thus, based upon the confidence given in the use of the method for several simpler approaches, it is now appropriated to apply it to several more complex problem, discussed subsequently.

Chapter 8

Characterisation of Optical Channel Waveguides Directional Couplers

8.1. Introduction

In chapters 5, 6, and 7 the solution of a planar waveguide directional coupler, in terms of various of its important operational parameters such as the width of the guide, and different values of refractive index and wavelength used, have been described. One of the practical dielectric waveguides of special interest for fabrication in integrated optics form is the channel waveguide, which is also known as the embedded strip waveguide. In its ideal form, it is a rectangular dielectric waveguide surrounded on three sides by a substrate which has a slightly smaller refractive index. The fourth side is generally exposed to the air, while most of the fields are confined in the central strip. The analysis of this type of guide is complex and no exact analytical solutions for the modes are available. The modes are nearly transverse electromagnetic as in a rectangular dielectric waveguide, having smaller longitudinal components. In order to understand the operating characteristics of such a device and to achieve an optimization of these directional

coupler-based devices, it is important to be able to predict the coupling properties between the guides. Since the design, modification, development and optimization of such devices can be both tedious and expensive, a clear need exists for an accurate and versatile design method to ensure high and consistent quality for the use of such a device.

Thus, over the years, there has been considerable interest in and importance given to the theoretical analysis of such devices. Many simple methods have been developed and used, such as the method of Marcatili (1969), and the effective index method (Knox and Toulios, 1970; Robson and Kendall, 1990; Cheng, 1991) for such analysis. However, in order to use these simple methods, the waveguide cross-section must be very much restricted to simpler cross-sections. The Beam Propagation method (Feit *et al.*, 1983) has been used to find the power transfer for axially variant coupled waveguides but with a restriction on small index differences, and it can provide only scalar solutions. The finite difference method (Schultz *et al.*, 1991) and scalar (Bersiner *et al.*, 1991) and vector (Rahman and Davies, 1984a; Koshiba *et al.*, 1984; Rahman and Davies, 1988a) finite element methods have also been used to characterise such devices. In this chapter the finite element analysis has been used to study the characterisation of optical channel waveguide directional couplers.

8.2. Application of the method

To show the usefulness of this method, some results for channel waveguide and coupled channel waveguides are presented. Such results can also be obtained for different types of waveguides, including optical fibres and semiconductor rib waveguides, with if necessary, graded or anisotropic or nonlinear materials.

Modes in channel waveguides are neither pure TE nor pure TM. In two-dimensional optical waveguides they are generally classified as the E^x_{mn} modes if the transverse electric field is primarily in the x-direction and E^y_{mn} mode if the transverse electric field is primarily in the y-direction. The m and n subscripts denote the number of maxima for the principal field component in the x and y directions, respectively. The E^x_{mn} can also be denoted as H^y_{mn} and similarly the E^y_{mn} modes as H^x_{mn} modes. The lowest order mode has $m = 1$ and $n = 1$. For most purposes, the E^x_{mn} modes can be considered as quasi-TE modes while the E^y_{mn} modes can be considered as quasi-TM modes.

8.2.1. Numerical Results for Channel Waveguide

In this example, the solutions of a simple channel waveguide are presented. The waveguide under consideration is shown schematically in Fig. 8.1. The refractive indices of the guide core, n_g, substrate, n_s, and top cladding, n_a, are 2.30 2.29 and 1.0 respectively. The dimensions of the guide core are given by the guide

width, W, and the guide depth, D, with operating wavelength, λ = 0.85 μm. The normalized propagation constant, V, used here is given as follows

$$V = \frac{\frac{\beta^2}{k^2} - n_s}{n_g - n_s} \tag{8.1}$$

where β is propagation constant and the wave number, $k = 2\pi/\lambda_0$.

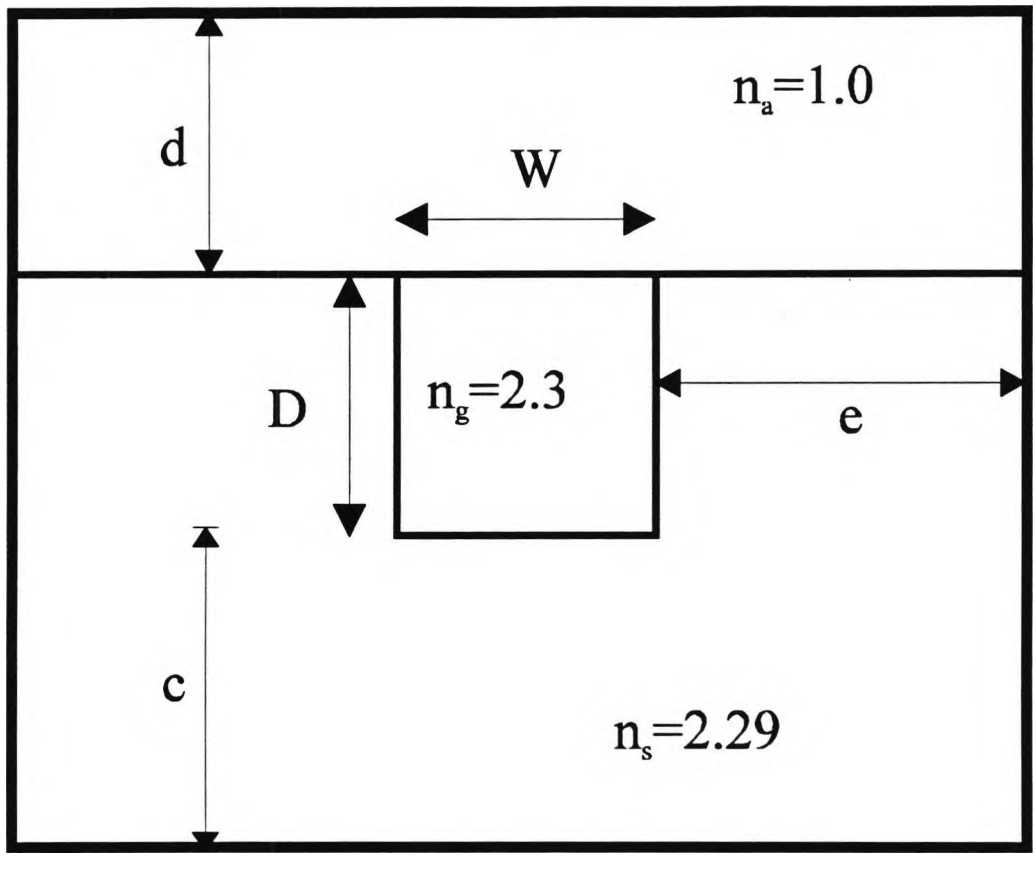

Fig. 8.1 Schematic of channel waveguide.

Fig. 8.2 shows the variation of the normalized refractive index, $n_e = \beta/k_o$, for the H_{11}^y and H_{21}^y modes (quasi TE modes) for the step index channel waveguide. In this example the guide depth, *D*, and the half-guide width, *W/2*, are varied. This wavelength structure has been analyzed using the vector **H**-formulation and 3200 first order elements. It is also necessary to select other dimensions, *c, d,* and *e* such that the orthodox boundary does not influence the solutions. Near to cut-off, the normalized propagation decreases very quickly.

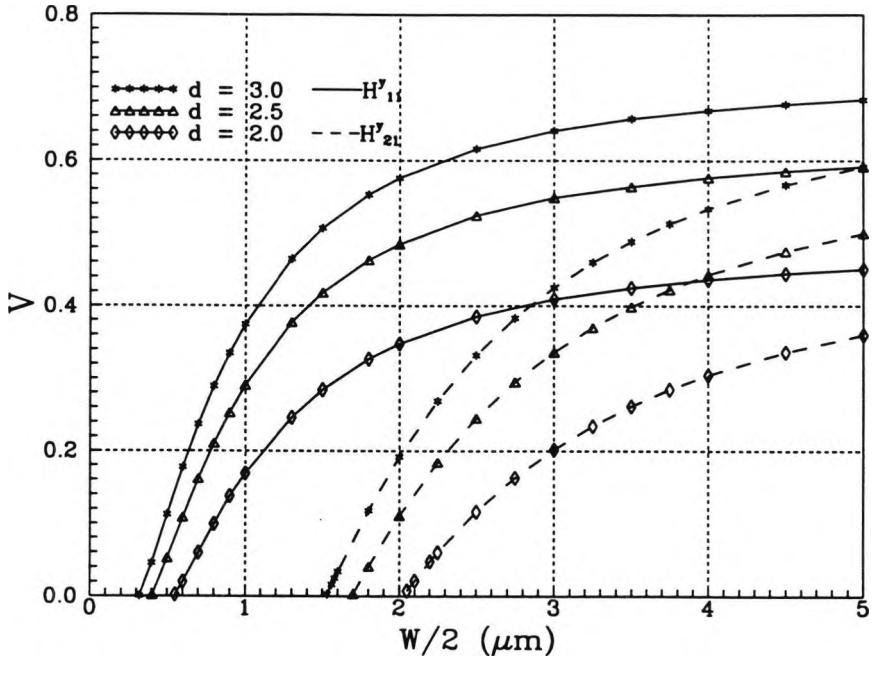

Fig. 8.2 Dispersion characteristics for a step-channel waveguide.

In the finite element method, the solution accuracy improves (Svedin, 1989) with the mesh refinement in a similar way to the finite difference method. Fig. 8.3 illustrates the effect of mesh divisions when W = 4.0 μm and D = 3.0 μm. This figure shows monotonic convergence with the mesh divisions. Note that in this figure the normalized propagation constant (which itself represents an expanded version of the propagation constant) is drawn in an enlarged scale to show this variation itself.

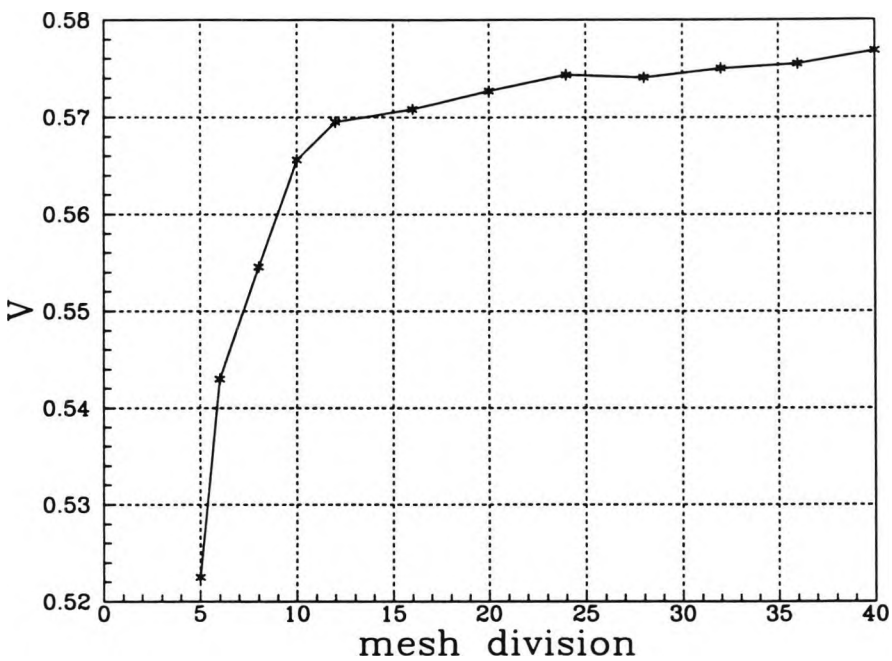

Fig. 8.3 The convergence of the finite element solution with the total number of elements.

Convergence of the finite element solution is often studied by refining the size of the elements. The accuracy of the results can be considerably increased by

the use of careful extrapolation techniques. The technique employed is based on solving the physical problem with, say, two or three rather coarse meshes and extrapolating systematically from these results, with considerable saving in computer time being produced. If the pattern of the element shapes is suitably preserved, then a powerful extrapolation procedure such as Aitken's extrapolation procedure can be employed. In this technique the mesh refinement should follow a fixed geometric ratio and the results for the three calculations may be put into the following extrapolation formula (Rahman and Davies, 1985).

$$x = x_{r+1} - \frac{(x_{r+1} - x_r)^2}{(x_{r+1} - 2x_r + x_{r-1})} \tag{8.1}$$

Table 8.1 shows the extrapolated result from the use of different mesh divisions, although the mesh divisions in the x and y directions need not be equal.

No. of division	V
9×9	0.55100
18×18	0.57200
36×36	0.57546
Extrapolated	0.57614
16×16	0.57082
24×24	0.57433
36×36	0.57546
Extrapolated	0.57600

Table 8.1 Results with the use of Aitken's extrapolation.

Perhaps the most serious difficulty in using some vector formulation is the appearance of extraneous nonphysical or spurious modes (Rahman and Davies, 1984). In the conventional vector finite element formulations such as are seen with equation (2.13), the associated Euler equation is consistent with the two Maxwell curl equations but does not imply $\nabla \cdot B = 0$, which is believed to be responsible for the spurious modes. By imposing the divergence constraint by using the penalty technique (Rahman and Davies,1984), spurious solutions can be effectively removed. Besides removing them from the region of interest, the penalty procedure also improves the eigenvector quality. A variational expression with the divergence-free constraint ($\nabla \cdot H = 0$) imposed in a least-squares sense is given by equation (2.51).

It is necessary to comment on the use of the free term α, the penalty coefficient because the accuracy of the solution depends on its value. Generally, with a larger α value, the modal solutions get more stable but their accuracy for the eigenvalues deteriorates. On the other hand, the smaller the values of α becomes, the better the accuracy of the physical solutions. However, with a smaller α value, the more spurious solution couples with a physical solution to form two degenerative eigenvectors, and then the accuracy of the physical solution may be considerably worse or be very unpredictable. By considering the eigenvalues λ_1 for $\alpha = \alpha_1$ and λ_2 for $\alpha = \alpha_2$ respectively, the correct eigenvalue λ_o ($\alpha = 0$) can be extrapolated (Hayata *et al.*, 1986). It is also observed, from our experience, that spurious solutions can be avoided by setting $\alpha \cong 1/n_s$. The error resulting is very

small for reasonable mesh refinement. Fig. 8.4 illustrates the effect of the penalty parameter for the H_{11}^{y} mode. It can be seen that an error becomes less with a finer mesh, for example the errors of mesh divisions 15×15, 20×20, 30×30 and 40×40 are 3.7%, 1.9%, 1.3% and 0.82% respectively. It can be also noticed that for below a certain value of $\alpha = 0.15$, the values of normalized propagation constants, V, are unpredictable.

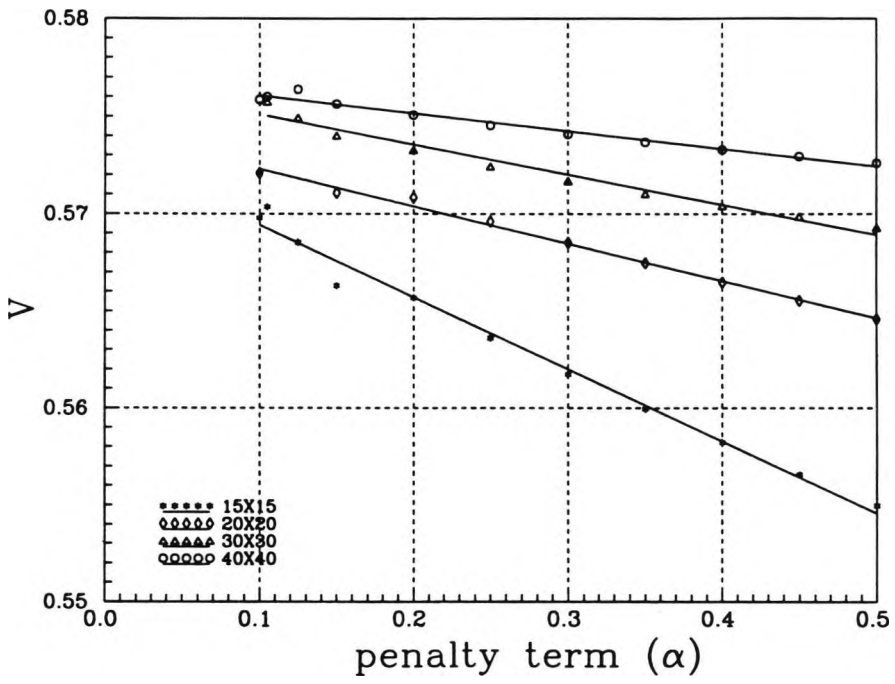

Fig. 8.4 Effect of the penalty parameter for the H_{11}^{y} mode with mesh division.

8.2.2. Solutions for the coupled channel waveguide

For this example, it is considered that the core, substrate and top cladding refractive indices are 2.30, 2.29 and 1.0 respectively as shown in Fig. 8.5, typical of

the channel waveguide used. The width and depth of the left guide are W_1, D_1, and those of the right guide are W_2, D_2 (microns) respectively. The operating optical wavelength in this example is considered to be 0.85 μm.

In a directional coupler, two optical waveguides are place in parallel, and at close proximity. The interaction of the overlapping evanescent fields of the guided modes in the individual guides causes power exchange between the coupled guides. This power exchange can be controlled by adjusting the synchronization and the coupling coefficient between the two guides. Complete energy transfer can occur between the two coupled identical waveguides if their length is equal to the coupling length, L_c, for a given separation between the guides, s. The coupling length, L_c, may be defined as the length required to achieve 180 degree relative phase shift between the two normal modes propagating along the directional coupler, *i.e.*

$$L_c = \frac{\pi}{\Delta\beta} = \frac{\pi}{\beta_e - \beta_o} \tag{8.2}$$

where β_e and β_o are the propagation constants of the even and odd supermodes of the coupled guides.

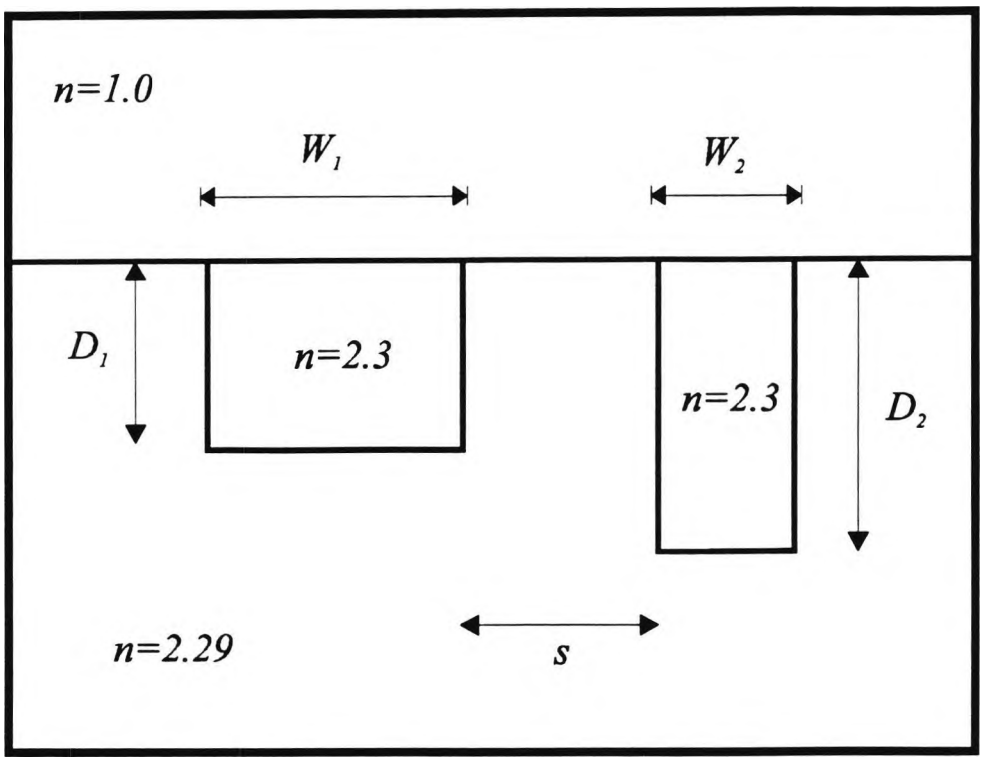

Fig. 8.5 Asymmetrical channel waveguide directional coupler.

Fig. 8.6 illustrates the variation of the propagation constants for the "even-like" and "odd-like" supermodes with the variation of the width of the second channel waveguide, W_2, for different guide separations, s. In this example the depth, D_1, and the width, W_1, of the first guide are 2.5 μm and 2.6 μm respectively and the depth of the second guide, D_2, is 3.0 μm. The two guides are not identical but when W_2 is 2.0 μm, the propagation constants of the two isolated guides are identical, that is they are phase matched. In this situation, the two supermodes are almost the even and odd types and there can be full transfer of power between the two guides. The top curves E_1 and E_2 are representative of the first supermodes which are even or even-like supermodes, whereas the lower curves O_1 and O_2 are for the second

supermodes which are odd or odd-like supermodes. When the width of the second guide, W_2, is larger than necessary for the synchronous condition (i.e. $W_2 > 2.0$ μm) then the first supermodes almost resemble the modes of the isolated second guide and second supermode resembles that of the isolated first guide.

However, when W_2 is smaller than 2.0 μm, the first supermodes resemble those of the first isolated guide and second supermodes resemble those of the second isolated guide. The above statement is true for all the values of waveguide separation, s, but when the guides are in close proximity, the coupling between them is larger. The effect of the separation distance on the field profiles for the same waveguide dimensions can also be seen from the eigenvectors drawn in Fig. 8.6. For the finite element results presented in this work, 4320 first order triangular elements are used to represent the complete coupled waveguide cross-section and the resulting order of the matrix eigenvalue equation is 6771. This takes about 20 minutes of CPU time on Sun Sparcstation 2, to find the propagation constant and the associated vector field profiles using a sparse solver.

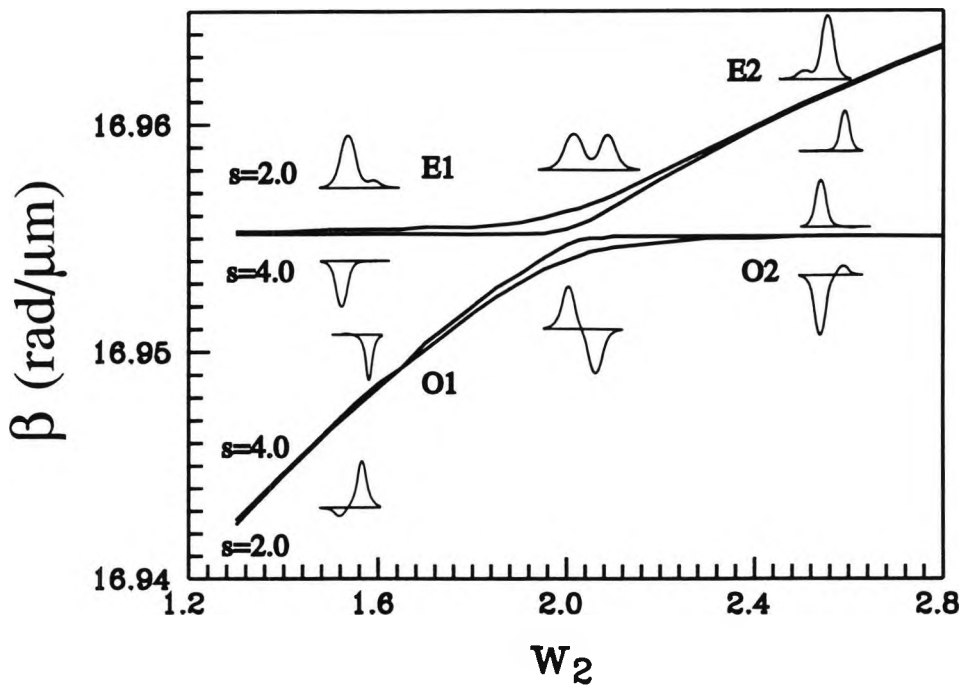

Fig. 8.6 Variation of propagation constants of the first two quasi-TE supermodes.

Fig. 8.7 shows the variation of the propagation constants for the "even-like" and "odd-like" supermodes with the variation of the separation, *s*. In this case, the depth, D_1, and width, W_1, of the first guide are 2.5 μm and 2.6 μm respectively and the depth and width of the second guide, D_2, are 3.0 μm and 2.01 μm respectively. The propagation constants of the two guide are almost those of the propagation of the isolated guide when the separation, *s*, increases.

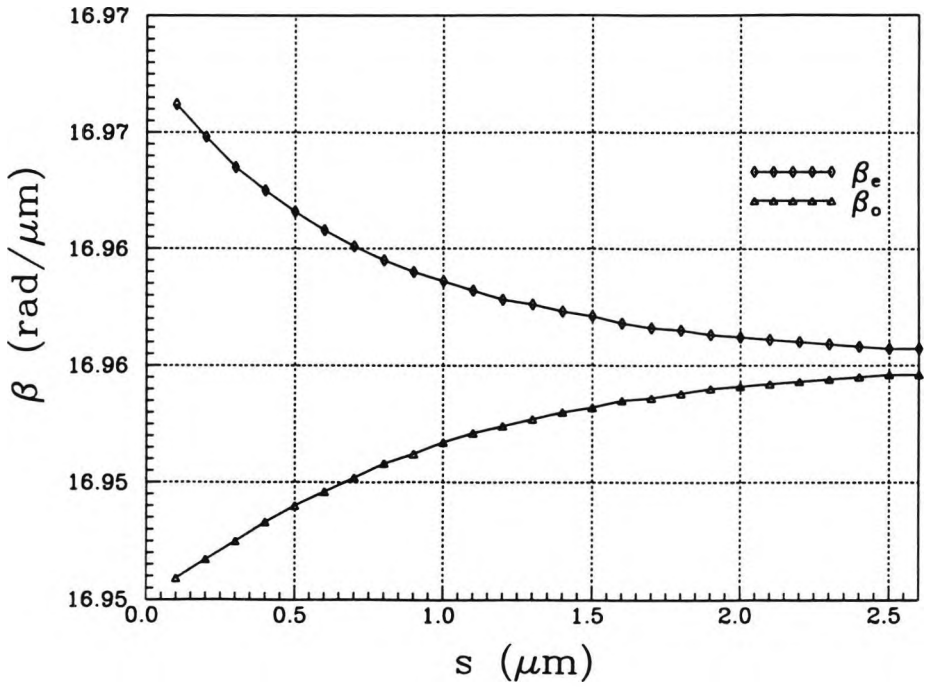

Fig. 8.7 Variation of the propagation constants for the even-like and odd-like supermodes with separation, *s*.

Fig. 8.8 shows the variation of the coupling length, L_c, with the half separation distance, *s*, for four different waveguide cross-sections when the two guides are identical, *i.e.*, $W_1 = W_2$, $D_1 = D_2$. It can be seen from this figure that L_c becomes larger with increasing *s* and follows an exponential law, so the L_c vs *s* plot is linear on a log-linear scale. To reduce the device length, a benefit in practical applications where space may be limited, it is important to have a shorter value of L_c which in turn requires a strong coupling between the guides. Unlike the finite element method, many simple methods of analysis which are based on the perturbation of the normal modes of the two individual guides fail to preserve the orthogonality of the supermodes and power conservation criteria in strong coupling situations.

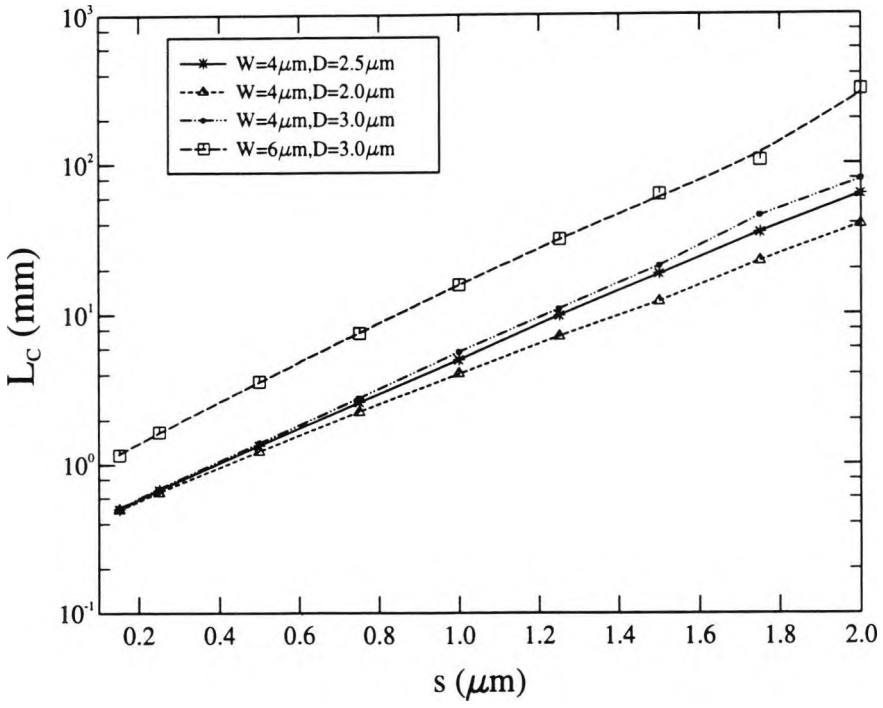

Fig. 8.8 Variation of the coupling length with the separation distance.

Due to fabrication tolerances, it is not always possible precisely to control the waveguide dimensions W and D or the refractive indices in different regions. It is important to see the effect of such a variation on the coupling lengths. Fig. 8.9 shows this variation of the coupling length with the change in the width fraction (W/W_0) for two different half-separation distances, s. When the half-separation distance, s = 0.5 μm, the central coupling length required is 0.688 mm, compared to 2.13 mm when s = 1.0 μm. Although $\Delta L_c/\Delta W$ is smaller for smaller separation distances, its effect on the power transfer will be detrimental as $\Delta L_c/L_c$ becomes higher, which introduces significant cross-talk. It can be also noticed that slope increases with larger separation, s, *i.e.*, the effect of coupling length, L_c, becomes

more significant with longer device length. The percentage changes are of 1.13% and 5.03% when the half-separation distances, *s*, are 0.5 μm and 1.0 μm respectively.

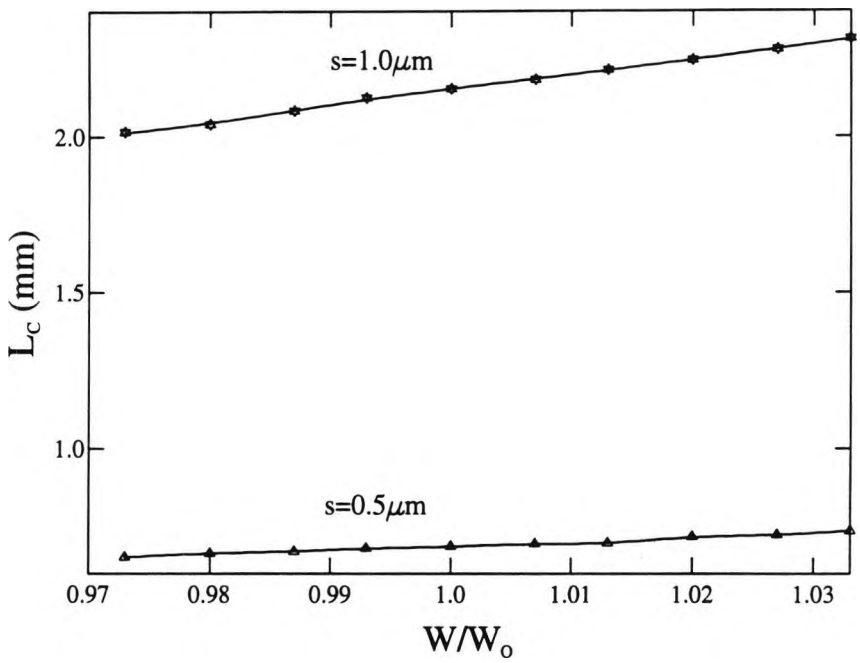

Fig. 8.9 Variation of the coupling length with W/W_o for different half-separation distances.

Similarly Fig. 8.10 shows the variation of the coupling length with the tolerance of the guide depth (D/D_0). It can be seen that the effect of tolerances of guide depth and guide width are in the same law, *i.e.*, slope is more sharp with larger separation, *s*. The variation of the coupling length changes 0.5% and 4.1% when the half-separation are 0.5 μm and 1.0 μm respectively.

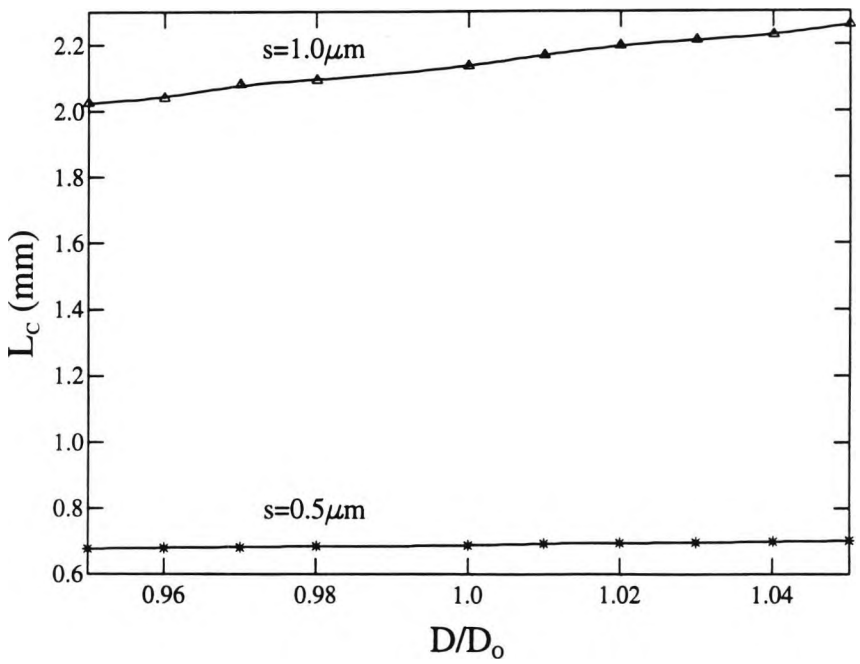

Fig. 8.10 Variation of the coupling length with D/D_o for different half-separation distances.

However, the effect of structural asymmetry due to the fabrication procedure is much more severe in its effect on their performance than the symmetrical structural deviations. This is because the two modes in the two isolated nonidentical guides will have different propagation constants, β, and will not be phase matched to transfer power effectively between the guides. Fig. 8.11 shows the variation of the coupling length, L_c, with the second waveguide width, W_2, for various waveguide separations when W_1, D_1 and D_2 are 2.6 μm, 2.5 μm and 3.0 μ m respectively. When the two waveguides are phase matched, Δβ is a minimum and so the value of L_c is highest at that point. L_c decreases steadily away from the synchronous position and in this condition only negligible power can be transferred

between the waveguides as their propagation constants are different. When the separation between the guides, s, increases L_c is very high at the phase matching condition and decreases very sharply away from this point, in which case a very sharp frequency response is possible. Although such unintentional loss of phase matching in couplers, designed to be symmetrical may not be desirable, specially designed asymmetrical couplers have excellent wavelength-dependent coupling ratios and find their application in the construction of wavelength division multi/demultiplexing systems.

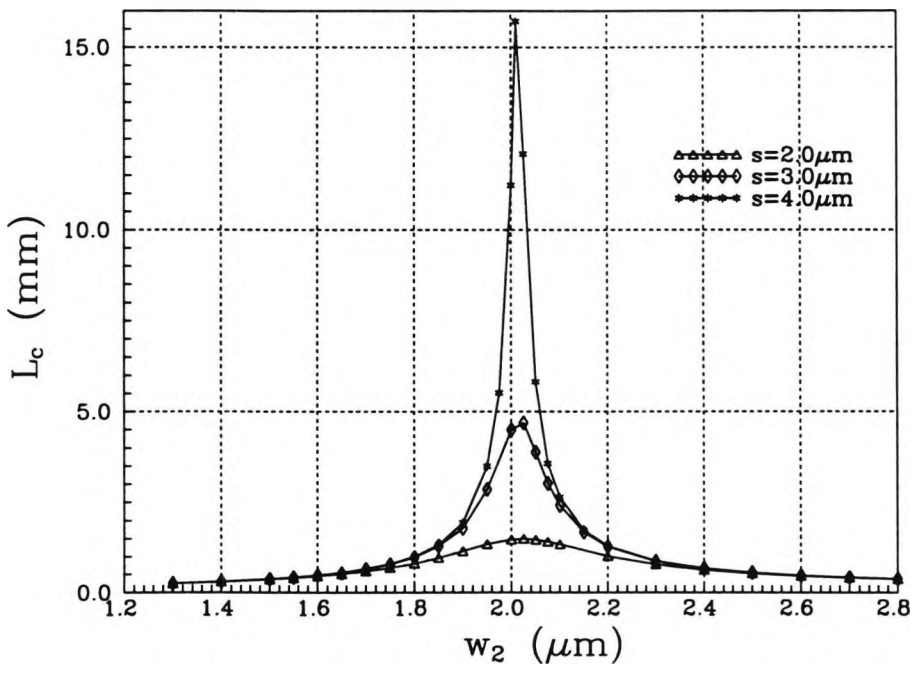

Fig. 8.11 Variation of the coupling length with W_2.

Fig. 8.12(a) shows the H_y field (the dominant component) for the H_{11}^y even mode, when the two isolated guides are phase matched. It can be observed that the supermode is nearly symmetrical but reflecting only the slight asymmetry of the individual guide cores. Fig. 8.12(b) shows the H_y field contour for the H_{11}^y odd supermode which is nearly antisymmetrical. Fig. 8.12(c) shows the H_y field of the even-like mode at W_2 = 1.8 μm and in this case the two waveguides are not phase matched. In this situation, as the eigenvalue of the left isolated guide is higher than that of the isolated right guide and so for this, in the first supermode (even-like) more power is concentrated in the left-hand side. By contrast, the second supermode (odd-like) carries more power in the right-hand side guide, as shown in Figure 8.12(d).

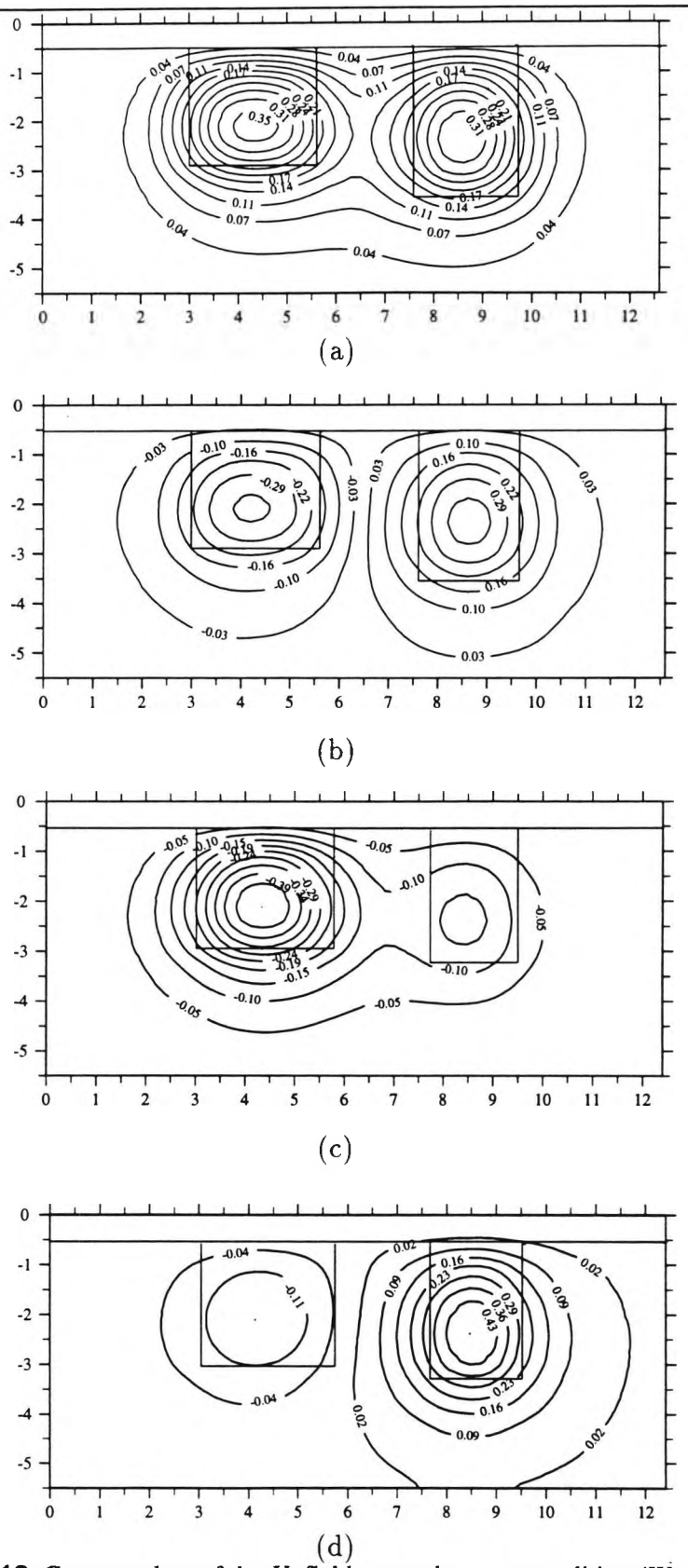

Fig. 8.12 Contour plots of the H_y field at synchronous condition (W_2 = 2.0 μm) (a) Even supermode, (b) odd supermode; Nonsynchronous modes at W_2 = 1.8 μm, (c) Even-like supermode, (d) Odd-like supermode.

In optical circuits, it is essential to have bent or curved guiding sections to connect the directional coupler region to other optical devices which may be employed, such as optical fibres. The separation between the guides is increased outside the coupling region either by introducing a sloped straight or a curved *S* section, as shown in Fig. 8.13(a) and 8.13(b). These bent or curved sections will introduce an offset or radiation loss. It is desirable that power transfer should be only in the actual directional coupler region and there should not be any power transfer between the two connecting guides, but in fact, there will always be some transfer of power in this region.

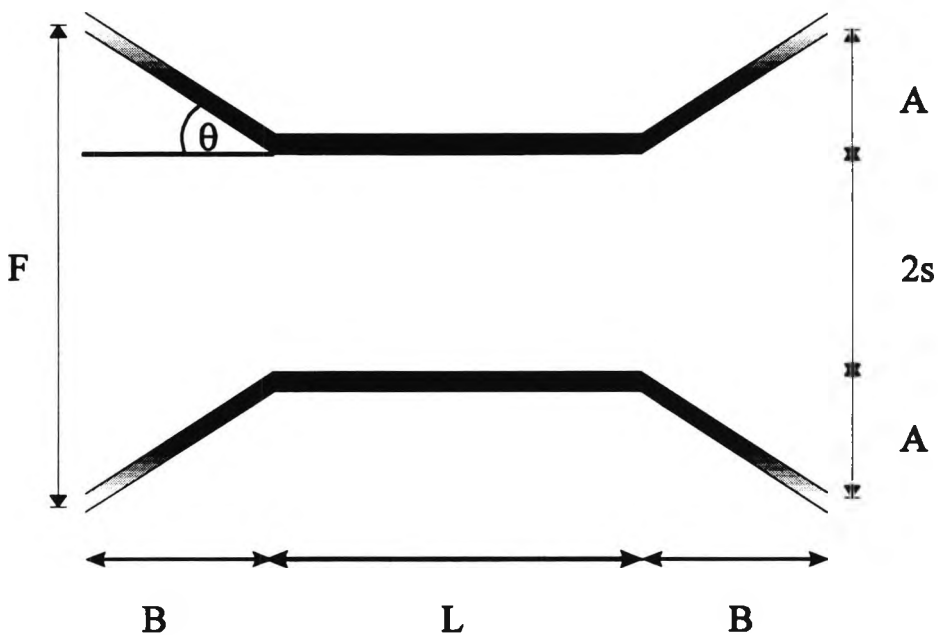

(a)

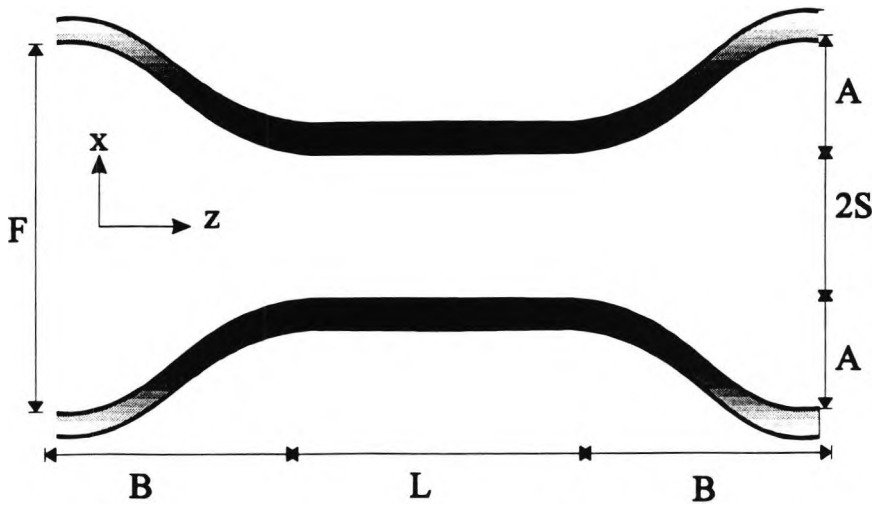

(b)

Fig. 8.13 Input and output sections of directional couplers (a) straight line approach (b) curved *S* shaped approach.

If the angle, θ, is smaller, to obtain a certain final waveguide separation, a longer transition length, *B*, is required making the total device length longer. These tapered transition sections leading towards and away from the coupler region will also introduce an additional power transfer between the guides which can be written as an additional phase shift, ΔΦ, from the two transition regions. Fig. 8.14 shows the variation of ΔΦ with angle, θ, for different separation distances, with F is fixed at 50 μm. When the angle, θ, is increased, for a given *F*, the required horizontal distance *B* will be smaller and the additional ΔΦ will also be reduced, but it will introduce more loss due to sharp transitions. It can be observed that ΔΦ reduces with θ, and also for higher separation distances. Similarly Fig. 8.15 shows the variation of the additional phase with the A/B ratio.

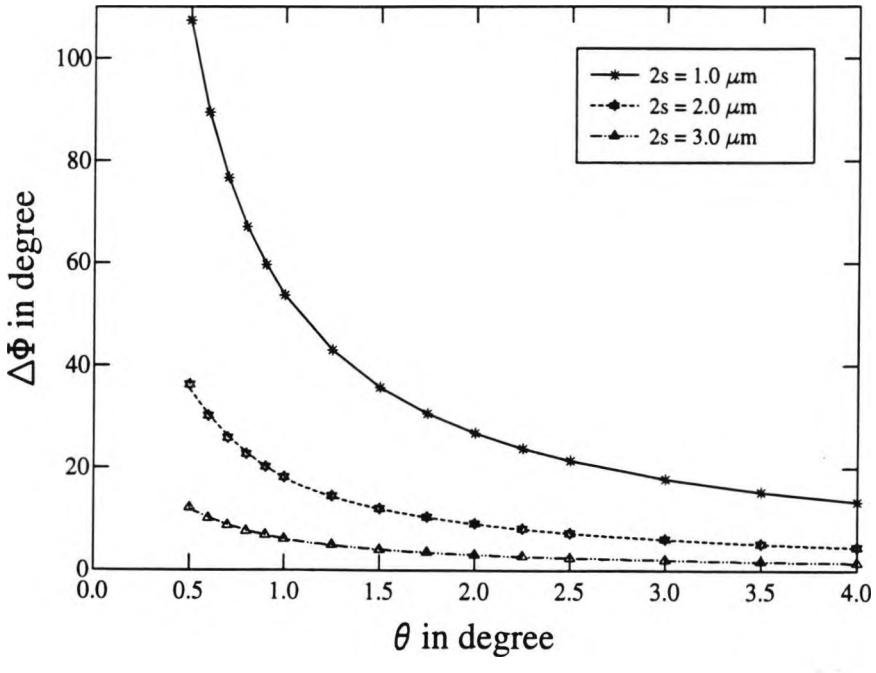

Fig. 8.14 Variation of the additional phase shift, $\Delta\Phi$ with the slope angle θ.

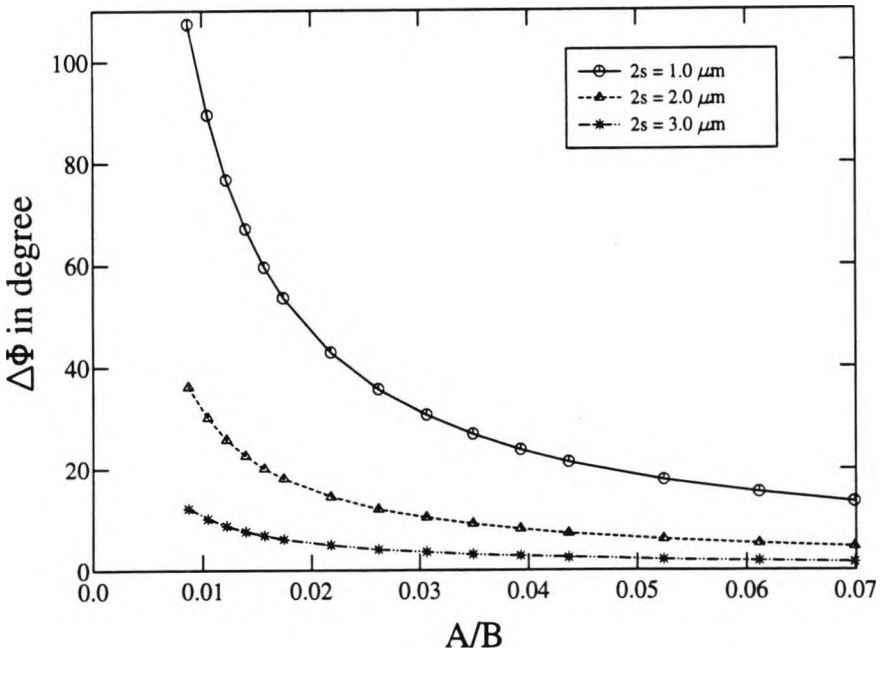

Fig. 8.15 Variation of the additional phase with *A/B* ratio.

In the design of a practical directional coupler, its effective length, L_e, is usually chosen so that

$$\Delta\beta\ L_e = n\pi \tag{8.3}$$

where n is an odd integer. If the additional phase shift $\Delta\Phi$ is not taken into account, the effective length of the directional coupler is not exactly equal to an odd number of times the coupling length, and so the performance of the directional coupler will be degraded and the power output from port 1, P_1, is not be exactly zero. This cross-power ratio, when the effect of $\Delta\Phi$ is neglected may be given by:

$$P_1/P_0 = \sin^2(\Delta\Phi/2) \tag{8.4}$$

where P_0 is the total power. However, as this additional phase shift can be accurately calculated for different designs, if the length of the parallel section(L_c') is shortened appropriately so that $L_e = L_c$, only then may 100 percent power transfer will be possible. Fig. 8.16 shows the length of the parallel section for a straight line approach for different angles, θ, and separation distances. Similarly, Fig. 8.17 shows the actual coupling length for the use of the curved section approach.

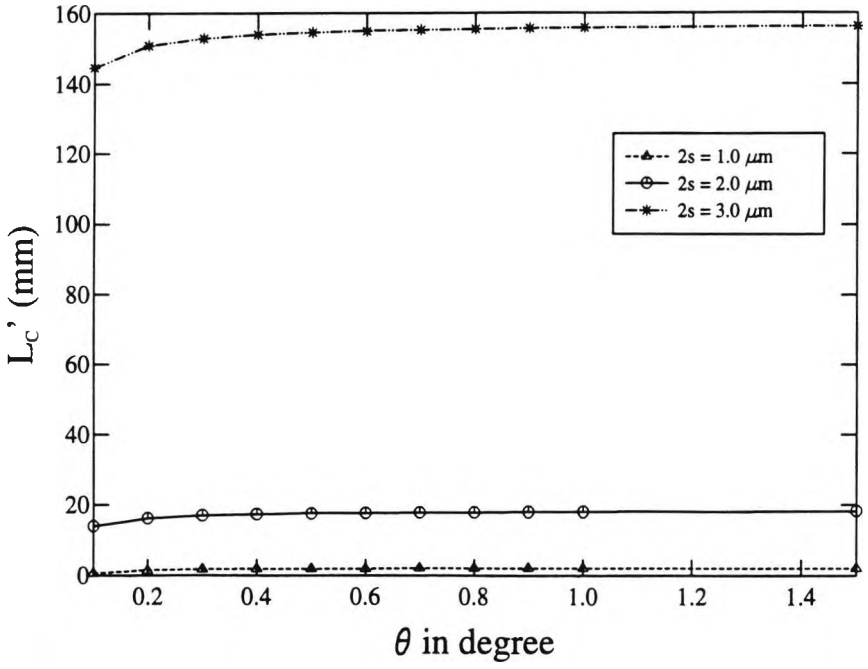

Fig. 8.16 Effective coupling length variation for straight line approach.

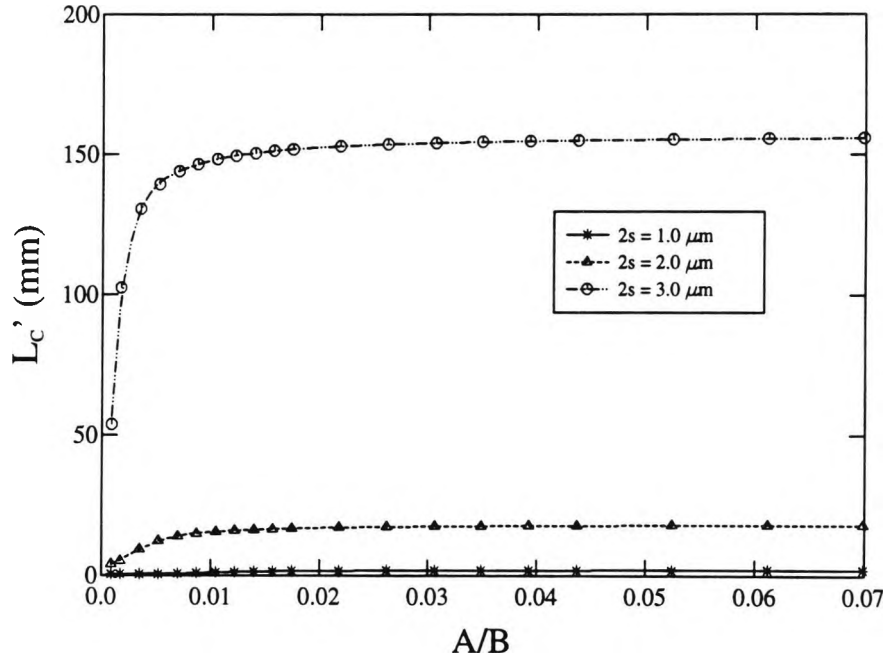

Fig. 8.17 Effective coupling length variation for curved *S* section approach.

8.3 Summary

Initially modal solutions for channel waveguides, including the effect of mesh division and penalty parameter were presented. It can be noted that the solutions become unique with the use of a finer mesh. The effect of separation distance, fabrication tolerances of the guide width and the guide depth, W/W_o and D/D_o, were also discussed. The coupling length for nonidentical guides and the supermode field profiles for synchronous and nonsynchronous waveguides were also illustrated. Additionally, the effect of curved section in terms of the additional phase shift, $\Delta\Phi$, and the length of the parallel section (L_c) were discussed. As an illustration of further applications, the power transfer between the two guides on an electro-optic directional coupler switch in 2-D confinement will be presented in the next Chapter.

Chapter 9

Electro-Optic Channel Waveguides Directional Coupler Switch

9.1 Introduction

In chapter 6, the solutions of the coupled-mode equations for electro-optic planar waveguide directional couplers have been described. The coupling properties of the directional coupler were also presented in Chapter 8, where an electro-optic directional coupler with two-dimensional confinement is presented. As has been mentioned in chapter 5, the finite element method can provide a means to obtain accurate modal field profiles and propagation constants for all the modes of each individual guide or for all the supermodes for a coupled structure consisting of two or more waveguides. Once the modal properties of the supermodes are known, the least squares boundary residual (LSBR) method can be applied to calculate the first and second supermode coefficients, b_1 and b_2. To carry out the calculations of power transfer efficiency, equation (5.5) is integrated over the cross section of the waveguides and their values are substituted into equation (5.6) and finally the

results of an analysis of the electro-optic directional coupler, in two dimensional channel waveguides are presented as follows.

9.2 Design Example

A two-parallel-channel-waveguide system is considered, which consists of five dielectric layers in x-direction and three dielectric layers in y-direction. In this example, a titanium-diffused $LiNbO_3$ electro-optic directional coupler switch is viewed together with its simplified equivalent channel structure, as shown in Fig 9.1.

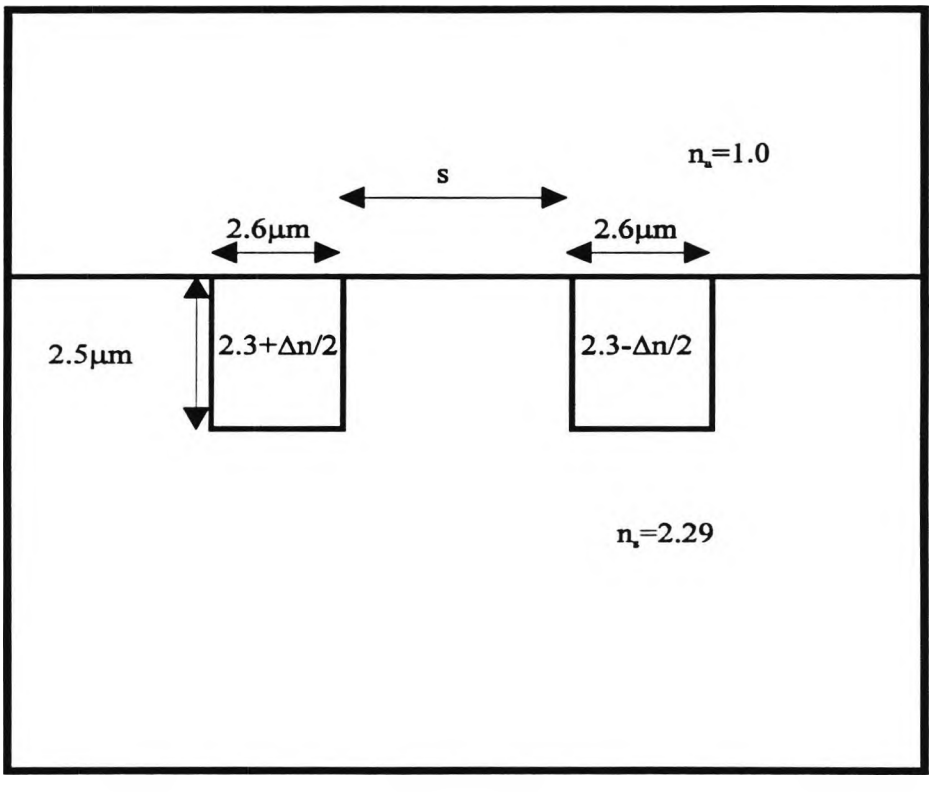

Fig. 9.1 Schematic diagram of channel waveguides directional coupler.

The unperturbed guides are 2.6 μm wide and 2.5 μm in depth and with a refractive index of 2.3, when no modulation is applied. The separation region between the guides is *s* μm wide with a refractive index in this region of 2.29. The operating wavelength is 1.3 μm. In this work, it is assumed that when a positive modulation field is applied, the refractive index in the left guide is increased by Δn/2 and decreased by Δn/2 in the right guide due to the opposite sign of the electric field, and the guides are no longer identical. Fig. 9.2 shows the variation of the propagation constants for the "even-like" and "odd-like" TE supermodes with Δn. It can be observed that the propagation constants of the two guides are almost those of the propagation of the isolated guide when the separation, *s*, increases. It can also be noted that when Δn = 0, the difference of their values of β, Δβ, is very small and it almost zero when the separation is very large.

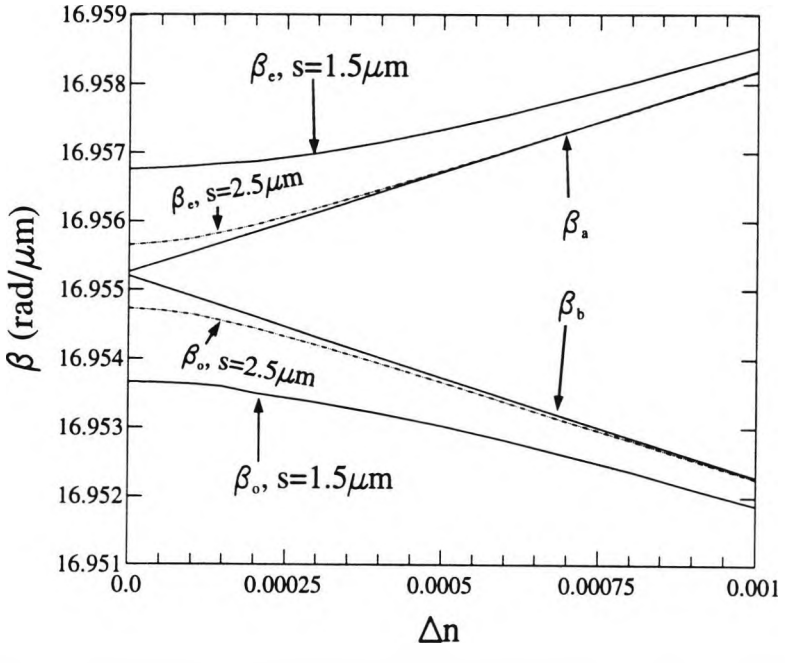

Fig. 9.2 Variation of the propagation constants for the even-like and odd-like supermodes with separation, *s*.

The electric modal field profiles for the first TE supermode are shown in Fig. 9.3 for $\Delta n = 0$ when the guide separation, s, is 1.5 μm. The dominant field is the H_y field. When no modulation is applied, in this case $\Delta n = 0$, the two guides are identical and the even and odd supermodes are symmetrical along the centre of the separation region as shown in Fig. 9.3 (a) and (b). The peak values of even field are positive for both sides and along the symmetry plane whereas the values of the odd field occur with positive and negative peaks and the field become zero at the centre of the guide.

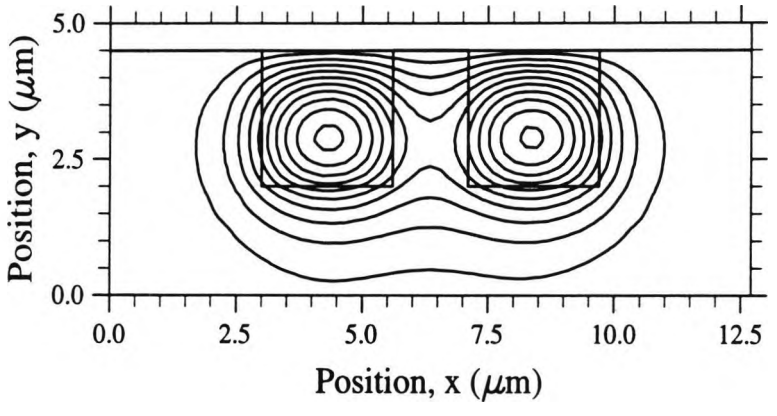

(a)

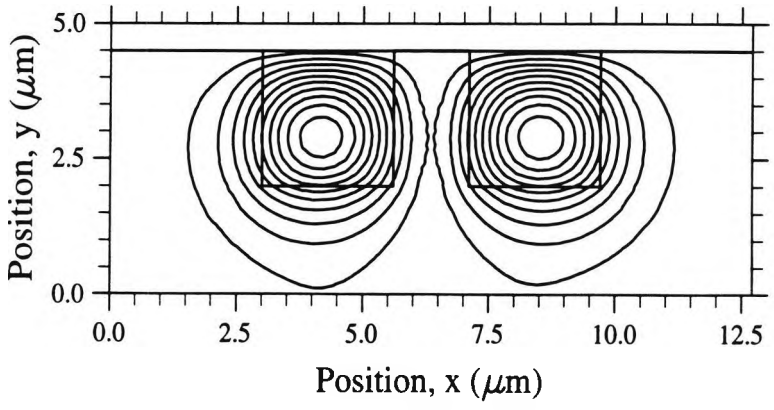

(b)

Fig. 9.3 Contour plots of the H_y field at $\Delta n = 0$ and the separation, s, is 1.5 μm (a) Even supermode (b) Odd supermode.

However, when a modulation is applied, it can be observed that the first supermode is the deformed even-like mode with more power confined in the left guide which has a higher refractive index than the right guide. Similarly the second odd-like supermode will be more confined in the right guide, which is shown in Fig. 9.4 (a) and (b) at $\Delta n = 0.0005$ for the separation, s, is 1.5 μm. When the modulating voltage is increased further, the coupled waveguides are far away from synchronous condition and then the even-like and the odd-like modes almost resemble the mode of isolated guide, as shown in Fig. 9.5 (a) and (b) at $\Delta n = 0.001$ where the separation, s, is 1.5 μm.

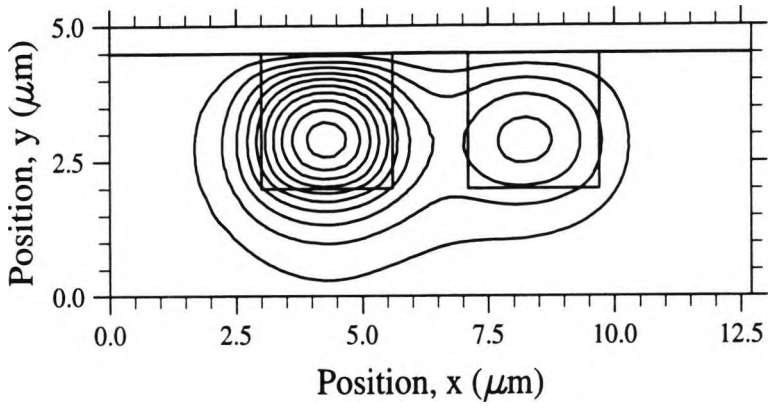

(a)

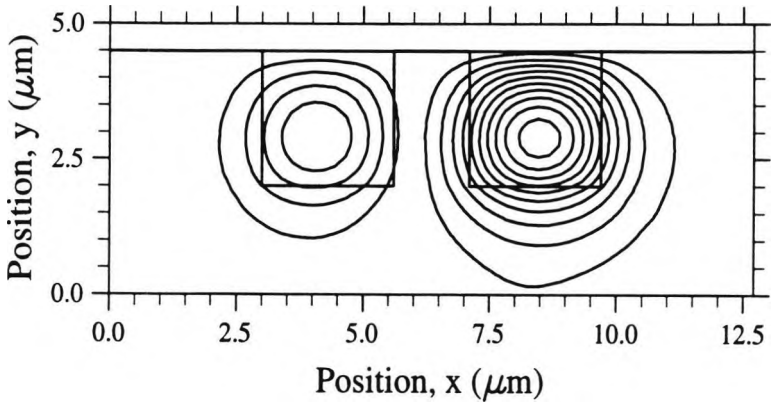

(b)

Fig. 9.4 Contour plots of the H_y field at $\Delta n = 0.0005$ (a) Even supermode (b) Odd supermode.

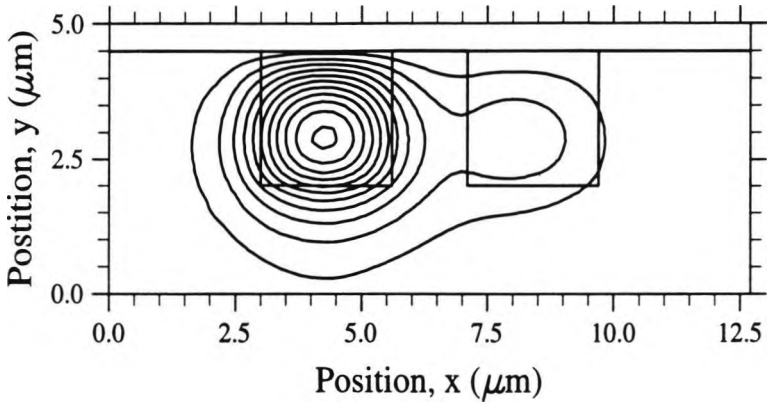

(a)

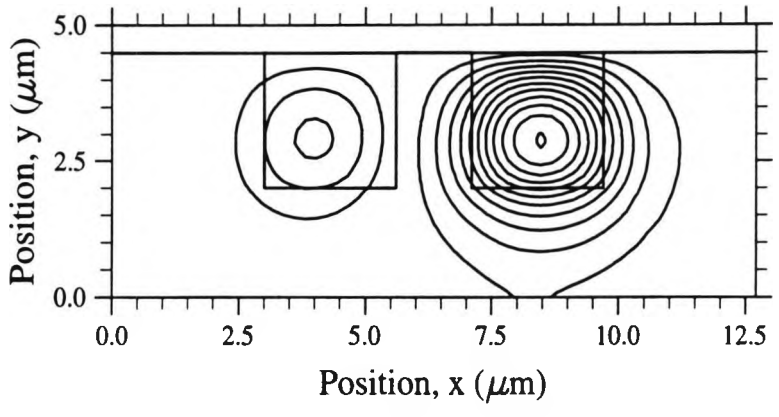

(b)

Fig. 9.5 Contour plots of the H_y field at $\Delta n = 0.001$ (a) Even supermode (b) Odd supermode.

Fig. 9.6 (a) and (b) shows the contour plots of the H_y field for the first supermode and the second supermode when $\Delta n = 0.0005$ and in this case the separation, s, is increased to 2.5 μm. It can be observed that when the separation, s, is increased the two guides become weakly coupled and the even-like mode has most of the power in the left guide compared to the case when $s = 1.5$ μm as shown

in Fig. 9.4(a). Similarly, the second odd-like mode is more confined in the right guide. It can be seen that at the same Δn but where the separation is larger, the two waveguides become further apart so the modal interaction is less, and the supermodes lose their synchronicity faster as compared to the situation in Fig. 9.4 (a), (b).

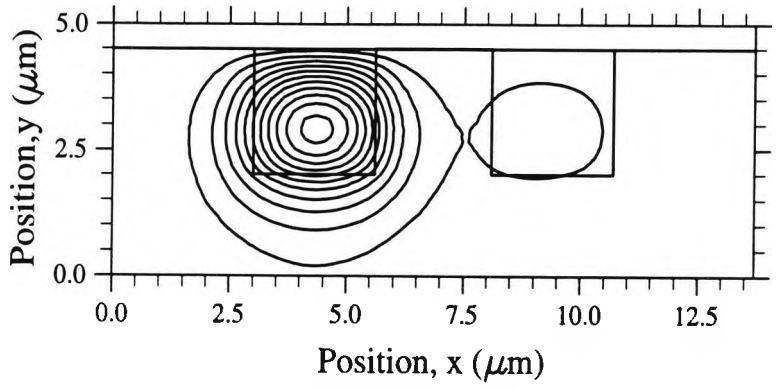

(a)

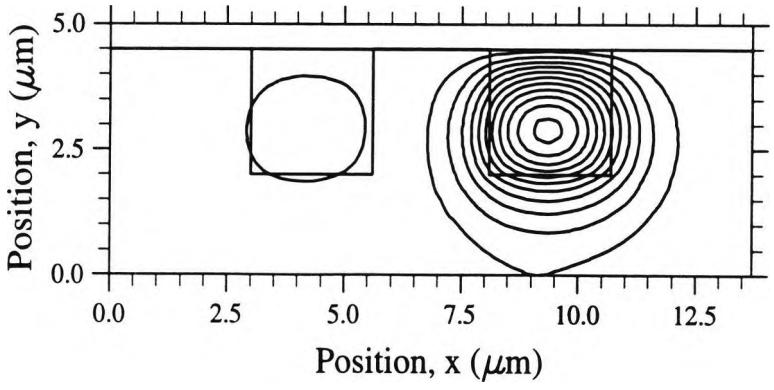

(b)

Fig. 9.6 Contour plots of the H_y field at Δn = 0.0005 and the separation, s, is 2.5 μm. (a) Even supermode (b) Odd supermode.

Fig. 9.7 shows the variation of the coupling length, L_c, with Δn for different values of the separation distance, s. It can be seen that L_c decreases with increasing Δn since $\Delta\beta$ increases when Δn increases. It can also be noted that with the increase in separation, the coupling length decreases more rapidly with the change in refractive index, Δn, since the coupling length, L_c, depends on the difference of the propagation constants, $|\beta_a - \beta_b|$. At small values of Δn, the coupling length, L_c is more sensitive to the separation, s, as $\beta_a \approx \beta_b$.

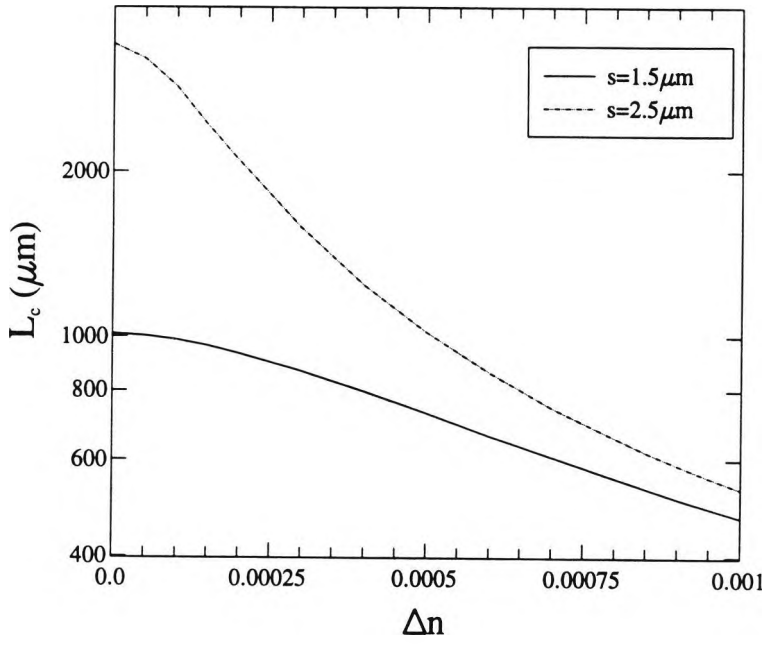

Fig. 9.7 Variation of the coupling length with Δn for different separation distances, s.

Next, the least squares boundary residual method is applied to obtain the coefficients of the two supermodes excited at the directional coupler interface, when excited by the fundamental mode in the guide *b*. Fig. 9.8 shows the variation of the supermode coefficients with Δn for different separations between the guides, *s*. It can be observed that when Δn = 0 and the separation distance is large, $b_1 \equiv b_2 \equiv 0.707$. It can be seen that the coefficient of the even supermode, b_1, decreases with Δn, whereas that of the odd supermode, b_2, increases. From the curve, when the separation distance, s = 2.5 μm the odd supermode, b_2 converges to 1.0 faster and in the same time the even supermode, b_1, also converges to zero faster.

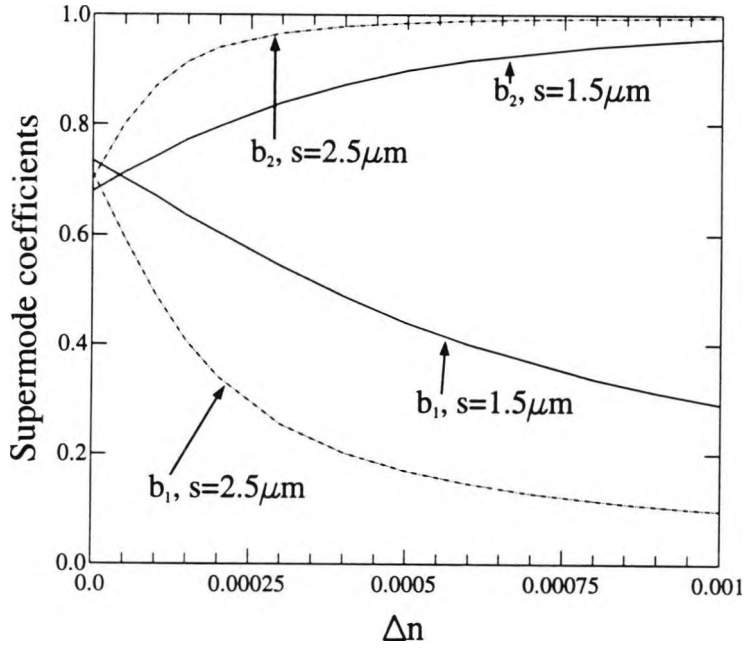

Fig. 9.8 The variation of the supermode coefficients with Δn.

Fig. 9.9 and Fig. 9.10 show the variation of the maximum power transferred and the output power from guide *b* to guide *a* with the change of refractive index difference, Δn, at values of the separation, *s*, of 2.5 μm and 1.5 μm respectively. The output power is the power transferred from guide *b* to guide *a* when the device length is kept fixed at $L_c = L_{co}$ = 3414.77 μm and 1013.42 μm when the separation distances, *s*, are 2.5 μm and 1.5 μm respectively, which are the coupling lengths when no modulation is applied. The maximum power means the power transfer from guide *b* to guide *a* when the device length is changed for a particular coupling length, L_c, which is changing with Δn. Results show that the power efficiency becomes nearly equal to unity, only when the guides are weakly coupled. With increasing Δn, the two guides lost their synchronicity and thus complete transfer of power between them can no longer occur and it falls nearly to zero. Here, the power transfer efficiency is significantly lower than the maximum power transfer. This reduced power transfer is due to the additional effect of the coupling length mismatching as the value of L_c changes with Δn, whereas the device length is kept fixed. It can be seen from the results that the output power increases to maximum and decreases to minimum alternatively when Δn is greater than 0.0003, due to the effect of the coupling length. The output power increases to maximum and decreases to minimum when the coupling length is equal to an even multiple of L_c and an odd multiple of L_c respectively. The output power and the maximum power curves when the separation, *s* = 2.5 μm decrease more rapidly compared to the case when the separation, *s* = 1.5 μm in Fig. 9.10. However, with the decrease of the

separation, *s*, the two guides have a greater interaction, the coupling length does not change much, but the output power starts increasing when Δn is greater than 0.00092, as shown in Fig. 9.10. The comparison of the effect of separation, *s*, will be shown in Fig. 9.11.

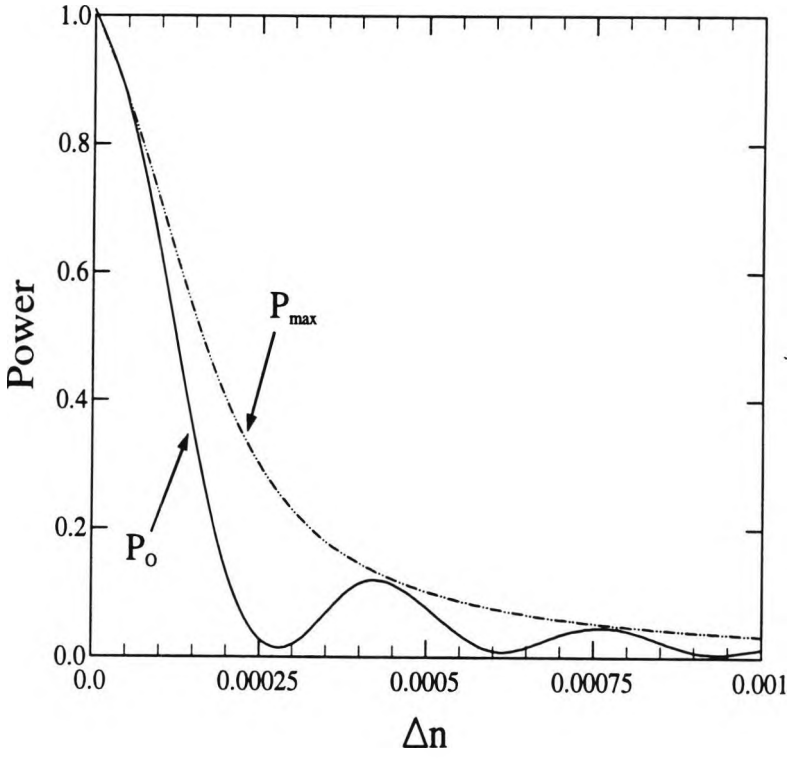

Fig. 9.9 Maximum power transfer and the output power transfer between two coupled waveguides at a separation, *s*, of 2.5 μm.

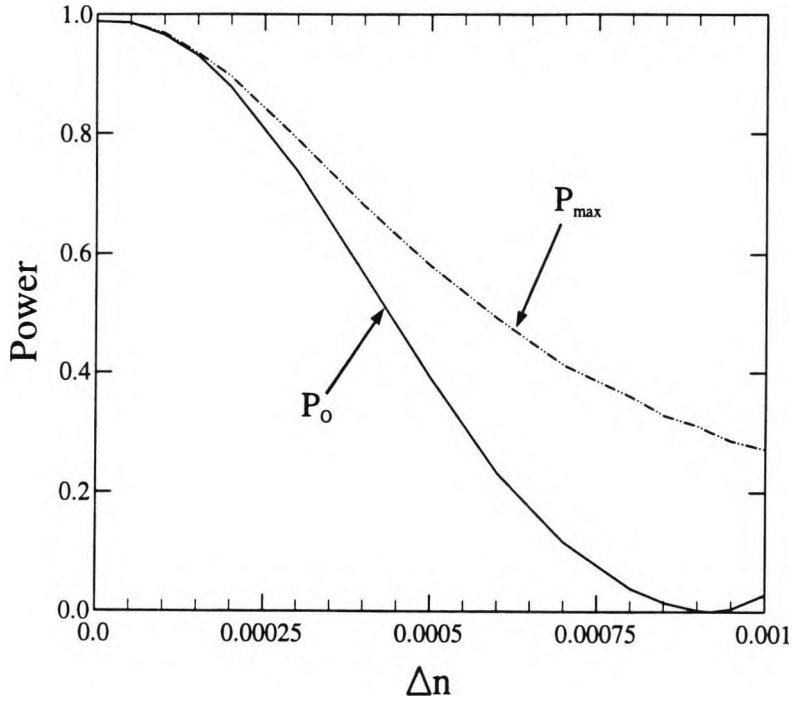

Fig. 9.10 Maximum power transfer and the output power transfer between two coupled waveguides at the separation, *s*, is 1.5 μm.

Fig. 9.11 shows the variation of the output power transfer from guide *b* to guide *a* with the change of refractive index, Δn, between the guides, when the separations, *s*, are 1.5 μm and 2.5 μm respectively. It shows that with the increase in the separation, *s*, the output power decreases more rapidly with the change in refractive index, Δn, since the waveguides loose their synchronicity faster under these circumstances.

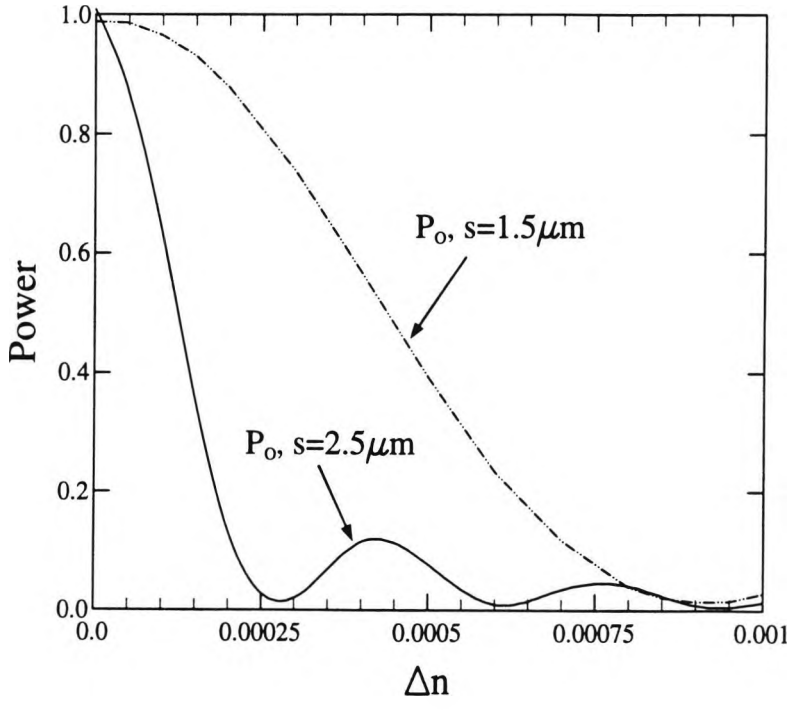

Fig. 9.11 Variation of the coupled output power in guide *a* with the refractive index change Δn.

9.3 Summary

Results for the coupling length, L_c, the modal solution field profiles, the supermode coefficients, b_1 and b_2, and the power transfer in 2-D confinement were presented in this Chapter. An accurate field profile and the coupling length were obtained from the use of the finite element method. Both synchronous and nonsynchronous field profiles were also illustrated. It can be noted that the waveguides will loose their synchronisity when Δn increases. The supermode coefficients, b_1 and b_2 were calculated from the least squares boundary residual

approach. It can be noticed from Fig. 9.8 that b_2 must be greater than b_1 because b_1 and b_2 are the coefficients which need to make the sum of $b_1E_e + b_2E_o$ equal to the incident mode in guide b. From the values of supermode coefficients, b_1 and b_2, the power transfer from guide b to guide a could be calculated. The effect of the separation, s, between the two guides was also shown.

It can be seen that complete power transfer is not possible when Δn increases and its transfer is faster with larger separation, s. The effect of the coupling length that makes the output power increase to maximum and decrease to minimum alternatively can be used in the design of an optical switch. It is important to note that the 2-D confinement approach is valid for diffused $n(x,y)$ and anisotropic material and in future work an optical filter and $\Delta n(x,y)$ can be considered. In the next Chapter, an overall conclusion of this work will be discussed, and also further work in this research theme will be suggested.

Chapter 10

Discussion and Suggestions for further work

10.1 Discussion of aims and objectives of this thesis

The objectives set out at the beginning of the study were essentially achieved during the course of the work. The results obtained were, in general satisfactory in showing agreement where possible with the results of other numerical experimental work and the use of other methods and they provide encouragement for further applications of the technique in a range of practical optical waveguides. The prime objective of this work was to develop numerical procedures to characterize directional couplers and directional coupler-based devices in terms such as the fabrication tolerances in the dimensions of the waveguides, and the bend input and output sections for a range of directional couplers and devices such as optical filters, modulators or electo-optic switches. An important objective of this work was to provide a straightforward technique to solve problems whose solutions are of significant practical interest in the optoelectronics industry. Most of the industrial interest in waveguides is in two

dimensional confinement that needs better and more accurate design methods to which most of simpler approaches may not applicable. The finite element method is one of the most powerful numerical methods which can handle a wide range of optical waveguide problems such as the arbitrary cross section waveguide, including open boundaries, the arbitrary refractive index profile $n(x,y)$ and the use of anisotropic materials. In this work, emphasis was placed on developing the finite element based techniques for further use in the design and understanding of practical waveguides. The characterization of the TE mode coupling in planar structures is presented only to make a comparison with published results using different procedures and to confirm the validity of the procedure used in this work. The method was then developed for hybrid modes in optical waveguides with two-dimensional confinement, which so far has not been reported and represents an important advance in this work. The results obtained on the power transfer in two-dimensional confinement are satisfactory, showing the validity of the method in this approach.

10.2 Use of Numerical Techniques in Problem Solving

Unfortunately the range of available analytical techniques is inadequate to solve the problems of most the optical waveguides available. In this thesis it has been demonstrated why numerical analysis has become standard for most of the dielectric waveguide structures which are usable at optical frequencies, due to its success in problem solving. The finite element method has undoubtedly become a powerful tool for the analysis of electromagnetic problems and it stands as one of

the most important techniques for carrying out such numerical analysis for a wide range of optical waveguides. In this thesis, the finite element method was implemented to obtain the modal solution for supermode field profiles, to obtain accurate propagation constants and the coupling length, L_c, of coupler devices. A specific finite element formulation involving the vector magnetic field, **H**, and a penalty function term to eliminate spurious modes has been used for the solution of optical waveguide problems, mostly for application to directional couplers of real practical interest. Several different types of directional coupler have been analyzed and the results obtained compared with others from alternative approximate methods, showing the value of the method.

The main advantages of the finite element method, over other approximate techniques, are its generality and suitability for the development of efficient and flexible computer programs. While most analytical and numerical approximate methods are mainly applicable to guides with relatively regular or slightly perturbed shape and material composition, the finite element method has been shown in this work to be suitable to treat waveguide structures with quite complicated shape and material properties. Another advantage is that its index distribution can be arbitrary, which is important for many practical waveguides. Hence it has been shown that it can be used to solve a wide range of practical waveguide problems.

For integrated optics problems, there is the need for special boundary conditions at the dielectric interfaces. As a result, the formulation involving the magnetic field vector **H** is the most advantageous, since **H** is naturally continuous

across the dielectric interfaces, and the associated natural boundary condition is that of an electric wall, which is also convenient to consider in most practical situations. However, with this formulation, there is an appearance of spurious modes amongst the physical modes. To eliminate the spurious modes, the penalty function technique was added to impose the constraint $\nabla \cdot H = 0$, and it has proved to be very effective and quite easy to implement, as demonstrated in this work.

The structures analyzed in this thesis have been two-core directional couplers. These dielectric configurations exploit the interchange of modal power between the two adjacent guides and their importance is seen in that they are at the heart of many important optical devices, such as modulators, wavelength filters and sensors. Their analytical treatment may be quite complicated and in most cases reported this has involved approximations that are not always realistic. The finite element method has proved to be very useful in that respect in this work, since it has enabled the evaluation of the basic coupling parameters, such as the coupling length and the transferred power, in a generalized and conceptually straightforward manner, showing its superiority over the analytical methods.

10.3 Specifics of the Application of the Finite Element Method in this work

With this method, the modal solution field profile and the propagation characteristics of a wide range of practical optical waveguides are easily attainable. The results show the validity of the method even when used with strongly coupled,

synchronous or nonsynchronous waveguides. The effect of fabrication tolerances, D/D_o, W/W_o, and the bend input and output sections were shown in Chapter 8. It can be noted that the effect of fabrication tolerances, D/D_o and W/W_o on the coupling length become higher when the device length is longer and it will introduce significant cross-talk. For the case of bend input and output sections, it can be seen that the transition sections will introduce an additional power transfer between the guides in the two transition regions. The effect of an additional phase shift on different parameters can accurately be calculated, as shown in Fig 8.14 to Fig. 8.17. The effect of two free parameters, the penalty term (α) and the mesh division has also been presented. There are a few types of errors which have become clear in the total solution of the problem. One is called the discretization error, which is due to the replacement of the continuous problem by a discrete model. It is necessary to use a large number of elements and nodal points to achieve a satisfactory convergence with the finite element methods. This is due to the fact that the shape functions provide only approximate representations of the true fields. The resulting error decreases as the mesh number increases, because the numerical model comes closer to an accurate representation of the continuous physical problem.

Once the accurate modal solution field profile and the coupling length, L_c, are obtained from the finite element approach, the coupled mode formulation was applied to describe a wide range of directional couplers. The application of improved coupled mode theories along with the use of accurate eigenvectors and eigenvalues obtained by the finite element method provide the power transfer ratio

between such coupled waveguides. Different coupled mode approaches have been considered to study some of the coupled guided structures. Explicit expressions for the coupling coefficients, which play a central role in this theory, are given. The formalism treats the case of slab dielectric waveguides, thus assuming no variation in one *(y)* direction. In this work, three such approaches, namely, the coupled mode approaches, the least squares boundary residual approach and the propagation model approach, were considered to test the applicability of the formulations. The coupling coefficient and the overlap integral has been tested by varying three different parameters of the waveguides, as follows in:

- Simulation of strongly coupled nonidentical waveguides by changing the width of the second guide b, where the results in Chapter 5 show excellent agreement with those of Hardy and Streifer (1985),

- Simulation of optical modulators/switches by changing refractive index different, Δn, where the results in Chapter 6 show good agreement with those of Chuang (1987),

- Simulation of optical filters by changing the wavelength, λ, where the results in Chapter 7 show close agreement with those of Huang (1992).

Alternative methods, such as the least squares boundary residual method and the propagation model method were used to test the accuracy of the result. Here the results from the least squares boundary residual method have also been

presented, and the power transfer efficiency has been shown to agree well with the results obtained from the coupled mode approaches.

Finally, these approaches presented were developed for hybrid modes in optical waveguides with two-dimensional confinement. The extension to guides where the confinement is in both the x and y directions principally involves replacing the integration over all x, in the expressions for the coupling coefficients, by an integration over both x and y. For the cases where the modes are very well confined in the y direction, the numerical correction is small. The applications of the coupled mode formulations to the two dimensional confinement has not been discussed. However, these approaches presented are valid for hybrid modes in optical waveguides with two-dimensional confinement, and the results obtained on the power transfer shown in Chapter 9 are reasonably satisfactory. The calculation of important device parameters, such as power transfer, cross-talk, and filter bandwidth, for practical optical waveguides, will be very useful in the optimization of the design of modern directional coupler-based photonic devices.

10.4 Further potential of this work

It has been shown that the use of the finite element method, the coupled-mode theory, and the least squares boundary residual method are of fundamental importance for the design and understanding of a wide variety of integrated optics and optoelectronic devices based on the coupling of optical waves. A further application of this work could be in the consideration of waveguides with different

index profiles, as well as anisotropic guides. Some important integrated optical devices are made of anisotropic materials in practice. The permittivities of these waveguide systems are characterized by a dielectric tensor, $\hat{\varepsilon}$, given by:

$$\hat{\varepsilon} = \begin{pmatrix} \varepsilon_{xx} & \varepsilon_{xy} & \varepsilon_{xz} \\ \varepsilon_{yx} & \varepsilon_{yy} & \varepsilon_{yz} \\ \varepsilon_{zx} & \varepsilon_{zy} & \varepsilon_{zz} \end{pmatrix}$$

Generally, $\hat{\varepsilon}$ is complex when there exists loss or gain in waveguide systems. For the lossless case, it is Hermitian, and for isotropic media, it degenerates to a scalar. As has been shown in this study, the finite element method can be applied to any guided mode (TE, TM, or hybrid) in a waveguide of arbitrary cross section, dissimilar index and nonidentical shape. In the finite element method, the guide cross section is divided into a finite number of triangular elements to represent the problem, thus allowing each element to have a different tensor permittivity. This property enables the finite element to be applied to the analysis of a range of arbitrarily shaped anisotropic waveguides. The modal solutions and the propagation constant of the waveguide using anisotropic materials can thus be obtained by using the finite element method. A future orientation of the work in this field could lie in the development of the coupled mode equations and the least squares boundary residual methods to calculate the coupling coefficient, the power transfer and cross-talk from the solutions obtained by the use of the finite element method. This work would also serve as a useful basis for the modelling of vertical cavity devices such as wavelength selective waveguides, carrier induced

semiconductors switches, multimode interference systems (MMI) and in the investigation of the use of lateral coupling for efficient laser-fibre coupling.

Appendix 1

Infinite Elements

The components of $[B_e]$ matrix in eq. (2.30) which represents the denominator of the eq. (2.13) can be evaluated as:

$$B_e(1,1) = \mu \int N_1^2 ds$$

$$= \mu \int \frac{y^2}{b^2} e^{(-2x/L)} dxdy$$

$$= \frac{\mu bL}{6}$$

$$B_e(1,4) = \mu \int N_1 N_2 ds$$

$$= \frac{\mu bL}{12}$$

where b and L are the width of infinite strip and the free parameter related to the field decay respectively.

Similarly the other matrix components can be also calculated.

The numerator of the equation (2.13) can also be calculated as follows:

$$\int \{H\}^* [\nabla \times [N]]^* \varepsilon^{-1} [\nabla \times [N]] \{H\} ds = \{H\}^* [A_e] \{H\} \qquad [A1.1]$$

where

$$[A_e] = \frac{1}{\varepsilon}\int [\nabla \times [N]]^* [\nabla \times [N]]\, ds \qquad \text{[A1.2]}$$

Any particular component of $[A_e]$ matrix can be easily evaluated, and as an example,

$$A_e(1,1) = \frac{1}{\varepsilon}\left[\frac{\beta^2 bL}{6} + \frac{L}{b^2}\right]$$

and similarly other components of $[A_e]$ matrix can also be calculated. The infinite elements extending in the y direction, or being extended in both the transverse directions can be solved by using similar approach.

Appendix 2

Matrix generation

From equation (2.44) the 9x9 $[B_e]$ matrix can be calculated, and as an example the *ijth* component as

$$B_{e_{ij}} = \mu \iint i_{th} \text{ row of } N^*, j_{th} \text{ column of } N \, d\Omega \qquad \text{[A2.1]}$$

From eq. (2.36), the integral of this form (2.45) can be evaluated numericallly as following:

$$B_e(1,1) = \iint N_1^2 d\Omega = \frac{A}{6} \qquad \text{[A2.2]}$$

$$B_e(1,2) = 0 \qquad \text{[A2.3]}$$

$$B_e(1,3) = 0 \qquad \text{[A2.4]}$$

$$B_e(1,4) = \frac{A}{12} \qquad \text{[A2.5]}$$

The shape functions for the first order case can be written as

$$N_i = a_i + b_i x + c_i y \qquad \text{[A2.6]}$$

From eq. (2.49) a few components of [Q] matrix can be shown as

$$Q_{11} = 0 \qquad \text{[A2.7]}$$

$$Q_{12} = -\frac{\partial N_1}{\partial z} = -j\beta N_1 \qquad \text{[A2.8]}$$

$$Q_{13} = \frac{\partial N_1}{\partial y} = c_1 \qquad \text{[A2.9]}$$

From eq. (2.50)the 9×9 [A_e] matrix can be calculated as:

$$A_e(1,1) = \iint \left(\frac{\partial N_1}{\partial y}\right)^2 + \beta^2 N_i^2 dW \qquad \text{[A2.10]}$$

$$= \frac{c_1^2 A}{\varepsilon} + \frac{\beta^2}{\varepsilon} \cdot \frac{A}{6}$$

$$A_e(1,2) = -\frac{b_1 c_1 A}{\varepsilon} \qquad \text{[A2.11]}$$

$$A_e(1,3) = -j\beta b_1 \frac{1}{\varepsilon} \cdot \frac{A}{3} \qquad \text{[A2.12]}$$

Appendix 3

List of Publications by the author relevant to the thesis

1. Wongcharoen, T., Rahman, B.M.A., Grattan, K.T.V. and Buah, P.A. (1995). Characterization of an Optical Filter using a nonsynchronous Directional Coupler. In: IEEE Singapore International Conference on Networks/International Conference on Information Engineering, Singapore 1995. Proceedings. pp. 41-45

2. Wongcharoen, T., Rahman, B.M.A. and Grattan, K.T.V. (1995). Characterization of Directional Coupler-based optical guided-wave device. In: International Microwave and Optoelectronics Conference, Rio de Janeiro, Brazil 1995. Proceedings.

3. Rahman, B.M.A., Wongcharoen, T. and Grattan, K.T.V. (1995). Characterisation of Directional Coupler based Optical Guided-Wave devices. In: Progress in Electromagnetics Research Symposium, Seattle, Washington, U.S.A., July 1995. Proceedings.

4. Wongcharoen, T., Rahman, B.M.A. and Grattan, K.T.V. (1995). Characterisation of MQW Photonic devices. In: The First Conference on Low Dimensional Structure and Devices, Singapore 1995. Proceedings. p.6.

5. Wongcharoen, T., Rahman, B.M.A. and Grattan, K.T.V. (1995). Characterization of Directional Coupler-based Modulators and Switches. (has been submitted to IEEE Lasers and Electro-Optics Society 1995 Annual Meeting, San Francisco, C.A.).

6. Wongcharoen, T., Rahman, B.M.A. and Grattan, K.T.V. (1995). Electro-optic directional coupler switches characterization (has been submitted to Journal. of Lightwave Technology).

7. Rahman, B.M.A., Rajarajan, M., Wongcharoen, T. and Grattan, K.T.V. (1995). Improved Laser-Fiber Coupling by Using Spot-size Transformer. (has been submitted to IEEE Photonic Technology Letters).

8. Wongcharoen, T., Rahman, B.M.A. and Grattan, K.T.V. (1995). Finite Element analysis of Optical Directional Couplers. Journal. of Science Society of Thailand 21. September 1995.

9. Wongcharoen, T., Rahman, B.M.A. and Grattan, K.T.V. (1994). Power Coupling Efficiency for Electro-Optic Directional Coupler Switch. In: Guided-Wave Optoelectronics. Book. New York: Plenum Publishing corporation, pp. 213-219.

10. Wongcharoen, T., Rahman, B.M.A. and Grattan, K.T.V. (1994). Wavelength-Selective Coupling between Optical Waveguides. European COST Workshop 94 Optical Telecommunications, 1721, pp. 215.

11. Rahman, B.M.A., Wongcharoen, T. and Grattan, K.T.V. (1994). Finite Element Analysis of Nonsynchronous Directional Couplers. Fibre and Integrated Optics 13, (3): 331-336.

12. Wongcharoen, T., Rahman, B.M.A. and Grattan, K.T.V. (1994). Finite Element Modelling of Semiconductor Optical Filters and Polarisers. In: Semiconductor and Integrated Optoelectronics Conference, Cardiff, Wales, UK. 1994. Proceedings.

13. Wongcharoen, T., Rahman, B.M.A. and Grattan, K.T.V. (1993). Design and Characterisation of Optical Directional Couplers using the Finite Element Method. In: Sensors and Application VI, Manchester 1993. Proceedings. pp. 311.

References

- Adachihara, H., Moloney, J.V. and Polky, J.N. (1990). Pulsed spatial switching at the Interface separating Kerr-Like instantaneous and relaxing dielectric media. Physical Review A 41 (9): 5000-5011.

- Alferness, R.C. (1982). Waveguide electrooptic modulators. IEEE Transactions on. Microwave Theory and Techniques MTT-30 (8): 1121-1137.

- Alferness, R.C. and Veselka, J.J. (1985). Simultaneous modulation and wavelength multiplexing with a tunable Ti: $LiNbO_3$ directional coupler filter. Electronics Letters 21 (11): 466-467.

- Armstrong, J.A., Bloembergen, N., Ducuing, J. and Pershan, P.S. (1962). Interactions between light waves in a nonlinear dielectric. Physical Review 127 (6): 1918-1939.

- Auracher, F., Schicketanz, D. and Zeitler, K.H. (1984). High-speed $\Delta\beta$-reversal directional coupler modulator with low insertion loss for 1.3 μm in $LiNbO_3$. Journal of Optical Communication 5: 7-9.

- Bathe, K.J. and Wilson, E.L. (1976). Numerical methods in finite element analysis. (New Jersey : Prentice Hall).

- Berk, A.D. (1956). Variational principles for electromagnetic resonators and waveguides. IRE Transactions on Antennas and Propagation AP-4: 104-111.

- Bersiner, L., Hempelmann, U. and Strake, E. (1991). Numerical analysis of passive integrated-optical polarisation splitters : comparison of finite-element method and beam-propagation method results. Journal of the Optical Society of America B 8 (2): 422-433.

- Bossavit, A. and Mayergoyz, I. (1989). Edge-elements for scattering problems. IEEE Transactions on Magnetics 25 (4): 2816-2821.

- Broberg, B., Lindgren, B.S., Oberg, M.G. and Jiang, H. (1986). A Novel Integrated Optics Wavelength Filter in InGaAsP-InP. Journal of Lightwave Technology LT-4 (2): 196-203.

- Broberg, B. and Lindgren, S. (1984). Refractive index of $In_{1-x}Ga_xAs_yP_{1-y}$ layers and InP in the transparent wavelength regions. Journal of Applied Physics 55 (9): 3376-3381.

- Chen, C.H. and Lien, C. (1980). The variational principle for non-self-adjoint electromagnetic problems. IEEE Transactions on Microwave Theory and Techniques MTT-28 (8): 878-886.

- Chen, K.L. and Wang, S. (1984). Cross-talk problems in optical directional couplers. Applied Physics Letters 44 (2): 166-168.

- Cheng, H.C. and Ramaswamy, R.V. (1991). Symmetrical directional coupler as wavelength multiplexer-demultiplexer: Theory and experiment. IEEE Journal of Quantum Electronics QE-27 (3): 567-574.

- Chuang, S. (1987). Application of strongly coupled-mode theory to integrated optical devices. IEEE Journal of Quantum Electronics QE-23 (5): 499-509.

- Chuang, S.L. (1987a). A coupled-mode formulation by reciprocity and a variational principle. Journal of Lightwave Technology LT-5 (1): 5-15.

- Chuang, S.L. (1987b). A coupled-mode theory for multiwaveguide systems satisfying the reciprocity theorem and power conservation. Journal of Lightwave Technology LT-5 (1): 174-183.

- Crosignani, B., Papas, C.H. and Porto, P.D. (1981). Coupled-mode theory approach to nonlinear pulse propagation in optical fibers. Optics Letters 6 (2): 61-63.

- Crosignani, B., Cutolo, A. and Diporto, P.D. (1982). Coupled-mode theory of nonlinear propagation in multimode and single-mode fibers: envelope solitons and self-confinement. Journal of the Optical Society of America 72 (9): 1136-1141.

- Csendes, Z.J. and Silvester, P. (1970). Numerical solution of dielectric loaded waveguides: I-Finite-element analysis. IEEE Transactions on Microwave Theory and Techniques MTT-18 (12): 1124-1131.

- Davies, A.J. (1980). The finite Element Method: A First Approach. (New York: Oxford University Press).

- Davies, J.B. (1993). Finite-element analysis of wave-guides and cavities-A Review. IEEE Transactions on Magnetics 29 (2): 1578-1583.

- English, W.J. and Young, F.J. (1971). An **E** vector variational formulation of the Maxwell equations for cylindrical waveguide problems. IEEE Transactions on Microwave Theory and Techniques MTT-19 (1): 40-46.

- English, W.J. (1971a). Vector variational solutions of inhomogeneously loaded cylindrical waveguide structures. IEEE Transactions on Microwave Theory and Techniques 19 (1): 9-18.

- Feit, M.D., Fleck, Jr., J.A. and McCaughan, L. (1983). Comparison of calculated and measured performance of diffused channel-waveguide couplers. Journal of the Optical Society of America 73 (10): 1296-1304.

- Fernandez, F.A. and Lu, Y. (1990). Variational finite element analysis of dielectric waveguides with no spurious solutions. Electronics Letters 26 (25): 2125-2126.

- Gantmacher, F.R. (1959). The theory of Matrices vol. I. (New York: Chelsea): 331-338, 322.

- Glembocki, O.J. and Piller, H. (1985). Indium Phosphide (InP). In: Handbook of Optical constants of solids, ed. by E.D. Palik (New York: Academic Press).

- Gould, R.W. (1955). A coupled mode description of the backward wave oscillator and the kompfner dip condition. I.R.E. Transactions on Electron Devices PGED-2: 37-42.

- Hardy, A. and Streifer, W. (1985). Coupled mode theory of parallel waveguides. Journal of Lightwave Technology LT-3 (5): 1135-1146.

- Hardy, A. and Streifer, W. (1986). Coupled modes of multiwaveguide systems and phase arrays. Journal of Lightwave Technology LT-4 (1): 90-99.

- Hardy, A. and Streifer, W. (1986a). Coupled mode solutions of multiwaveguide systems. IEEE Journal of Quantum Electronics QE-22 (4): 528-534.

- Harrington, R.F. (1968). Field computation by moment methods. (Florida: R.E. Krieger Publishing company).

- Haus, H.A. (1958). Electron beam waves in microwaves tubes. In: SYMPOSIUM ELECTRONIC WAVEGUIDES .New York 1958. Proceedings. New York: Polytechnic Institute of Brooklyn.

- Haus, H.A. and Fonstad, C.G. (1981). Three waveguide couplers for improved sampling and filtering. IEEE Journal of Quantum Electronics QE-17 (12): 2321-2325.

- Haus, H.A. and Whitaker, N.A. (1985). Elimination of cross talk in optical directional couplers. Applied Physics Letters 46 (1): 1-3.

- Haus, H.A., Huang, W.P., Kawakami, S. and Whitaker, N.A. (1987). Coupled-mode theory of optical waveguides. Journal of Lightwave Technology LT-5 (1): 16-23.

- Haus, H.A., Huang, W.P. and Snyder, A.W. (1989). Coupled-mode formulations. Optics Letters 14 (21): 1222-1224.

- Hayata, K., Eguchi, M., Koshiba, M. and Suzuki, M. (1986). Vectorial wave analysis of side-tunnel type polarization-maintaining optical fibers by variational finite elements. Journal of Lightwave Technology LT-4 (8): 1090-1096.

- Hayata, K., Koshiba, M., Eguchi, M. and Suzuki, M. (1986a). Vectorial finite-element method without any spurious solutions for dielectric waveguiding problems using transverse magnetic-field component. IEEE Transactions on Microwave Theory and Techniques MTT-34 (11): 1120-1124.

- Hayata, K., Misawa, A. and Koshiba, M. (1990). Split-Step Finite-Element Method applied to Nonlinear Integrated Optics. Journal of the Optical Society of America B-Optical Physics 7 (9): 1772-1784.

- Hermansson, B., Yevick, D., Bardyszewski, W. and Glasner, M. (1990). The Unitarity of Split-Operator Finite-Difference and Finite-Element Method-Applications to Longitudinally varying Semiconductor Rib Wave-Guides. Journal of Lightwave Technology 8 (12): 1866-1873.

- Huang, H.C. (1981). Coupled modes and nonideal waveguides. (Collected papers) Microwave Research Institute (MRI), Polytechnic Institute of Brooklyn New York.

- Huang, W.P. (1989). Modelling and analysis of guided-wave optoelectronic devices. PhD thesis: Massachusetts Institute of Technology, Cambridge.

- Huang, W.P., Xu, C.L. and Choudhuri, S.K. (1992). Application of the finite difference vector beam propagation method to directional coupler devices. IEEE Journal of Quantum Electronics QE-28 (6): 1527-1532.

- Hunsperger, R.G. (1984). Integrated Optics: Theory and Technology. 2nd ed. (Berlin Heidelberg New York: Springer Verlag).

- Ikeuchi, M., Sawami, H. and Niki, H. (1981). Analysis of open-type dielectric waveguides by the finite-element iterative method. IEEE Transactions on Microwave Theory and Techniques MTT-29 (3): 234-239.

- Katz, J. (1982). Novel solution of 2-D waveguides using the finite element method. Applied Optics 21 (15): 2747-2750.

- Knox, R.M. and Toulios, P.P. (1970). Integrated Circuits for the millimeter through Optical frequency range. In: MRI SYMPOSIUM ON SUBMILLIMETER WAVES, J.FOX, ed., Brooklyn 1970. Proceedings. New York: Polytechnic Press, pp. 497-515.

- Kogelnik, H. (1969). Coupled wave theory for thick hologram gratings. The Bell System Technical Journal 48 (9): 2909-2947.

- Kogelnik, H. (1975). Theory of dielectric waveguides: In: Integrated Optics, ed. by T. Tamir. (New York: Springer-Verlag).

- Koshiba, M., Hayata, K. and Suzuki, M. (1982). Approximate scalar finite-element analysis of anisotropic optical waveguides. Electronics Letters 18 (10): 411-413.

- Koshiba, M., Hayata, K. and Suzuki, M. (1984). Vectorial Finite-Element Method without spurious solutions for dielectric waveguide problems. Electronics Letters 20 (10): 409-410.

- Koshiba, M. (1992). Optical Waveguide Analysis. (New York: McGraw-Hill, Inc.).

- Koshiba, M. and Inoue, K. (1992). Simple and efficient finite-element analysis of microwave and optical waveguides. IEEE Transactions on Microwave Theory and Techniques 40 (2): 371-377.

- Lance, A.L. (1964). Introduction to Microwave Theory and Measurements. (New York: McGraw-Hill). 116-117.

- Lee, D.L. (1986). Electromagnetic Principles of Integrated Optics. (New York: John Wiley and Sons).

- Louisell, W.H. (1955). Analysis of the single tapered mode coupler. The Bell System Technical Journal 33 (6): 853-870.

- Louisell, W.H. (1960). Coupled-mode and Parametric Electronics. (New York: Wiley). and the references therein.

- Mabaya, N., Lagasse, P.E. and Vandenbulcke, P. (1981). Finite element analysis of optical waveguides. IEEE Transactions on Microwave Theory and Techniques MTT-29 (6): 600-605.

- Marcatili, E.A.J. (1969). Dielectric rectangular waveguide and directional coupler for integrated optics. The Bell System Technical Journal 48 (7): 2071-2102.

- Marcatili, E. (1986). Improved coupled-mode equations for dielectric guides. IEEE Journal of Quantum Electronics QE-22 (6): 988-993.

- Marcuse, D. (1971). The coupling of degenerate modes in two parallel dielectric waveguides. The Bell System Technical Journal 50 (6): 1791-1816.

- Marcuse, D. (1973). Coupled mode theory of round optical fibers. The Bell System Technical Journal 52 (6): 817-842.

- Marcuse, D. (1989). Light Transmission Optics. 2nd ed., (New Jersey: Van Nostrand Reinhold, Princeton, (1982) Robert E. Krieger, Malabar Florida).

- Miller, S.E. (1954). Coupled wave theory and waveguide applications. The Bell System Technical Journal 33 (5): 661-719.

- Miller, S.E. (1968). On solutions of two waves with periodic coupling. The Bell System Technical Journal 48 (8): 1801-1822.

- Miller, S.E. (1969). Some theory and applications of periodically coupled waves. The Bell System Technical Journal 49 (7): 2189-2218.

- Miniowitz, R. and Webb, J.P. (1991). Covariant-projection quadrilateral elements for the analysis of waveguides with sharp edges. IEEE Transactions on Microwave Theory and Techniques 39 (3): 501-505.

- Mitchell, C.S. and Moloney, J.V. (1990). Propagation and stability of Optical Pulses in Nonlinear Planar structures with instantaneous and Finite Response-times. IEEE Journal of Quantum Electronics 26 (12): 2115-2129.

-

- Morishita, K. and Kumagai, N. (1977). Unified approach to the derivation of variational expression for electromagnetic fields. IEEE Transactions on Microwave Theory and Techniques MTT-25 (1): 34-40.

- Neyer, A. (1984). Integrated-optical multi-channel wavelength multiplexer for monomode systems. Electronics Letters 20 (18): 744-746.

- Noda, J., Fukuma, M. and Mikami, O. (1981) Design calculations for directional couplers fabricated by Ti-diffused $LiNbO_3$ waveguides. Applied Optics 20 (13): 2284-2290.

- Pierce, J.R. (1954). Coupling of modes of propagation. Journal of Applied Physics 25 (2): 179-183.

- Rahman, B.M.A. and Davies, J.B. (1984). Finite-element analysis of optical and microwave waveguides problems. IEEE Transactions on Microwave Theory and Techniques MTT-32 (1): 20-28.

- Rahman, B.M.A. and Davies, J.B. (1984a). Finite-element solution of integration optical waveguides. Journal of Lightwave Technology LT-2 (5): 682-688.

- Rahman, B.M.A. and Davies, J.B. (1984b). Penalty function improvement of waveguide solution by finite elements. IEEE Transactions on Microwave Theory and Techniques MTT-32 (8): 922-928.

- Rahman, B.M.A. and Davies, J.B. (1985). Vector-**H** finite element solution of GaAs/GaAlAs rib waveguides. IEE Proceedings-J Optoelectronics 132 (6): 349-353.

- Rahman, B.M.A. and Davies, J.B. (1988). Analysis of Optical Waveguide Discontinuities. Journal of Lightwave Technology LT-6 (1): 52-57.

- Rahman, B.M.A. and Davies, J.B. (1988a). Analysis of optical wave-guides and some discontinuity problems. IEE Proceedings-J Optoelectronics 135 (5):339-342.

- Rahman, B.M.A. (1989). Finite element solution of nonlinear optical waveguides. In: INTEGRATED OPTICS AND OPTOELECTRONICS. Boston, Massachusetts 1989. Proceedings SPIE 1177. pp. 228-235.

- Rahman, B.M.A., Fernandez, F.A. and Davies, J.B. (1991). Review of finite element method for microwave and optical waveguides. Proceedings of the IEEE 79 (10): 1142-1148.

- Reddy, J.N. (1993). An Introduction to the Finite Element Method. (Singapore: McGraw-Hill, Inc.).

- Robson, P.N. and Kendall, P.C. (1990). Rib Waveguide Theory by the Spectral Index Method. (England: Research studied Press LTD.)

- Schelkunoff, S.A. (1955). Conversion of Maxwell's equations into generalized telegraphist's equations. The Bell System Technical Journal 34 (7): 995-1043.

- Schultz, N., Bierwirth, K. and Arndt, F. (1991). Rigorous finite-difference analysis of couple channel waveguides with arbitrary varying index profiles. Journal of Lightwave Technology LT-9 (10): 1244-1253.

- Shi, TT. and Chi, S. (1991). Beam Propagation Method analysis of Transverse-Electric Waves Propagating in a Nonlinear Tapered Planar wave-guide. Journal of the Optical Society of America B-Optical Physics 8 (11): 2318-2325.

- Silvester, P. (1969). A general high-order finite-element waveguide analysis program. IEEE Transactions on Microwave Theory and Techniques MTT-17 (4): 204-210.

- Snyder, A.W. (1970). Coupling of modes on a tapered dielectric cylinder. IEEE Transactions on Microwave Theory and Techniques MTT-18 (7): 383-392.

- Snyder, A.W. (1972). Coupled mode theory for optical fibers. Journal of the Optical Society of America 62 (11): 1267-1277.

- Snyder, A.W., Ankiewicz, A. and Altintas, A. (1987). Fundamental error of recent coupled mode formulations. Electronics Letters 23 (20): 1097-1098.

- Somekh, S. (1974). Theory, Fabrication and Performance of some Integrated optical Devices. PhD thesis: California Institute of Technology, University Microfilms, Ann Arbor. pp. 46.

- Somekh, S., Garmire, E., Yariv, A., Garvin, H.L. and Hunsperger, R.G. (1974a). Channel Optical Waveguides and Directional Couplers in GaAs-Imbedded and Ridged. Applied Optics 13 (2): 327-330.

- Streifer, W., Osinski, M. and Hardy, A. (1987). Reformulation of coupled-mode theory of multiwaveguide systems. IEEE Journal of Lightwave Technology LT-5 (1): 1-4.

- Suematsu, Y. and Kishino, K. (1977). Coupling coefficient in strongly coupled dielectric waveguides. Radio Science 12 (4): 587-592.

- Svedin, J.A.M. (1989). A numerically efficient finite-element formulation for the general waveguide problem without spurious modes. IEEE Transactions on Microwave Theory and Techniques MTT-37 (11): 1708-1715.

- Syms, R.R.A. and Peall, R.G. (1988). Explanation of asymmetric switch response of three-arm directional couplers in Ti: $LiNbO_3$ using strong coupling theory. Optics Communications 66 (5-6): 260-264.

- Tang, C.C.H. (1969). Mode conversion in nonuniform multimode waveguides and transitions. Advances in Microwaves, L. Young, Ed. 4 pp. 301-372. and references therein.

- Taylor, H.F. (1973). Frequency-selective coupling in parallel dielectric waveguides. Optics Communications 8 : 421-425.

- Taylor, H.F. and Yariv, A. (1974). Guided wave optics. Proceedings of the IEEE 62 (8): 1044-1060.

- Turner, M.J., Clough, R.W., Martin, H.C. and Topp, L.T. (1956). Stiffness and deflection analysis of complex structures. Journal of the Aeronautical Sciences 23 (9): 805-823.

- Vandenbulcke, P. and Lagasse, P.E. (1976). Eigenmode analysis of anisotropic optical fiber or integrated optical waveguides. Electronics Letters 12 (5): 120-122.

- Vassallo, C. (1987). Condensed formula for coupling coefficients between parallel dielectric waveguides. Electronics Letters 23 (7): 334-335.

- Veselka, J.J. and Korotky, S.K. (1986). Optimization of Ti: $LiNbO_3$ optical waveguides and directional coupler switches for 1.56 μm wavelength. IEEE Journal of Quantum Electronics QE-22 (6): 933-938.

- Yariv, A. (1973). Coupled-mode theory for guided wave optics. IEEE Journal of Quantum Electronics QE-9 (9): 919-933.

- Yariv, A. (1976). Introduction to Optical Electronics. 2nd, ed. (New York: Holt, Rinehart and Winston).

- Yeh, C., Dong, S.B. and Oliver, W. (1975). Arbitrary shaped inhomogeneous optical fiber or integrated optical waveguides. Journal of Applied Physics 46 (5): 2125-2129.

- Zienkiewicz, O.C. (1977). The finite element method in engineering science. 3rd ed. (London: McGraw-Hill).